Departamento de Matemáticas
UNIVERSIDADE DA CORUÑA

PhD. Thesis

Contributions to the numerical simulation of coupled models in glaciology

Raquel Toja Gómez

March 2010

Departamento de Matemáticas
UNIVERSIDADE DA CORUÑA

The undersigned hereby certify that they are supervisors of Thesis entitled "**Contributions to the numerical simulation of coupled models in glaciology**" developed by **Raquel Toja Gómez** inside the Ph.D Program "**Mathematical Modelling and Numerical Methods in Applied Sciences and Engineering**" at the Department of Mathematics (University of A Coruña).

Dated: April 5, 2010

Research Supervisors: ______________________________
José Durany Castrillo

____
Carlos Vázquez Cendón

Table of Contents

List of Tables

List of Figures

Acknowledgements

I would like to thank José Durany and Carlos Vázquez, my supervisors, for their many suggestions and constant support during this research. I am also thankful to Natividad Calvo for her supervision all these years.

I will always be grateful to Andrew Fowler. He is not only a brilliant research but also a wonderful person and their contributions makes research like this possible.

I had the pleasure of meeting Carlos Parés and Manuel Castro. I will never forget the kindness to me and specially his hospitality when I arrived in Malaga.

I should also mention Francisco Navarro and their research team. They are wonderful people and he always inform us about activities in Cryosphere research.

Thanks as well to my colleagues at the University of A Coruña.

Of course, I am grateful to my parents for their support, patience and *love*. Without them this work would never have come into existence (literally). And I am grateful to my brother David and to Raquel because they give us a wonderful present and to Sara (because she asked me when she can talk).

Finally, I wish to thank the following: CirsP, CrisS, Hoki and Gema; Patri and Gore; and the PhD students of the Mathematics Department: Aldana, Carmen, María and Marta, and Gonzalo too.

I would also like to mention that this research has been supported by Grants MTM2004-05796-C02-01, MTM2007-67596-C02-01 and PGIDIT06PXIB105230PR.

Raquel Toja Gómez

A Coruña, April 1, 2010

Resumen

En las épocas de glaciación, las masas de hielo llegaron a ocupar el 30% de la superficie terrestre. En la actualidad cubren un 10% de la misma y, además, otro 10% está permanentemente congelada. Aproximadamente la mitad del suelo del hemisferio norte está cubierto por nieve y hielo durante el invierno (ver Figura 1). Los glaciares almacenan más del 75% del agua dulce del mundo y proporcionan agua de riego para algunas de las zonas más pobladas del planeta. En la actualidad, los grandes mantos de hielo (*ice sheets*) de Groenlandia y la Antártida contienen 99% del hielo existente en la tierra. Estos grandes mantos de hielo están en zonas remotas, alejadas de toda actividad humana. Por ello, no sorprende que los glaciares pequeños de las zonas montañosas fuesen los primeros en llamar la atención debido a su ubicación cercana a zonas habitadas por el hombre. Durante los últimos 150 años, los glaciares y la Glaciología han centrado la atención creciente de la comunidad científica internacional, pero ya podemos encontrar descripciones de glaciares en la literatura islandesa del siglo XI. En Paterson [69], por ejemplo, se pueden encontrar detalles sobre la evolución histórica de la investigación en Glaciología.

Las investigaciones recientes se centran más en los mantos de hielo que en los glaciares. Esto se debe principalmente a que la amenaza del calentamiento global se cierne sobre el mundo y los mantos de hielo son reconocidos como el mayor componente en el sistema climático después de los océanos [57]. El gran volumen de agua contenida tanto en los glaciares como en los mantos de hielo representan un peligro potencial para las actividades humanas en las zonas costeras. El colapso de la capa de hielo de la Antártida Occidental puede conllevar un aumento del nivel de los mares

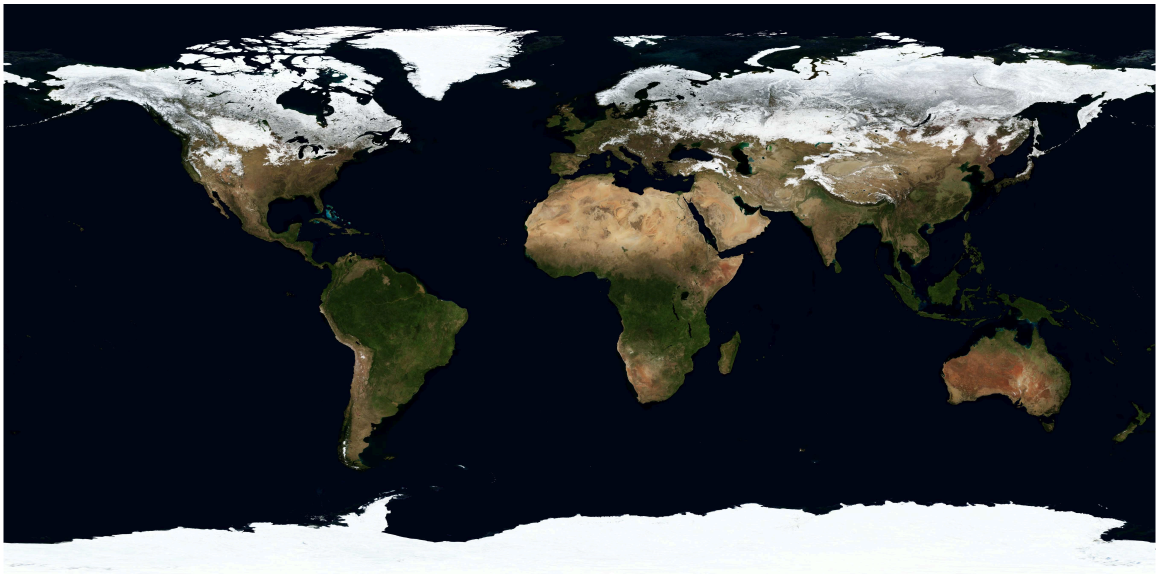

Figure 1: Northern Hemisphere in February 2004 [75]

y océanos de 7 metros en, quizás, menos de un siglo, y si este colapso es seguido por el derretimiento de la capa de hielo de la Antártida Oriental, entonces el nivel del mar podría incrementarse otros 50 metros [57].

No es difícil encontrar otras aplicaciones para la Glaciología. Las personas que viven en los países nórdicos y en tierras montañosas a veces están tan cerca de los glaciares que sus vidas se pueden ver gravemente alteradas si esos glaciares avanzan de forma similar a como se han retraído durante el siglo pasado en muchas partes del planeta. El avance del *Mer de Glace* en Francia presentó un problema de este tipo durante la *Little Ice Age* [47].

Existen poblaciones próximas a arroyos que drenan lagos represados por glaciares. El derretimiento de ese tipo de presas de hielo ha dado lugar a algunas de las mayores inundaciones archivadas en los registros geológicos y a la devastación de comunidades enteras en los Alpes y en el Himalaya [72].

El Programa de las Naciones Unidas para el Medio Ambiente (*PNUMA*) y la Organización Meteorológica Mundial (*OMM*) establecieron un Grupo Intergubernamental de Expertos sobre Cambio Climático (*IPCC*) para proporcionar al mundo una visión científica sobre el estado actual del cambio climático y sus posibles consecuencias ambientales, sociales y económicas.

Esta memoria pretende contribuir, desde un punto de vista matemático, al establecimiento de modelos y técnicas de simulación numérica de los fenómenos físicos involucrados en la evolución de los glaciares. Con ello se pretende ayudar a una mejor comprensión del comportamiento de los glaciares y así poder llevar a cabo tratamientos riguroso de distintos problemas tanto en el campo de la ingeniería como medioambientales preocupantes para el ser humano.

Un manto de hielo es una capa gruesa de hielo permanente que cubre un área extensa. Los únicos mantos de hielo que existen actualmente en la tierra son la Antártida y Groenlandia (el Ártico en un océano y su hielo es hielo marino), pero durante el último periodo glacial el manto de hielo conocido como Laurentide llegó a cubrir gran parte de Canadá y América del Norte, el manto de hielo Fennoscandia ocupó el norte de Europa y el manto de hielo Patagónico se extendía por el sur de América del Sur. Las magnitudes de los mantos de hielo son del orden de miles de kilómetros de extensión, y kilómetros de espesor (hasta cuatro kilómetros en la Antártida). Los mantos de hielo son el equivalente a gotas de hielo, pero a gran escala. Cuando un continente entero (o al menos una parte sustancial de él) tiene clima polar, entonces la nieve se acumula en las alturas, se comprime el hielo y fluye para cubrir el continente, de la misma forma que una gota de un fluido sobre una mesa se extiende por la acción de la gravedad. Sin embargo, mientras las gotas alcanzan un estado estacionario debido al efecto contráctil de las tensiones superficiales, esto no es tan relevante en el caso de los mantos de hielo. En los mantos de hielo el equilibro se mantiene por un balance de masas entre la acumulación en el centro y la ablación en los márgenes. Ésta puede ocurrir tanto debido al derretimiento del hielo, porque los márgenes se encuentran en regiones de clima más cálido, como al desprendimiento de icebergs.

Los glaciares son grandes masas de hielo perenne que se mueven lentamente sobre la tierra como ríos de hielo. Se forman en lugares donde durante muchos años la acumulación de nieve y hielo excede a la ablación. Alaska, los Alpes, Spitzbergen o el Himalaya son algunos ejemplos de su localización actual. Los glaciares drenan las zonas donde se acumula la nieve, de la misma forma que los ríos drenan las zonas donde cae la lluvia. Los glaciares también fluyen de la misma forma en que lo hacen los ríos. Aunque los glaciares son sólidos, se pueden deformar por la lenta expansión de la red de cristales de hielo que los forman. Así, el hielo de los glaciares se comporta como un material viscoso, con una viscosidad muy elevada, sobre 10^{16} veces la viscosidad del agua. Como consecuencia de su enorme viscosidad, los glaciares se mueven de forma lenta, con velocidades típicas en el rango de 10–100 metros por año, que, aunque sin duda son velocidades pequeñas, son muy importantes.

Tanto el movimiento de los mantos de hielo como el de los glaciares pueden ser explicados mediante la teoría de la viscosidad, sin embargo, ocurren ciertos fenómenos relevantes que no se pueden explicar utilizando esta teoría. El principal es el hecho de que el hielo puede alcanzar temperaturas de fusión en la base del glaciar debido al calentamiento por fricción o a la entrada de calor geotérmico. En ese caso se produce agua y el hielo se puede deslizar. Así, a diferencia de un fluido viscoso ordinario, el deslizamiento de los glaciares puede ocurrir en la base.

Es importante destacar que la Matemática Aplicada, con herramientas de modelización basadas en ecuaciones en derivadas parciales (EDPs), técnicas para el análisis matemático de los modelos, y una amplia variedad de métodos para la simulación numérica de fenómenos termo-mecánicos, es una parte de la familia multidisciplinar que estudia la Glaciología teórica (ver Díaz [26], por ejemplo). Otras ciencias de esta familia como, por ejemplo, la Geofísica, la Geografía, o la Mecánica de Medios Continuos, han reconocido el papel primordial de la modelización matemática y la simulación numérica en este campo, como se puede ver en los libros de Fowler [35], Greve y Blatter [46], Hutter [54], Lliboutry [62] y Paterson [69], entre otros.

El contenido de esta memoria se puede enmarcar dentro de los modelos matemáticos de glaciares y su simulación numérica. Una de las principales motivaciones de este trabajo es formular las ecuaciones matemáticas de la dinámica del hielo, teniendo en cuenta de forma destacada que no se conoce a priori la región ocupada por el hielo, de modo que el dominio forma parte de la solución del problema. Otra motivación importante es que se tienen que considerar modelos globales donde hay agua y hielo a punto de fusión. Ambas motivaciones llevan a ejemplos típicos de problemas de frontera móvil o libre.

La formulación matemática de los modelos globales que establecen el comportamiento mecánico y termohidrodinámicos de los glaciares es compleja, porque, como se ha comentado previamente, todavía hay cuestiones abiertas sobre algunas condiciones de flujo tanto en el interior del glaciar como en las fronteras. Esto se evidencia cuando se observan las diferentes simplificaciones y los desacoplamientos de los distintos fenómenos físicos que se han estado utilizando desde el primer modelo matemático a finales de los años cincuenta. Existen modelos termodinámicos, modelos isotermos de la dinámica del hielo, modelos termomecánicos, modelos específicos para la Antártida, entre otros, lo que evidencia la dificultad de los problemas.

El lector interesado puede consultar la Tesis Doctoral de Huybrechts [55]. En ella se indican las particularidades de los distintos modelos matemáticos que se han manejado en los últimos cuarenta años, también se recomienda la lectura del libro de Hutter [54], donde se incluyen los progresos hechos por Nye, Glen, Lliboutry, Weertman y Fowler, entre otros. Esta tesis se centra en modelos simplificados, ya que todos los modelos que se resuelven son de este tipo. En particular, las formulaciones basadas en el trabajo de Fowler–Larson [36] y, de forma más concreta, Fowler [34].

El Capítulo 1 es una introducción general a esta memoria.

El Capítulo 2 es una revisión de los modelos matemáticos de glaciares. En él se establecen las ecuaciones básicas de los problemas de frontera móvil estudiados en los siguientes capítulos. En teoría, se puede calcular el tamaño de un glaciar, su distribución de temperatura, su campo de velocidades y sus tensiones, así como la variación temporal de estas magnitudes con unas condiciones inicial y de frontera dadas. Las ecuaciones básicas que se resuelven para el cálculo de esas magnitudes son las leyes de conservación de la masa, el momento y la energía, acompañadas por la ley de comportamiento del hielo y las condiciones de contorno apropiadas. Sin embargo, se tiene que considerar algún tipo de simplificación, física o empírica, para conseguir una solución factible. Incluso con estas simplificaciones, el problema matemático es lo suficientemente complejo como para no tener solución analítica. Por una parte, las simplificaciones obvian algunos fenómenos locales en tiempo y espacio, como por ejemplo: la formación y propagación de grietas dentro del glaciar, la acumulación de tensiones en ciertas partes del mismo, el desprendimiento de icebergs en los márgenes, etc. Por otra parte, la importancia de las escalas de tiempo en años, y no en segundos o minutos, hace posible excluir ciertos efectos como los movimientos sísmicos, entre otros. Las ecuaciones adimensionales, basadas en el escalado de hielo poco profundo y bajo la hipótesis de aproximación de hielo poco profundo, también permiten despreciar ciertos términos en el modelo matemático, y además, la imposición de ciertas hipótesis relacionadas con los órdenes de magnitud de las distintas incógnitas conduce a unos modelos que pueden ser tratados con técnicas analíticas y numéricas conocidas.

Se debe indicar que, aunque la exclusión de ciertos fenómenos y las simplificaciones de las ecuaciones que se han incluido pueden limitar la aplicabilidad de los modelos matemáticos propuestos en el Capítulo 2, estas restricciones no evitan que, desde un punto de vista práctico, las soluciones matemáticas sean físicamente relevantes, como se discute a lo largo de este trabajo, y que forman, desde una perspectiva teórica, problemas visiblemente difíciles enmarcados en el campo de la resolución numérica de ecuaciones en derivadas parciales.

Concretamente, en el Capítulo 2 se propone un problema acoplado para el cálculo del perfil, la distribución de temperaturas y el campo de velocidades para modelar el comportamiento termo-mecánico de los glaciares, utilizando una condición de frontera móvil para el cálculo de la superficie del glaciar que está en contacto con la atmósfera. Esta caracterización da lugar a un problema de frontera móvil gobernado por una ecuación no lineal en derivadas parciales.

Por otro lado, otras formas de energía interna distintas de la energía térmica se desprecian, de modo que, la distribución de temperatura en una sección longitudinal está determinada por un balance entre los mecanismos de conducción, convección y reacción, junto con las distintas leyes constitutivas (Glen y Arrhenius). Además, la difusión horizontal del calor se omite, debido a que los gradientes en esta dirección son muy pequeños si se comparan con los grandes gradientes verticales de la temperatura, como se indica en el escalado de hielo poco profundo.

El problema acoplado propuesto en el Capítulo 2, sirve como base para los siguientes capítulos de la memoria.

En el Capítulo 3 se propone una aproximación isoterma para el problema del perfil descrito en el Capítulo 2 y así se desacopla el cálculo del perfil de los problemas de distribución de temperatura y campo de velocidades. Además, se desarrollan un conjunto de técnicas numéricas para la simulación de la evolución del perfil que se enmarcan en el campo de los modelos isotermos de hielo poco profundo. Las diferentes formulaciones matemáticas se proponen en términos de una ecuación parabólica altamente no lineal. Una primera no linealidad viene de la frontera móvil asociada al desconocimiento a priori de la extensión basal de la región ocupada por el glaciar. Esta característica se trata con una técnica de dominio fijo aplicada a formulaciones de complementariedad que son resueltas numéricamente por un método de dualidad. La formulación en términos de un problema de obstáculo asociado con ecuaciones altamente no lineales de convección-difusión es una de las principales novedades de este trabajo. El término difusivo no lineal es tratado de forma explícita en el esquema de avance en tiempo. Al tratarse de un problema de convección dominante, se propone un esquema de características para la discretización en tiempo, mientras que para la discretización espacial se utilizan elementos finitos de Lagrange lineales a trozos. La presencia de pendientes infinitas en los regímenes polares motivan una formulación alternativa basada en la prescripción de una condición de contorno donde interviene el flujo en el nacimiento del glaciar en vez de la condición de tipo Dirichlet homogénea que se había utilizado. Al final del Capítulo 3, se incluyen varios ejemplos numéricos para ilustrar el comportamiento de los métodos propuestos. Para comprobar la validez del método que se propone, entre los ejemplos se plantean casos analíticos en los que se han construido soluciones exactas artificiales de forma similar a las de Bueler y otros [11] para el caso de mantos de hielo. Además, bajo ciertas condiciones de contorno se puede calcular la posición del frente del glaciar de forma analítica, así que también se proponen algunos ejemplos para comprobar que la posición del frente del glaciar obtenida con la simulación numérica coincide con el valor analítico que debería tener.

En el Capítulo 4 se propone y resuelve un modelo termoacoplado para la simulación numérica de la termo-mecánica de los glaciares utilizando técnicas numéricas eficientes. Una novedad en este capítulo es la formulación de problema de tipo obstáculo asociado a la ecuación integro-diferencial no lineal para el problema del perfil. Para tener en cuenta de forma adecuada el modelo no isotermo es preciso que los coeficientes de esta ecuación dependan en forma no local de la temperatura. Esta formulación se basa en la característica de la frontera libre y la influencia de la temperatura en el perfil. Se trata de un modelo no isotermo completamente acoplado. En cuanto a la ecuación de la temperatura, en la superficie el valor de la temperatura se prescribe de forma dinámica. Este valor de temperatura atmosférica decrece a medida que la altura aumenta. Como las ecuaciones de la temperatura y el perfil están completamente acopladas, se tiene un sistema no lineal de EDPs donde las incógnitas principales son el perfil del glaciar, el campo de velocidades y la temperatura. Junto a las dificultades numéricas asociadas a la ecuación del perfil, para la resolución numérica de la temperatura, la velocidad y las magnitudes basales se han considerado varias técnicas: formulaciones en entalpía, métodos de características para la discretización en tiempo, discretizaciones de elementos finitos en 2D, métodos de dualidad asociados a operadores monótonos, métodos de Newton para problemas no lineales y fórmulas de cuadratura numérica para el cálculo del campo de velocidades. Para resolver el sistema acoplado global de EDPs no lineales se realiza una iteración de punto fijo que trata de forma secuencial cada uno de los problemas implicados (perfil, velocidad y temperatura). Al final del Capítulo 4 se proponen varios ejemplos ilustrativos de glaciares con base polar, glaciares con base politérmica y glaciares con base temperada. Además, como en el Capítulo 3, se consideran dos posibles condiciones de contorno en el nacimiento del glaciar: flujo prescrito o valor del perfil impuesto. Como ocurre en el Capítulo 3, tras las simulaciones numéricas, los resultados obtenidos para los casos de flujo impuesto son más realistas que los que se consiguen con un valor fijado para el flujo en el nacimiento del glaciar. Además, se ha desarrollado la misma técnica que en el Capítulo 3 para calcular la posición de la frontera libre en los casos en los que se impone el flujo como condición de contorno y se ha comprobado que el valor calculado en las simulaciones numéricas se aproxima bien al valor teórico.

En el Capítulo 5 se propone otro modelo de aproximación de hielo poco profundo de valles glaciares para reconsiderar si el fenómeno conocido como fugas térmicas puede ser un mecanismo viable en el inicio de las inestabilidades en los glaciares que comienzan a moverse hasta 100 veces más rápido de lo normal y avanzan de forma sustancial (*surge glaciers*). Para ello se plantea una solución aproximada a la distribución de la temperatura dentro del glaciar. Dicha aproximación se fundamenta en que las tensiones se concentran en la base del glaciar. Con esta hipótesis se muestra que existe una ecuación evolutiva para el perfil. Aunque esto es bien conocido para flujos iso-viscosos, no había sido planteado antes para flujos de viscosidad variable. Durante el proceso de obtención de las ecuaciones se demuestra que las fugas térmicas no pueden ocurrir. Un resultado particular de este capítulo ha sido la inesperada inadecuación del calor geotérmico. Si se calcula utilizando los valores típicos para el flujo de calor geotérmico, entonces el calor geotérmico resultante es demasiado pequeño como para que el hielo de la base alcance el punto de fusión. En la naturaleza es extraño encontrar glaciares con la base completamente fría, y esta consideración lleva a replantearse la importancia de la liberación de calor latente producido por el agua del deshielo y de la lluvia que pasa de la superficie a partes interiores del glaciar. En ausencia de tales fenómenos la base de los glaciares permanece completamente congelada.

En el Apéndice A, se incluyen definiciones y resultados clásicos relacionados con operadores maximales monótonos. Además, se detallan los cálculos para obtener las aproximaciones Yosida de los operadores monótonos que aparecen en los distintos modelos.

En el Apéndice B se muestran detalles de la implementación en ordenador. Así, se describe la herramienta de software específica para la simulación de glaciares, GLANUSIT, que se ha construido y también se indican las técnicas de paralelización utilizadas en la implementación del problema.

Para finalizar, se ha de indicar que un resumen de los distintos apartados del Capítulo 3 se encuentran en los trabajos [14], [17] y [19]. Una primera aproximación a los resultados obtenidos en el Capítulo 4 se puede encontrar en las referencias [17] y [18]. El Capítulo 5 ha sido publicado en *Proceedings of the Royal Society A* (ver [40]). Los detalles de la versión para mantos de hielo de la herramienta de software GLANUSIT ha sido publicada en *Advances in Engineering Software* (ver [15]), y algunos de los resultados de la versión paralela de los códigos de simulación numérica para mantos de hielo están incluidos en *Proceedings in Applied Mathematics and Mechanics* (ver [16]).

Chapter 1

Introduction

Glaciers once covered 30% of the land area of the Earth, nowadays they cover the 10% and a further 10% of Earth's surface is permanently frozen. About 50% of the land is covered by snow and ice in the northern-hemisphere during winter. More than 75% of the world's fresh water is contained in glaciers, which provide irrigation water for some of the most densely populated areas of the world. However, at present, all but about 1% of this ice is located in areas remote from human activities, the great ice sheets of Greenland and Antarctica. Thus, it is not surprising that relatively small glaciers on mountain areas were the first to attract attention due to their location near to human activities. Glaciers and glaciology have focused the attention of a growing international research community for a little more than 150 years, but we can find descriptions of glaciers in the Icelandic literature of the 11^{th} century. Details about the history evolution of research in Glaciology can be found in Paterson [69], for example, and the bibliography that is referenced there.

Recently research is centered on ice sheets more than in glaciers. This is mainly because the ice sheets are recognized as the second largest component of the climate system after the oceans [57] and nowadays the threat of global warming is hanging over the world. The large volume of water locked up in glaciers and ice sheets represents a potential hazard for human activities in coastal areas. Collapse of the West Antarctic ice sheet could lead to a worldwide rise in sea level of seven meters in, perhaps, less

Figure 1.1: Le Mer De Glace

than a century and whether this event is followed by melting of the East Antarctic ice sheet, sea level could rise around additional fifty meters or so [57].

Other applications of Glaciology are not hard to find. An increasing number of people in northern and mountainous lands live so close to glaciers that their lives would be severely altered by ice advances comparable in magnitude to the retreats that have taken place during the past century in many parts of the world. The *Mer de Glace* in France, see Figure 1.1, present a particular problem during the *Little Ice Age* [47].

Other people live in proximity to streams draining lakes dammed by glaciers. Some of the biggest floods known from the geologic record resulted from failure of such ice dams, and smaller floods of the same origin have devastated communities in the Alps and Himalayas [72].

The United Nations Environment Programme (*UNEP*) and the World Meteorological Organization (*WMO*) established the Intergovernmental Panel on Climate Change (*IPCC*) to provide the world with a clear scientific view on the current state of climate change and its potential environmental and socio-economic consequences.

This memory tries to contribute, from a mathematical perspective, to the statement of the models and the numerical simulation of the physical phenomenon involved on glaciers evolution. In this way, we also try to contribute to a better comprehension of the glaciers behaviour for a rigorous treatment of various engineering and environmental problems of concern humans.

An ice sheet is a thick, permanent mass of ice that covers a very large area. The only current ice sheets on Earth are in Antarctica and Greenland (the Arctic is an ocean, and its ice is sea ice), but during the last glacial period at Last Glacial Maximum the Laurentide ice sheet covered much of Canada and North America, the Fennoscandian ice sheet covered northern Europe and the Patagonian ice sheet covered southern South America. Their magnitudes are on the order of thousands of kilometers in extend, and kilometers deep (up to four in Antarctica). Ice sheets are the equivalent of droplets, but on a larger scale. When an entire continent (or at least a substantial portion thereof) has a polar climate, then snow accumulates on the uploads, it compressed from ice, and flows out to cover the continent, much as a drop of fluid on a table will spread under the action of gravity. However, whereas droplets can reach a steady state though the contractile effect of surface tension, this is not so relevant in the case of large ice sheets. Nevertheless, in ice sheets equilibrium can be maintained through a balance between accumulation in the center and ablation at the margins. This can occur either though melting of the ice in the warmer climate regions located at the ice margin, or though calving of icebergs.

Glaciers are huge perennial masses of ice which move slowly over land like rivers of ice. A glacier forms in locations where the mass accumulation of snow and ice excess ablation over many years. Alaska, the Alps, Spitzbergen or Himalayas are just current examples of their localization. They drain areas in which snow accumulates, much as rivers drain catchment areas when rain falls. Glaciers also flow in the same basic way as rivers do. Although glaciers are solid, they can deform by the slow creep of dislocations within the lattice of ice crystal which form the fabric of ice. Thus, the glacier ice effectively behaves like a viscous material, with, however, a very large viscosity, about 10^{16} times the water viscosity. As a consequence of their enormous viscosity, glaciers move slowly, a typical velocity would be in the range of 10–100 meters per year, certainly measurable but hardly dramatic.

While the motion of ice sheets and glaciers can be understood by means of viscous theory, there are some relevant complex phenomena which can occur. Chief among these is that ice can reach the melting point at the glacier bed, due to frictional heating or geothermal heat input, in which case water is produced, and the ice can slide. Thus, unlike an ordinary viscous fluid, slip can occur at the base.

It is important to emphasize that Applied Mathematics, with its modelization tools based on partial differential equations, its techniques for the mathematical analysis of the models, and its wide range of methods for the numerical simulation of the thermo-mechanical phenomenon, is a part of the multidisciplinary family that studies the theoretical glaciology (see Díaz [26], for example). Other different subjects of this family, as for example: Geophysics, Geography, Materials Science and Continuum Mechanics, have recognized the important role of the mathematical modelization and numerical simulation in this field, as you can see in the books of Fowler [35], Greve and Blatter [46], Hutter [54], Lliboutry [62] and Paterson [69], among others.

The content of this memory can be framed into the field of mathematical models of glaciers and their numerical simulation. One of the main motivations of this work is to formulate the mathematical equations of the ice dynamics, specially keeping in mind that we do not know a prior the ice region so that this unknown domain is part of the solution of the problem. Other important motivation is that we have to consider global models where there are ice and water at melting point and solidification areas. Both motivations lead to typical examples of free or moving boundary problems.

The mathematical formulation of the global models that state the mechanical and thermodynamical behaviour of glaciers is complex, because, as we have previously mentioned, there are still questions about some flow conditions inside the domain and at the boundaries. This is evidenced when you observe the different simplifications and the uncoupling of the different physical phenomena that have been used since the advent of the first comprehensive mathematical models at the late fifties. Thermodynamical models, isothermal models of the ice dynamics, thermomechanical models, specific models for the Antarctic, are clear examples of the difficult of these problems.

We refer the interested reader to the PhD thesis of Huybrechts [55], where he referenced the particularities of different mathematical models that have been handled in the past forty years and the book wrote by Hutter [54] that includes the progress made by Nye, Glen, Lliboutry, Weertman and Fowler, among others. Accordingly, we direct our attention to certain simplified models and sets the guideline of this work. In particular, the formulations based on the work of Fowler-Larson [36] and more specifically Fowler [34].

Chapter 2 in this memory is a review of the mathematical models of glaciers and the statement of the basic equations appearing in the moving boundary problems that we study in the following chapters. In theory, we can compute the size of a glacier, its temperature and its velocity and stress distribution, just as the time variation of these magnitudes with prescribed boundary and initial conditions. The basic equations that we have to solve in order to compute these values are the conservation laws of mass, momentum and energy, accompanied by the ice rheology law and boundary conditions. However, we have to consider some kind of simplification, physical or empirical, to get a feasible solution. Even with this simplifications, the mathematical problem is complex enough so that we cannot get an analytical solution. On one hand, this simplifications neglect some local phenomena in time and space, as for example the cracks formation and propagation inside the glacier, the stress accumulation in certain places, the calving at margins, etc. On the other hand, the relevance of the time scales in years, and not in seconds or minutes, makes it possible to exclude certain effects such as seismic waves, among others. The dimensionless equations, based on a shallow ice scaling under the hypothesis of *shallow ice approximation*, also neglect certain terms in the mathematical model, and the imposition of certain assumptions related orders of magnitude of some unknowns, lead to models that can be treated with known analytical and numerical techniques. In this work, we propose a coupled model to compute the profile, temperature and velocity of a glacier.

We must indicate that, although the exclusion of certain phenomena and simplifications can limit the applicability of the mathematical models posed in Chapter 2, these restrictions do not prevent that from an application perspective, the mathematical solutions are physically relevant, as discussed throughout this work, and that from a theoretical perspective, the problems notoriously difficult within the framework of numerical solution of partial differential equations.

Specifically, in Chapter 2 we pose a coupled problem to model the thermo-mechanical behaviour of the glacier using a moving boundary condition to compute the boundary of the glacier that is in contact with the atmosphere. This characterization gives rise to a free boundary problem governed by a non-linear partial differential equation.

On the other hand, we can neglect other internal energy forms apart from the thermal energy so that the temperature distribution in a longitudinal section is determined by a balance between the mechanisms of conduction, convection and reaction, also involving different constitutive laws (Glen and Arrhenius). Moreover, the horizontal heat diffusion is omitted, due those gradients in this direction are very small compared with the vertical gradients of temperature, as illustrated by the shallow ice scaling.

The coupled problem posed in Chapter 2, is the basis for the next chapters in the memory.

In Chapter 3 we propose an isothermal approximation to the profile problem described in Chapter 2 and so we uncouple this profile problem from the temperature and velocity problems. Moreover we develop a set of numerical techniques for the simulation of the profile evolution included in the framework of isothermal shallow ice approximation models. The different mathematical formulations are posed in terms of a highly nonlinear parabolic equation. A first nonlinearity comes from the free boundary problem associated to the unknown basal extent of the glacier region. This feature is treated by a fixed domain complementarity formulation which is numerically solved by a duality method. The formulation in terms of a new obstacle problem associated to a highly nonlinear convection-diffusion equation is one main novelty. The nonlinear diffusive term is explicitly treated in the time marching scheme. A convection dominated problem arises so that a characteristics scheme is proposed for the time discretization (see Pironneau and co-workers [2, 71] for example), while piecewise linear finite elements are used for spatial discretization. The presence of infinite slopes in polar regimes motivates an alternative formulation based on a prescribed flux boundary condition at the head of the glacier instead a homogeneous Dirichlet one. At the end of the Chapter 3, several numerical examples illustrate the performance of the proposed methods. Some of these examples are analytical, so we build artificial exact solutions to check the validity of the proposed method. The artificial solutions are built similarly to those ones proposed by Bueler et al. [11] to ice sheets. Moreover, under certain boundary conditions we can compute the position of the glacier front analytically, so we also propose several examples to check if the position of the glacier front in the simulation results coincide with the analytical value.

In Chapter 4 the shallow ice thermocoupled model for the complex nonlinear polythermal glacier dynamics is proposed and solved by means of efficient numerical methods. A novelty of this chapter is the obstacle problem formulation associated to a nonlinear integro-differential equation for the glacier profile. The coefficients of this equation depend in a non local way on temperature in order to account properly for the non-isothermal setting. This formulation is motivated by the free boundary feature and the influence of the temperature on the profile, because it is a fully non-isothermal model. Concerning the temperature equation, a dynamically prescribed surface temperature that decreases with altitude is posed. As the profile and the temperature equations are fully coupled, a nonlinear PDE system governing the upper glacier profile, the velocity field, and the temperature is stated. In addition to the numerical difficulties associated to the new profile equation, several techniques have been considered for the numerical solution of the temperature, velocity and basal magnitudes: enthalpy formulations, upwind methods for time discretization, 2D finite element discretizations, duality methods associated to monotone operator, Newton methods for nonlinear problems, and numerical quadrature formulae for velocity computation. For solving the global coupled system of nonlinear PDEs a fixed point iteration which sequentially treats each subproblem has been developed. At the end of Chapter 4 several examples are proposed. Thus, illustrative examples concerning the case of cold, polythermal and temperate-based ice have been considered. Moreover, as in Chapter 3, we consider two possible boundary conditions at the head of the glacier: a prescribed a flux or an imposed profile value. Also as in Chapter 3, the computed numerical results show that flux imposed boundary results are more realistic. Moreover, in the case of flux imposed boundary condition, the same technique developed in Chapter 3 allows to obtain the exact position of the free boundary. This value has been very accurately verified by the computations.

In Chapter 5 we propose other two-dimensional *shallow ice approximation* model for a valley glacier in order to reconsider the question of whether thermal runaway could be a viable mechanism for the onset of creep instability in surging glaciers. We do this by providing an approximate solution for the temperature field based on the idea that shear is concentrated at the glacier bed. With this assumption, we show that a closed form evolution equation for the glacier profile exists in this case. While this is well-known for iso-viscous flows, it has not previously been derived for variable viscosity flows. During the process of deriving these equations, we show that thermal runaway does not occur. A particular revelation of this chapter has been the unexpected inadequacy of geothermal heat. If it is computed using normal values of geothermal heat flux, we find that it is so small that basal ice will never reach the melting point. In reality, entirely cold-based glaciers are something of a rarity, and we consider this to be due to the overwhelming importance of latent heat release by buried surface meltwater and rainwater. In the absence of such enhanced basal heating, glaciers would remain frozen at their base.

In Appendix A, some definitions and classical results related to maximal monotone operators are included. Moreover, we develop some calculus to obtain the Yosida approximations of several maximal monotone operators appearing in the different models. Appendix B is devoted to some features related to computer implementation. Thus, some details about the specific software toolbox GLANUSIT and the parallelization of numerical algorithms are described.

Finally, we point out that a summary of different parts of Chapter 3 are contained in the works [14], [17] and [19]. A first approach to the results obtained in Chapter 4 is contained in references [17] and [18]. Chapter 5 has been published in *Proceedings of the Royal Society A* (see [40]). The details of the GLANUSIT software toolbox version for ice sheets has been published in *Advances in Engineering Software* (see [15]), and some results on the parallel version for ice sheets simulation codes are included in *Proceedings in Applied Mathematics and Mechanics* (see [16]).

Chapter 2

Shallow Ice Glacier Model

2.1 Introduction

Glaciers and ice sheets have been subject of interest over the last few decades due to their importance in the study of climate change. Glaciers can be thought as large and slow moving rivers of ice. They drain areas in which snow accumulates, much as rivers drain catchment areas where rain falls. Glaciers also flow in the same basic way that rivers do. Although glacier ice is solid, it can deform by the slow creep of dislocations within the lattice of ice crystals which form the fabric of ice. Thus, glacier ice behaves like a viscous material with a very large viscosity, about 10^{16} times the water viscosity. As a consequence of its enormous viscosity, glaciers move slowly – a typical velocity would be in the range 10–100 my^{-1}. More awesome are the glacier dimensions, typical values are depths of hundreds of metres, widths of kilometres and lengths of tens of kilometres. Thus glaciers can have an important effect on the human environment in their vicinity. They are also indirect monitors of climate; for example, many lithographs of Swiss glaciers show that they have been receding since the nineteenth century, a phenomenon thought to be due to the termination of the *Little Ice Age* which lasted from about 1500 to about 1900. Glaciers can be formed in places of high elevation, such as the Himalayas or the Alps, as well as in polar regions , such as Alaska or Antarctica. For example, the Bering Glacier is one of the longest with 200 km in length.

In this chapter we study the motion of a valley glacier using the *shallow ice approximation* (*SIA*). The *SIA* keeps in mind the orders of magnitude of the real glaciers with the purpose of neglecting some terms in the original mass, momentum and energy conservation equations of the original continuum mechanics model (see Hutter [54], among others). Previously to obtain the *SIA* model, we carry out a shallow ice scaling of the continuum mechanics model equations that gives rise to introduce a small parameter $\varepsilon = d_2/d_1$ in the scaled model, where d_1 and d_2 are length and depth orders of magnitude, respectively. After this shallow ice scaling, we neglect the terms of $O(\varepsilon^2)$ and obtain our *SIA* model. This fact restricts the limits of the approach to ice masses geometries for which that ratio of characteristic thickness to characteristic length is small compared to 1. Traditionally, mountain glaciers can indeed develop typical thickness of the same order as their length. However, some mountain glaciers have intermediate geometries with an overall aspect ratio still allowing for a correct expansion series to have any meaning. For example, the Glacier Saint Sorlin, in the French Alps, whose geometrical characteristics give rise to an $\varepsilon = 5 \times 10^{-2}$ [61]. Moreover, in Le Meur et al. [61] it is concluded that the applicability of *SIA* is also related to the presence of small bedrock slopes and not only to small enough aspect ratio. The authors arrive to this conclusion by comparing the obtained results for *SIA* and full Stokes models under very simple basal conditions and no sliding. The use of *SIA* presents the huge advantage of being very efficient in terms of computing resources concerning memory and CPU time consumptions. In order to simplify the glacier model, a two dimensional ice flux is commonly assumed so that the same profile is considered for the different longitudinal sections.

This chapter is organized as follows: Section 2.2 is dedicated to the glacier profile model in real variables. The shallow ice scaled model is proposed in Section 2.3 and the shallow ice approximation of the scaled model is described in Section 2.4. To get a more detailed information about the ice constitutive relations and about the glaciers modelling see Hutter [54] and Paterson [69], for example.

2.2 Initial problem

In this section we propose the equations in real variables that model the behaviour of a glacier situated over a valley. For this purpose, first we consider that glaciers flow is nearly two dimensional and we restrict ourselves to the glaciers where the profiles are the same for different longitudinal sections [33]. More precisely, by neglecting the width effect, we consider a section in the longitudinal and depth directions, the geometry of which is shown in Figure 2.1. Thus, we take the X-axis in the direction of the valley downslope and the Z-axis upwards and transverse to the mean valley slope. The angle between the valley axis and the horizontal line is denoted by δ. Moreover, the bedrock geometry below the glacier is characterized by the function b^*, and η^* is the unknown function defining the glacier profile in real coordinates. Therefore,

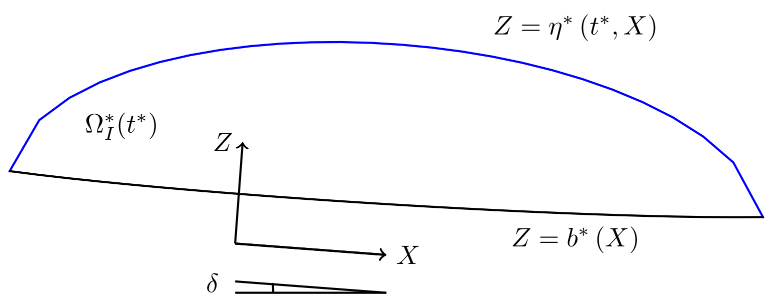

Figure 2.1: Typical profile of a valley glacier.

the ice region at time t^* is denoted by $\Omega_I^* (t^*) = \{(X, Z) \ / \ b^* (X) \leq Z \leq \eta^* (X, t^*)\}$. Moreover, if t_A^* is the final time, we denote $\Omega_I^* = \bigcup_{t^* \in [0, t_A^*]} (\{t^*\} \times \Omega_I^* (t^*))$.

The basic equations for the ice displacement are those ones of mass and momentum conservation, which for an incompressible ice flow (neglecting inertial terms) are [49]:

$$\nabla \cdot \vec{U} = 0 \tag{2.1}$$

$$\nabla \cdot \mathbf{T} = -\rho \vec{g}, \tag{2.2}$$

where $\vec{U} = (U, V)$ denotes the velocity field, $\mathbf{T}$ is the Cauchy stress tensor, ρ is the ice density and $\vec{g}$ is the acceleration due to gravity. Moreover, the stress tensor can be decomposed into an isotropic and a deviatoric part, namely:

$$\mathbf{T} = -P\mathbf{I} + 2\nu\mathbf{D}$$

where P is the ice pressure, ν is the effective viscosity and $\mathbf{D}$ denotes the stress rate tensor:

$$\mathbf{D} = \frac{1}{2}\left(\nabla\vec{U} + \nabla\vec{U}^T\right). \tag{2.3}$$

Then, field equations (2.1) and (2.2)can be equivalently written in the form:

$$0 = U_X + V_Z \tag{2.4}$$

$$0 = -P_X + \tau^*_{11X} + \tau^*_{12Z} + \rho\, g\, \sin\delta \tag{2.5}$$

$$0 = -P_Y + \tau^*_{12X} + \tau^*_{22Z} + \rho\, g\, \cos\delta, \tag{2.6}$$

where τ^*_{11}, τ^*_{22} and τ^*_{12} are longitudinal and transversal stresses in the XZ-plane, respectively, and the subscripts X and Z denote the partial derivatives with respect to X and Z, respectively.

Other forms of internal energy different from heat are neglected so that the temperature distribution in polar ice is governed by a balance among the mechanisms of reaction, conduction and convection. Thus, the temperature verifies the energy equation:

$$\rho c_p \dot{\Theta} = -\nabla \cdot \vec{q} + Q \tag{2.7}$$

where c_p is the specific head, Θ denotes the temperature, $\vec{q}$ is the energy flux and Q is the internal heat source. Notice that $\dot{\Theta}$ denotes the material derivative of Θ respect to time, t^*, i.e.:

$$\dot{\Theta} = \frac{\partial\Theta}{\partial t^*} + \vec{U}\cdot\nabla\Theta.$$

More precisely, the energy heat flux is given by:

$$\vec{q} = -k\nabla\Theta, \tag{2.8}$$

where k is the thermal conductivity, and the internal heat source, Q, is associated to viscose dissipation and takes the form:

$$Q = \tau^*_{ij} e^*_{ij} \tag{2.9}$$

where e^*_{ij} denotes the components of the strain tensor of the material (2.3) that are defined by:

$$e^*_{11} = \frac{\partial U}{\partial X}, \qquad e^*_{12} = \frac{1}{2}\left(\frac{\partial U}{\partial Z} + \frac{\partial V}{\partial X}\right) = e^*_{21}, \qquad e^*_{22} = \frac{\partial V}{\partial Z}. \tag{2.10}$$

The joint consideration of (2.7), (2.8) and (2.9) leads to the following equivalent expression for the energy equation:

$$\rho\, c_p \left(\frac{\partial \Theta}{\partial t^*} + \vec{U} \cdot \nabla \Theta\right) = k\, \nabla^2 \Theta + \tau^*_{ij}\, e^*_{ij}, \tag{2.11}$$

In the case of an isotropic ($\tau^*_{ij} = \tau^*_{ji}$, $e^*_{ij} = e^*_{ji}$), incompressible ($\tau^*_{11} + \tau^*_{22} = e^*_{11} + e^*_{22} = 0$) and viscous material, a classical model represents the deformation rate in the fluid due to the efforts through the second invariants of the stress and strain tensors, respectively. These invariants are defined as:

$$2\,(e^*)^2 = e^*_{ij}\, e^*_{ij}, \qquad 2\,(\tau^*)^2 = \tau^*_{ij}\, \tau^*_{ij}. \tag{2.12}$$

Notice that e^* and τ^* represent the effective strain and stress rates, respectively. Moreover, the stress and strain rates are related by the effective viscosity $\bar{\epsilon}$ as follows:

$$\tau^*_{ij} = 2\, \bar{\epsilon}\, e^*_{ij}. \tag{2.13}$$

The most common choice of nonlinear rheology flow law for glaciers links again the stress and strain tensors through Glen's law $Gl\,(\tau^*)$ (see Glen [43]) and Arrhenius type function $A^*\,(\Theta)$ as indicates the following expression:

$$e^*_{ij} = A^*\,(\Theta)\; Gl^*\,(\tau^*)\; \tau^*_{ij}/\tau^*. \tag{2.14}$$

Moreover, the definitions of the Glen's law and the Arrehnius function in this case are:

$$Gl^*\,(\tau^*) = (\tau^*)^n\,, \tag{2.15}$$

$$A^*\,(\Theta) = A^*_0\, \exp\left(-Q/R\,\Theta\right), \tag{2.16}$$

where n is the Glen's law exponent (typically, $n = 3$), A^*_0 is a constant depending on the material, Q is the activation energy and R is the Boltzmann's universal constant.

Notice that the set of equations (2.14)–(2.16) can be summarized in the following non Newtonian law for the viscosity:

$$\nu = \frac{1}{2} A^{-\frac{1}{n}} \left(\frac{1}{2} \mathrm{tr} \left(\mathbf{D} \cdot \mathbf{D} \right) \right)^{\frac{1-n}{2n}} \tag{2.17}$$

Although expression (2.16) is classical, its validity at temperatures between $263K$ and $273K$ has been questioned. In this rank of temperatures, some authors have developed more appropriate variants which are based on experimental values. There is a detailed study of this expression in Hutter [54], where there are precise proposals by Smith and Morland [74].

In brief, the equations that model the behaviour of ice in cold region are:

$$\begin{aligned} U_X + V_Z &= 0 && (2.18) \\ 0 &= -P_X + \tau^*_{11X} + \tau^*_{12Z} + \rho\, g\, \sin\delta && (2.19) \\ 0 &= -P_Y + \tau^*_{12X} + \tau^*_{22Z} + \rho\, g\, \cos\delta && (2.20) \\ \rho\, c_p \left(\frac{\partial \Theta}{\partial t^*} + \vec{U} \cdot \nabla\Theta \right) &= k\, \nabla^2\Theta + \tau^*_{ij}\, e^*_{ij} && (2.21) \\ e^*_{ij} &= A^*\left(\Theta\right)\, Gl^*\left(\tau^*\right)\, \tau^*_{ij}/\tau^*. && (2.22) \end{aligned}$$

The model (2.18)–(2.22) is posed over a domain, Ω^*_I, the upper boundary of which is defined at each time t by the function $Z = \eta^*\left(t^*, X\right)$. This upper boundary is an unknown of the problem and its location depends on, among other factors, the accumulation-ablation function and the displacement of the glacier. In this sense it is a kinematic boundary and it is characterized by the equation:

$$\frac{\partial \eta^*}{\partial t^*} + U \frac{\partial \eta^*}{\partial X} - V = a^*, \tag{2.23}$$

where a^* is the real accumulation-ablation function and (2.23) indicates the net mass-balance of the glacier. Accumulation includes all processes by which material is added to the glacier. Material is normally added as snow which is slowly transformed to ice. Avalanches, rime formation and freezing of rain within snowpack are some other accumulation processes. Ablation includes all processes by which snow and ice are lost from the glacier: melting followed by run-off, evaporation, removal of snow by wind of the calving of icebergs are some examples. Melting followed by refreezing at another part of the glacier is not ablation because the glacier does not lose mass. Almost all the ablation takes place at the surface or, in the case of calving, at the terminus. Some glaciers may lose ice by melting at their bases but, unless the ice is floating, the amount is usually negligible compared with the surface ablation. In glaciers, accumulation normally takes place in the upstream region of the glacier and ablation normally takes place in the downstream region of the glacier. The deduction of the kinematic boundary equation (2.23) of this problem can be found in Hutter [54] or Fowler [33].

In order to solve the problem (2.18)–(2.22), we impose upper and lower boundary conditions in addition to the kinematic upper boundary (2.23). These conditions are detailed in next paragraphs.

Following previous works of Fowler and Schiavi, for example [39], we prescribe no tangential stress condition at the upper boundary $Z = \eta^*(t^*, X)$ as follows:

$$\mathbf{T}\vec{n} = 0$$

or equivalently:

$$0 = (-P + \tau_{11}^*)\,\eta_X^* - \tau_{12}^* \text{ at } Z = \eta^*(t^*, X)\,, \tag{2.24}$$

$$0 = \tau_{12}^*\,\eta_X^* + P - \tau_{22}^* \text{ at } Z = \eta^*(t^*, X)\,, \tag{2.25}$$

and we also assume a prescribed temperature at that upper boundary $Z = \eta^*(t^*, X)$:

$$\Theta(t^*, X, \eta^*(t^*, X)) = \Theta_A(t^*, X, \eta^*(t^*, X)) \qquad \text{at } Z = \eta^*(t^*, X)\,. \tag{2.26}$$

Before describing boundary conditions at the base of the glacier we point out that glaciers can be classified in terms of their thermal characteristics, although a continuum exists between the end members. We normally think of water as freezing at $0\,^\circ C$, but we may overlook the fact that once all the water in a space is frozen, the temperature of the resulting ice can be lowered below $0\,^{\circ}C$ as long as heat can be removed from it. Thus, the temperature of glaciers ice in specially cold climates can reach below $0\,^{\circ}C$ temperatures. We call such glaciers *polar glaciers*. More specifically, polar glaciers are those ones in which the temperature is below the melting temperature of ice everywhere, except possibly at the bed. Glaciers that are not polar are either *polythermal* or *temperate*. Polythermal glaciers, which are sometimes called *subpolar* glaciers, contain large volumes of ice that are cold, but also large volumes that are at the melting temperature. Most commonly, the cold ice is present as a surface layer, tens of meters in thickness, on the lower part of the glacier (the ablation area). Polythermal glaciers can be found mainly at high latitudes, e.g. in the Canadian Arctic, in Svalbard or in Scandinavia but also can be found at high altitudes in the European Alps and in China. In simplest terms, a temperate glacier is one that is at the melting temperature throughout except for a surface layer, about $15\,m$ thick, that is subject to seasonal variations in temperature. However, the melting temperature varies on many length scales in a glacier [54]. Harrison suggests a more rigorous definition of a temperate glacier [50]. He suggested that a glacier is considered as temperate if its heat capacity is greater than twice the heat capacity of pure ice. In other words, this is when the temperature and liquid content of the ice are such that only half of any energy put into the ice is used to warm the ice, while the other half is used to melt ice in places where the local melting temperature is depressed. This definition, while offering the benefit of rigor, is not easily applied in the field. Thus, this discussion serves to emphasize that the class of glaciers that we loosely refer to as temperate may include ice masses with a range of physical properties that are as wide, or wider than, polar glaciers.

This classification of glaciers depending on their temperature is relevant to impose the thermal conditions at the base of the glacier, $b^*(x)$. We can distinguish two different basal boundary conditions: one for the polar case and another for the polythermal one.

In the case of polar glaciers, basal temperature is under melting point at each point, so we impose as condition at the base of the glacier that heat flow balances geothermal heat:

$$k\,\nabla\Theta \cdot \vec{n^*} = G_b, \tag{2.27}$$

where $\vec{n^*} = (b^*_X, -1)$ is the normal vector pointing outwards the domain Ω^* and G_b is the geothermal heat and it is considered as a constant (a typical value for polar glaciers is $60\,m\,W\,m^{-2}$).

In the case of polythermal glaciers, there are some points at the basal boundary at melting point and some others are under melting point, but their position is unknown a priori so, we impose the following Signorini type condition as basal boundary condition:

$$\Theta \leq \Theta_m, \quad (\Theta - \Theta_m)\left(k\frac{\partial\Theta}{\partial\vec{n^*}} - G_b\right) = 0, \quad 0 \leq k\frac{\partial\Theta}{\partial\vec{n^*}} \leq G_b \quad \text{at } Z = b^*(x)\,, \tag{2.28}$$

where Θ_m denotes the ice melting temperature.

The thermal boundary condition at the base is completed with a kinematic boundary condition. Thus, either a sliding velocity at the base, U_b is prescribed or a sliding law relation between basal shear stress, τ^*_b, and U_b is considered. In the isothermal problem treated in Chapter 3 we assume that the basal velocity is given while in the fully coupled model posed in Chapter 4 a sliding law is considered. Notice that in both cases, when no-slip conditions hold (such as, for example, in the case of cold-based regions) then $U_b = 0$.

In the framework of non isothermal lubrication problems with Newtonian and incompressible fluids a rigorous mathematical analysis for Tresca free boundary conditions has been carried out in Boukrouche–Saide [8]. Also the corresponding thin film approximation with Reynolds-like models is obtained in Boukrouche–Saide [9].

A lubrication phenomenon involves the temperate and polythermal regions, but following the same approach in the glacier framework is far more complex due to non Newtonian and phase change features among others.

2.3 Shallow ice scaling

The initial model and boundary conditions posed in Section 2.2 are written in real variables, so they do not consider the specific temporal and spacial scales. Depth in glaciers is small compared to their width or length, this difference in magnitude orders in the real domain of glaciers must allow us to neglect some terms in the model in order to obtain some simplifications in the original equations. This is one of the basic ideas in the *Shallow Ice Scaling* proposed mainly by Fowler and Larson [36] and detailed in the books of Hutter [54] and Fowler [33], for example. We develop this idea in this section and the next one.

New unknowns and magnitude order relations

Previously to deduce the *SIA* model, we introduce the following set of new variables and unknowns to establish the dimensionless equations:

$$X = d_1\, x, \quad Z = d_2\, z, \tag{2.29}$$

$$\tau^*_{12} = [\tau^*]\, \tau_{12}, \quad \tau^*_{11} = \varepsilon\, [\tau^*]\, \tau_{11}, \quad \tau^*_{22} = \varepsilon\, [\tau^*]\, \tau_{22}, \tag{2.30}$$

$$\Theta = \Theta_m + (\Delta\Theta)\; T, \quad A^* = [A^*]\, A, \quad Gl^* = [Gl^*]\, Gl, \tag{2.31}$$

$$\eta^* = d_2\, \eta, \quad U = [U]\, u, \quad V = \varepsilon\, [U]\, v, \tag{2.32}$$

$$P - P_a - \rho\, g\, \cos\delta\, (\eta^* - Z) = \varepsilon\, [\tau^*]\, p, \quad t^* = \frac{d_1}{[U]}\, t, \tag{2.33}$$

where d_1 and d_2 are the orders of magnitude for length and depth, respectively, and

$$\varepsilon = d_2/d_1 \tag{2.34}$$

is the aspect ratio for which we anticipate $\varepsilon \ll 1$. Moreover, P_a is the atmospheric pressure, magnitude orders $[\tau^*]$, $[U]$, $[A^*]$ and $[Gl^*]$ correspond to stress, horizontal velocity, Arrhenius term and Glen's law, respectively, and are used to define the different scaled functions. At last, considering that the melting point is $\Theta_m = 273\, K$ and maximum ice temperature prescribed on surface is $\Theta_A = 253\, K$, the temperature gap is $\Delta\Theta = 20\,K$ which motivates the definition of the dimensionless temperature T.

The choice of $[A^*]$ and $[Gl^*]$ is done so that the dimensionless functions A and Gl are $\mathcal{O}\,(1)$. Moreover, we get the following equalities as a result of the Glen's and Arrhenius's expressions, respectively:

$$[Gl^*] = [\tau^*]^n\,, \qquad [A^*] = A_0^* \mathrm{e}^{-\frac{Q}{R\,\Theta_m}}. \tag{2.35}$$

We choose the accumulation-ablation ratio $[a^*]$ via $[a^*] = \varepsilon\,[U]$, because it balances the vertical velocity with the accumulation-ablation rate. Besides, we choose $[\tau^*] = \rho g d_2 \sin\delta$, and define

$$\mu = \varepsilon\,\cot\delta. \tag{2.36}$$

On the other hand, the choice of d_2 and $[\tau^*]$ has to be determined self-consistently. The relation for choosing d_2 is determined by a balance in the flow law. So, if the viscosity scale is $[\bar{\epsilon}^*]$, then we choose

$$[\tau^*] = [\bar{\epsilon}^*]\,[U]\,/d_2. \tag{2.37}$$

With this relation and the Glen's law, we obtain the value of $[\bar{\epsilon}^*] = \frac{1}{2[A^*][\tau^*]^{n-1}}$, and we set the value of d_2:

$$d_2 = \left[\frac{[a^*]\,d_1}{2\,[A^*]\,(\rho\,g\,\sin\delta)^n}\right]^{\frac{1}{n+2}}, \tag{2.38}$$

which leads (with sensible choices of $[A^*]$, d_1, $[a^*]$ and n) to values of d_2 comparable to those ones experimentally observed ($d_2 \sim 100$ m).

Now, we introduce the changes of variables proposed in the previous paragraphs, (2.29)–(2.33), in the set of original equations (2.18)–(2.22) to obtain our shallow ice scaled model.

Shallow ice scaling in mass and momentum equations

To obtain the shallow ice scaling equation of the mass conservation law, we write equation (2.18) in the new variables:

$$0 = U_X + V_Z = \frac{[U]\,u_x}{d_1} + \frac{[U]\,\varepsilon\,v_z}{d_2} = \frac{[U]}{d_1}\,(u_x + v_z)\,,$$

so we can deduce that:

$$u_x + v_z = 0. \tag{2.39}$$

On the other hand, to obtain the shallow ice scaling equation for the momentum conservation, first we take derivatives with respect to X and with respect to Z in $(2.33)_1$, thus obtaining:

$$P_X = \frac{\varepsilon}{d_1}\,[\tau^*]\,p_x + \rho\,g\,\frac{d_2}{d_1}\,\cos\delta\,\eta_x, \qquad P_Z = -\rho\,g\,\cos\delta + \varepsilon\,\rho\,g\,p_z\,\sin\delta, \tag{2.40}$$

Next, we take derivatives with respect to X and Z in (2.30):

$$\tau^*_{11X} = \varepsilon\,[\tau^*]\,\frac{\tau_{11x}}{d_1}, \quad \tau^*_{12Z} = [\tau^*]\,\frac{\tau_{12z}}{d_2}, \quad \tau^*_{12X} = [\tau^*]\,\frac{\tau_{12x}}{d_1}, \quad \tau^*_{22Z} = \varepsilon\,[\tau^*]\,\frac{\tau_{22z}}{d_2}, \tag{2.41}$$

where $[\tau^*] = \rho\,g\,d_2\,\sin\delta$. So, we obtain the following shallow ice scaling equations of the momentum conservation law from (2.19)–(2.20):

$$\tau_{12z} = \varepsilon^2\,(p_x - \tau_{11x}) + \mu\,\eta_x - 1, \tag{2.42}$$

$$p_z = \tau_{12x} + \tau_{22z}. \tag{2.43}$$

Shallow ice scaling in temperature equation

In order to write the equation (2.21) in the new variables we apply (2.22), (2.29), (2.31) and (2.33). First, we use the chain rule and the expressions $(2.31)_1$ and $(2.33)_2$ to write the material derivative of the temperature, $\frac{D\Theta}{Dt^*}$, as follows:

$$\frac{D\Theta}{Dt^*} = (\Delta\Theta)\,\frac{[U]}{d_1}\frac{DT}{Dt},$$

and we use again the chain rule and the expressions $(2.31)_1$ and (2.29) to write the value of $\nabla^2\Theta$ in the new set of variables and unknowns:

$$\nabla^2\Theta = \frac{\partial^2\Theta}{\partial X^2} + \frac{\partial^2\Theta}{\partial Z^2} = \frac{\partial}{\partial X}\left((\Delta\Theta)\frac{\partial T}{\partial x}\frac{\partial x}{\partial X}\right) + \frac{\partial}{\partial Z}\left((\Delta\Theta)\frac{\partial T}{\partial z}\frac{\partial z}{\partial Z}\right) =$$
$$= \frac{\Delta\Theta}{d_1}\frac{\partial}{\partial X}\frac{\partial T}{\partial x} + \frac{\Delta\Theta}{d_2}\frac{\partial}{\partial Z}\frac{\partial T}{\partial z} = \frac{\Delta\Theta}{d_1^2}\frac{\partial^2 T}{\partial x^2} + \frac{\Delta\Theta}{d_2^2}\frac{\partial^2 T}{\partial z^2}.$$

So, we obtain the following expressions:

$$\frac{D\Theta}{Dt^*} = (\Delta\Theta)\frac{[U]}{d_1}\frac{DT}{Dt}, \tag{2.44}$$

$$\nabla^2\Theta = \frac{\Delta\Theta}{d_1^2}\frac{\partial^2 T}{\partial x^2} + \frac{\Delta\Theta}{d_2^2}\frac{\partial^2 T}{\partial z^2}. \tag{2.45}$$

On the other hand, to rewrite expression $\tau_{ij}^*\, e_{ij}^*$, we multiply by τ_{ij}^* the equation (2.14):

$$\tau_{ij}^*\, e_{ij}^* = \tau_{ij}^*\, A^*\left(\Theta\right)\, Gl^*\left(\tau^*\right)\, \tau_{ij}^*/\tau^*. \tag{2.46}$$

Moreover, we employ the definition of the Glen's law (2.15), its dimensionless expression (2.31) and the choice of $[Gl^*]$ in (2.35) to get a Glen's law function of $\mathcal{O}\left(1\right)$. So, we can relate dimensional and dimensionless Glen's law using the following expression:

$$Gl^*\left(\tau^*\right) = \left[Gl^*\right] Gl\left(\tau\right) = \left[Gl^*\right]\tau^n = \left[\tau^*\right]^n\tau^n. \tag{2.47}$$

In order to write $\tau_{ij}^*\tau_{ij}^*/\tau^*$ in the new set of variables and unknowns, we use the definition of stress invariants (2.12) and the expression which relates dimensional and dimensionless stress tensor:

$$\tau_{ij}^*\tau_{ij}^*/\tau^* = 2\left(\tau^*\right)^2/\tau^* = 2\tau^* = 2\left[\tau^*\right]\tau, \tag{2.48}$$

and now we include the expression (2.47) and (2.48) in (2.46) to obtain:

$$\tau_{ij}^* e_{ij}^* = 2\left[A^*\right] A\left(T\right)\left[\tau^*\right]^{n+1}\tau^{n+1}. \tag{2.49}$$

Now, we introduce the expressions (2.44), (2.45) and (2.49) in (2.21) to get:

$$\frac{DT}{Dt} = \frac{k\, d_1}{\rho\, c_p\, [U]}\left(\frac{T_{xx}}{d_1^2} + \frac{T_{zz}}{d_2^2}\right) + \frac{2\,\left[A^*\right]\,\left[\tau^*\right]^{n+1}\, d_1}{\rho\, c_p\,\left(\Delta\Theta\right)\,[U]} A\left(T\right)\tau^{n+1}, \tag{2.50}$$

and we can simplify this equation by using the relation between accumulation-ablation order and horizontal velocity order ($[a^*] = \varepsilon\;[U^*]$), the equation (2.38) and the selection of $[\tau^*]$ order ($[\tau^*] = \rho\, g\, d_2\, \sin\delta$). So, the equation (2.50) is written as follows:

$$\frac{DT}{Dt} = \frac{k\, d_1}{\rho\, c_p\;[U]}\left(\frac{T_{xx}}{d_1^2} + \frac{T_{zz}}{d_2^2}\right) + \frac{\left[\tau^*\right]\; d_1}{\rho\, c_p\;\left(\Delta\Theta\right)\; d_2}\, A\left(T\right)\;\tau^{n+1}. \tag{2.51}$$

Besides, we define the following parameters to simplify the previous expression:

$$\kappa = \frac{k}{\rho\, c_p}, \tag{2.52}$$

$$\beta = \frac{d_1\,\kappa}{d_2^2\,[U]} = \frac{\kappa}{d_2\,[a^*]}, \tag{2.53}$$

$$\alpha = \frac{[\tau^*]\,d_1}{\rho\, c_p\,\Delta\Theta\, d_2} = \frac{[\tau^*]}{\rho\, c_p\,\Delta\Theta\,\varepsilon} = \frac{g\,d_1\,\sin\delta}{c_p\,(\Delta\Theta)}, \tag{2.54}$$

where κ is the thermal diffusivity, β is the thermal diffusion coefficient and α is a dimensionless parameter. Next, we introduce them in the expression (2.50) to get:

$$\frac{DT}{Dt} = d_2^2\,\beta\left(\frac{T_{xx}}{d_1^2} + \frac{T_{zz}}{d_2^2}\right) + \alpha\,A\,(T)\;\tau^{n+1}.$$

Therefore, the shallow ice scaling of energy equation (2.21) is the following:

$$\frac{DT}{Dt} = \beta\left(\varepsilon^2\,T_{xx} + T_{zz}\right) + \alpha\,\tau\,Gl\,(\tau)\;A\,(T)\,. \tag{2.55}$$

Shallow ice scaling of the rheology flow law

In order to obtain the shallow ice scaled expression related to the rheology flow law (2.22), first we write the shallow ice scaling for the invariant τ^*:

$$\begin{aligned} 2\,(\tau^*)^2 = \tau^*_{ij}\tau^*_{ij} &= \left((\tau^*_{11})^2 + (\tau^*_{22})^2 + 2\tau^*_{12}\tau^*_{12}\right) = \\ &= \left([\tau^*]^2\;\varepsilon^2\,\tau_{11}^2 + [\tau^*]^2\;\varepsilon^2\,\tau_{22}^2 + 2\,[\tau^*]^2\;\tau_{12}^2\right) = \\ &= [\tau^*]^2\left(\varepsilon^2\,\tau_{11}^2 + \varepsilon^2\,\tau_{22}^2 + 2\,\varepsilon^2\,\tau_{12}^2\right) = 2\;[\tau^*]^2\;\tau^2, \end{aligned}$$

where

$$2\,\tau^2 = 2\,\tau_{12}^2 + \varepsilon^2\;\left(\tau_{11}^2 + \tau_{22}^2\right). \tag{2.56}$$

On the other hand, we write the shallow ice scaled expressions for strain using (2.10), the expressions (2.29) and (2.32):

$$e^*_{12} = \frac{1}{2}\left([U]\,\frac{\partial u}{\partial z}\frac{\partial z}{\partial Z} + \varepsilon\;[U]\,\frac{\partial v}{\partial x}\frac{\partial x}{\partial X}\right) = \frac{[U]}{2}\;\left(\frac{u_z}{d_2} + \varepsilon\frac{v_x}{d_1}\right), \tag{2.57}$$

$$e^*_{11} = [U]\,\frac{\partial u}{\partial x}\frac{\partial x}{\partial X} = \frac{[U]}{d_1}u_x, \tag{2.58}$$

$$e^*_{22} = \varepsilon\;[U]\,\frac{\partial v}{\partial z}\frac{\partial z}{\partial Z} = \frac{\varepsilon\;[U]}{d_2}v_z. \tag{2.59}$$

Besides we write equation (2.22) in new variables as follows:

$$
\begin{aligned}
e_{12}^{*} &= [A^{*}]\ A\,(T)\ [Gl^{*}]\ Gl\,(\tau)\ \tau_{12}/\tau, && (2.60)\\
e_{11}^{*} &= [A^{*}]\ A\,(T)\ [Gl^{*}]\ Gl\,(\tau)\ \varepsilon\,\tau_{11}/\tau, && (2.61)\\
e_{22}^{*} &= [A^{*}]\ A\,(T)\ [Gl^{*}]\ Gl\,(\tau)\ \varepsilon\,\tau_{22}/\tau. && (2.62)
\end{aligned}
$$

Now, identifying expressions (2.60)–(2.62) with their respective (2.57)–(2.59), we get:

$$
\begin{aligned}
\frac{2\,d_2\ [A^{*}]\ [Gl^{*}]}{[U]}\,A\,(T)\ Gl\,(\tau)\ \tau_{12}/\tau &= u_z + \varepsilon^2\,v_x, && (2.63)\\
\frac{2\,d_2\ [A^{*}]\ [Gl^{*}]}{[U]}\,A\,(T)\ Gl\,(\tau)\ \varepsilon\,\tau_{11}/\tau &= 2\,\varepsilon\,u_x, && (2.64)\\
\frac{2\,d_2\ [A^{*}]\ [Gl^{*}]}{[U]}\,A\,(T)\ Gl\,(\tau)\ \varepsilon\,\tau_{22}/\tau &= 2\,\varepsilon\,v_z. && (2.65)
\end{aligned}
$$

Moreover, if we keep in mind the selection of $[\bar{\epsilon}^{*}]$ $\left([\bar{\epsilon}^{*}] = \frac{1}{2\,[A^{*}]\,[\tau^{*}]^{n-1}}\right)$ and the relation between $[\tau^{*}]$ and $[\bar{\epsilon}^{*}]$, given by (2.37), we obtain:

$$
[\tau^{*}]^{n}\ [A^{*}] = [Gl^{*}]\ [A^{*}] = \frac{[U]}{2\,d_2}. \qquad (2.66)
$$

So, we finally obtain the shallow ice scaled equations of the rheology law:

$$
\begin{aligned}
A\,(T)\ Gl\,(\tau)\ \tau_{12}/\tau &= u_z + \varepsilon^2\,v_x, && (2.67)\\
A\,(T)\ Gl\,(\tau)\ \tau_{11}/\tau &= 2\,u_x, && (2.68)\\
A\,(T)\ Gl\,(\tau)\ \tau_{22}/\tau &= 2\,v_z. && (2.69)
\end{aligned}
$$

Shallow ice scaled model

Now, we can write the scaled model coming from equations (2.18)–(2.22) as:

$$\begin{aligned}
u_x + v_z &= 0 && (2.70)\\
0 &= -\mu\, \eta_x + \tau_{12z} + 1 - \varepsilon^2 \left(p_x - \tau_{11x}\right) && (2.71)\\
0 &= -p_z + \tau_{12z} + \tau_{22z} && (2.72)\\
\frac{DT}{Dt} &= \alpha\, \tau\, Gl\,(\tau)\; A\,(T) + \beta\, \left(\varepsilon^2\, T_{xx} + T_{zz}\right) && (2.73)\\
u_z + \varepsilon^2\, v_x &= A\,(T)\; Gl\,(\tau)\; \tau_{12}/\tau && (2.74)\\
2\, u_x &= A\,(T)\; Gl\,(\tau)\; \tau_{11}/\tau && (2.75)\\
2\, v_z &= A\,(T)\; Gl\,(\tau)\; \tau_{22}/\tau && (2.76)\\
2\, \tau^2 &= 2\, \tau_{12}^2 + \varepsilon^2\, \left(\tau_{11}^2 + \tau_{22}^2\right) && (2.77)
\end{aligned}$$

Next, we devote the rest of this section to apply shallow ice scaling to the boundary conditions and to complete the model (2.70)–(2.77).

Shallow ice scaling of the upper boundary conditions

First, by using the chain rule, the kinematic boundary condition (2.23) is transformed into:

$$d_2 \frac{\partial \eta}{\partial t} \frac{\partial t}{\partial t^*} + [U]\; u\, d_2 \frac{\partial \eta}{\partial x} \frac{\partial x}{\partial X} - \varepsilon\; [U]\; v = [U]\, \frac{d_2}{d_1} \frac{\partial \eta}{\partial t} + [U]\, \frac{d_2}{d_1} u \frac{\partial \eta}{\partial x} - \varepsilon\, [U]\, v = \varepsilon\, [U]\; a.$$

Thus, the shallow ice scaled kinematic boundary condition (2.23) leads to:

$$\frac{\partial \eta}{\partial t} + u \frac{\partial \eta}{\partial x} - v = a \quad\quad at \quad\quad z = \eta\,(t, x)\,. \qquad (2.78)$$

In order to write the previous equation in terms of flow conservation, we introduce the horizontal flux:

$$Q = \int_{b(x)}^{\eta(x,t)} (u, v)\; dz,$$

so that:

$$\begin{aligned}
\nabla\cdot Q &= \frac{\partial}{\partial x}\int_{b(x)}^{\eta(t,x)} u\left(x,z\right)\,dz+\frac{\partial}{\partial z}\int_{b(x)}^{\eta(t,x)} v\left(x,s\right)\,ds=\\
&= \int_{b(x)}^{\eta(t,x)} u_x\left(x,z\right)\,dz+u\left(x,\eta\left(t,x\right)\right)\frac{\partial\eta\left(t,x\right)}{\partial x}-u\left(x,b\left(x\right)\right)\frac{\partial b\left(x\right)}{\partial x}=\\
&= u\left(x,\eta\left(t,x\right)\right)\frac{\partial\eta\left(t,x\right)}{\partial x}-u\left(x,b\left(x\right)\right)\frac{\partial b\left(x\right)}{\partial x}-\int_{b(x)}^{\eta(t,x)} v_z\left(x,z\right)\,dz=\\
&= u\left(x,\eta\left(t,x\right)\right)\frac{\partial\eta\left(t,x\right)}{\partial x}-u\left(x,b\left(x\right)\right)\frac{\partial b\left(x\right)}{\partial x}-v\left(x,\eta\left(t,x\right)\right)+v\left(x,b\left(x\right)\right)=\\
&= u\left(x,\eta\left(t,x\right)\right)\frac{\partial\eta\left(t,x\right)}{\partial x}-v\left(x,\eta\left(t,x\right)\right)-u\left(x,b\left(x\right)\right)\frac{\partial b\left(x\right)}{\partial x}+v\left(x,b\left(x\right)\right)=\\
&= u\left(x,\eta\left(t,x\right)\right)\frac{\partial\eta\left(t,x\right)}{\partial x}-v\left(x,\eta\left(t,x\right)\right).
\end{aligned}$$

Next, we write equation (2.78) as:

$$:\frac{\partial\eta}{\partial t}+\nabla\cdot Q=a,$$

or equivalently:

$$\frac{\partial\eta}{\partial t}+\frac{\partial}{\partial x}\int_b^\eta u\left(x,s\right)\,ds=a. \tag{2.79}$$

On the other hand, equations (2.24)–(2.25) give us the upper surface boundary conditions, and we use the relations (2.29), (2.30), (2.32) and (2.33) to get their corresponding shallow ice scaling ones, as follows:

$$\begin{aligned}
0 &= \left(-\varepsilon\,\left[\tau^*\right]\,p-\rho\,g\,\cos\delta\,d_2\left(\eta-z\right)+\varepsilon\,\left[\tau^*\right]\,\tau_{11}\right)\frac{d_2}{d_1}\eta_x-\left[\tau^*\right]\,\tau_{12},\\
0 &= \left[\tau^*\right]\,\tau_{12}\frac{d_2}{d_1}\eta_x+\varepsilon\,\left[\tau^*\right]\,p+\rho\,g\,\cos\delta\,d_2\left(\eta-z\right)-\varepsilon\,\left[\tau^*\right]\,\tau_{22}.
\end{aligned}$$

At the surface $z=\eta\left(t,x\right)$, the previous equations are analogous to the following ones:

$$\begin{aligned}
0 &= \left(-\varepsilon\,\left[\tau^*\right]\,p+\varepsilon\,\left[\tau^*\right]\,\tau_{11}\right)\varepsilon\,\eta_x-\left[\tau^*\right]\,\tau_{12},\\
0 &= \varepsilon\,\left[\tau^*\right]\,\tau_{12}\,\eta_x+\varepsilon\,\left[\tau^*\right]\,p-\varepsilon\,\left[\tau^*\right]\,\tau_{22},
\end{aligned}$$

or, equivalently:

$$\tau_{12}=\varepsilon^2\,\left(\tau_{11}-p\right)\eta_x \qquad \text{at } z=\eta\left(t,x\right), \tag{2.80}$$

$$\tau_{22}=\tau_{12}\,\eta_x+p \qquad \text{at } z=\eta\left(t,x\right). \tag{2.81}$$

Shallow ice scaling of the basal boundary conditions

Concerning the basal conditions, we need to distinguish two possible cases: the polar case and the polythermal one. In the polar case, first we apply the change of variable (2.31) for temperature and the chain rule to obtain:

$$k\left(\frac{\partial\Theta}{\partial X},\frac{\partial\Theta}{\partial Z}\right)(\varepsilon\, b_x,-1)=k\left(\frac{\Delta\Theta}{d_1}\frac{\partial T}{x},\frac{\Delta\Theta}{d_2}\frac{\partial\Theta}{\partial Z}\right)(\varepsilon\, b_x,-1)\,. \tag{2.82}$$

Next, we replace (2.82) in (2.27) to establish:

$$\varepsilon^2\, b_x\frac{\partial T}{\partial x}-\frac{\partial T}{\partial z}=g_b, \tag{2.83}$$

where g_b is the dimensionless geothermal heat flux given by:

$$g_b=\frac{G_b\, d_2}{k\,\Delta\Theta}. \tag{2.84}$$

Analogously, in the polythermal case, first we pose:

$$\frac{\partial\Theta}{\partial\vec{n^*}}=\frac{\Delta\Theta}{d_2}\frac{\partial T}{\partial\vec{n}},$$

and next, we replace this expression and (2.31) in the boundary condition (2.27). Finally, we get:

$$T\le 0,\quad T\left(\varepsilon^2 b_x\frac{\partial T}{\partial x}-\frac{\partial T}{\partial z}-g_b\right)=0,\quad 0\le\varepsilon^2 b_x\frac{\partial T}{\partial x}-\frac{\partial T}{\partial z}\le g_b. \tag{2.85}$$

2.4 Shallow Ice Approximation

In the shallow ice scaled model that has been described in Section 2.3, we will neglect $\mathcal{O}\left(\varepsilon^2\right)$ terms to obtain a simplified model called *Shallow Ice Approximation* (*SIA*) model.

Moreover, we use the classic Frank-Katmeneskii's approximation to Arrhenius' law. More precisely, from equation (2.35) we get:

$$\begin{aligned} A\,(T) &= \exp\left(Q/R\Theta_m\right)\exp\left(-Q/R\left(\Theta_m+(\Delta\Theta)\,T\right)\right)= \\ &= \exp\left(Q/R\Theta_m\right)\exp\left(-Q/Rj\,(T)\right), \end{aligned}$$

with

$$j(T) = \frac{1}{\Theta_m + (\Delta\Theta)\, T}.$$

Next, by approaching $j(T)$ with the Taylor series at $T_m = 0$ we have:

$$\begin{aligned} A(T) &= \exp\left(Q/R\Theta_m\right)\exp\left(-Q/\left(R\Theta_m\right) + Q\Delta T/\left(R\Theta_m^2\right)\right) = \\ &= \exp\left(Q\Delta\Theta T/\left(R\Theta_m^2\right)\right) = \exp\left(\gamma T\right), \end{aligned}$$

where

$$\gamma = \frac{Q\,(\Delta\Theta)}{R\Theta_m^2}. \tag{2.86}$$

So, in the *SIA* model we use the Frank-Katmeneskii expression:

$$A(T) = e^{\gamma T} \tag{2.87}$$

to approximate the Arrhenius' law.

The *SIA* model mainly consist of three coupled *SIA* submodels: velocity, profile and temperature models. Next subsections are devoted to each one of them as follows: in Subsection 2.4.1 we set out the *SIA* velocity model, in Subsection 2.4.2 we state the *SIA* profile one and finally in Subsection 2.4.3 we pose the *SIA* temperature model.

2.4.1 *SIA* glacier velocity model

In order to obtain a *SIA* model for the velocity field $\vec{u} = (u, v)$, first we neglect $\mathcal{O}(\varepsilon^2)$ terms in equations (2.71), (2.74) and (2.77). Thus, we obtain the following expressions:

$$0 = -\mu\,\eta_x + \tau_{12z} + 1, \tag{2.88}$$

$$u_z = A(T)\, Gl(\tau)\, \tau_{12}/\tau, \tag{2.89}$$

$$\tau^2 = \tau_{12}^2. \tag{2.90}$$

Additionally, we neglect the terms of $\mathcal{O}\left(\varepsilon^2\right)$ in the upper boundary condition (2.80) and in equation (2.81). So, we obtain:

$$\tau_{12} = 0 \qquad \text{at } z = \eta(t,x), \tag{2.91}$$

$$\tau_{22} = p \qquad \text{at } z = \eta(t,x). \tag{2.92}$$

Moreover, we integrate respect to z in equation (2.88) to get the following expression:

$$f\left(x\right) = \left(1 - \mu\,\eta_x\right) z + \tau_{12}. \tag{2.93}$$

Next, we rewrite this expression at $z = \eta$ (and then $\tau_{12} = 0$ from (2.91)), to get:

$$f\left(x\right) = \left(1 - \mu\,\eta_x\right)\eta.$$

Therefore, we can conclude the following expression for τ_{12}:

$$\tau_{12} = \left(1 - \mu\,\eta_x\right)\left(\eta - z\right). \tag{2.94}$$

Now, by using (2.94) in equation (2.90), we obtain:

$$\tau = \left|\tau_{12}\right| = \left|1 - \mu\eta_x\right|\left(\eta - z\right). \tag{2.95}$$

Next, we use Glen's law in the equations (2.89) and (2.95), to obtain:

$$\begin{aligned} u_z &= A\left(T\right)\tau^{n-1}\tau_{12} = && (2.96)\\ &= A\left(T\right)\left(1 - \mu\,\eta_x\right)\left|1 - \mu\,\eta_x\right|^{n-1}\left(\eta - z\right)^n. && (2.97) \end{aligned}$$

Thus, by integrating the equation (2.97) between $b\left(x\right)$ and z we get:

$$\begin{aligned} u - u_b &= \int_b^z A\left(T\left(s\right)\right)\left(1 - \mu\,\eta_x\right)\left|1 - \mu\,\eta_x\right|^{n-1}\left(\eta - s\right)^n ds = \\ &= \left(1 - \mu\,\eta_x\right)\left|1 - \mu\,\eta_x\right|^{n-1}\int_b^z A\left(T\left(s\right)\right)\left(\eta - s\right)^n ds, \end{aligned}$$

u_b being the basal sliding velocity. Notice that, just for simplicity, we write $A\left(T\left(s\right)\right)$ instead of $A\left(T\left(t,x,s\right)\right)$. So, we can write the velocity component in downslope direction as follows:

$$u = u_b + \left(1 - \mu\,\eta_x\right)\left|1 - \mu\,\eta_x\right|^{n-1}\int_b^z A\left(T\left(s\right)\right)\left(\eta - s\right)^n ds. \tag{2.98}$$

Moreover, we can rewrite (2.98) by using the Frank-Katmeneskii's approximation to Arrhenius's law indicated in (2.87), as follows:

$$u = u_b + (1 - \mu\, \eta_x)\, |1 - \mu\, \eta_x|^{n-1} \int_b^z e^{\gamma T(s)}\, (\eta - s)^n ds. \tag{2.99}$$

Now, by introducing the transversal flow function:

$$\Upsilon\, (x, \eta\, (t, x)) = \int_b^\eta u\, dz, \tag{2.100}$$

where u is given by (2.99), we can write the vertical component of the velocity v as:

$$v\,(x, z) = -\frac{\partial \Upsilon}{\partial x}(x, z). \tag{2.101}$$

2.4.2 *SIA* glacier profile model

In this section we state the model governing the glacier profile evolution. For this purpose, we write the kinematic boundary equation (2.79) in terms of the horizontal velocity, as follows:

$$\frac{\partial \eta}{\partial t} + \frac{\partial}{\partial x}\left(\int_b^\eta u\, dz \right) = a, \tag{2.102}$$

where the expression of u is given by equation (2.98). In order to state a basic equation to obtain the glacier profile, we can solve the integral appearing in (2.102):

$$\begin{aligned} \int_b^\eta u\, dz &= \int_b^\eta \left[u_b + (1 - \mu\, \eta_x)\, |1 - \mu\, \eta_x|^{n-1} \int_b^z A\,(T\,(s))\, (\eta - s)^n ds \right] dz = \\ &= u_b\, (\eta - b) + (1 - \mu\, \eta_x)\, |1 - \mu\, \eta_x|^{n-1} \int_b^\eta \left[\int_b^z A\,(T\,(s))\, (\eta - s)^n ds \right] dz = \\ &= u_b\, (\eta - b) + (1 - \mu\, \eta_x)\, |1 - \mu\, \eta_x|^{n-1} \int_b^\eta A\,(T\,(s))\, (\eta - s)^{n+1} ds. \end{aligned}$$

Now, we introduce the previous calculus in (2.102) and we get the following profile equation:

$$\begin{aligned} \frac{\partial \eta}{\partial t} + \frac{\partial}{\partial x}\, [u_b\, (\eta - b)] + \\ + \frac{\partial}{\partial x} \left[(1 - \mu\, \eta_x)\, |1 - \mu\, \eta_x|^{n-1} \int_b^\eta A\,(T\,(s))\, (\eta - s)^{n+1} ds \right] = a, \end{aligned} \tag{2.103}$$

that we can rewrite (again by using the Frank-Katmeneskii's approximation to Arrhenius' law indicated in (2.87)) as follows:

$$\begin{aligned}\frac{\partial \eta}{\partial t}&+\frac{\partial}{\partial x}\left[u_b\left(\eta-b\right)\right]+\\&+\frac{\partial}{\partial x}\left[\left(1-\mu\,\eta_x\right)\left|1-\mu\,\eta_x\right|^{n-1}\int_b^\eta e^{\gamma T(s)}(\eta-s)^{n+1}ds\right]=a.\end{aligned}\tag{2.104}$$

2.4.3 *SIA* glacier thermal model

After neglecting $\mathcal{O}\left(\varepsilon^2\right)$ terms in equation (2.73) we get:

$$\frac{DT}{Dt}=\alpha\tau\,Gl\left(\tau\right)A\left(T\right)+\beta T_{zz}.$$

Moreover, the combination of (2.90) and (2.94) leads to:

$$\frac{DT}{Dt}=\alpha\left(\left|1-\mu\,\eta_x\right|\left(\eta-z\right)\right)^{n+1}A\left(T\right)+\beta T_{zz},$$

or, equivalently:

$$\frac{\partial T}{\partial t}+\overrightarrow{v}\cdot\nabla T-\beta\frac{\partial^2 T}{\partial z^2}-\alpha e^{\gamma T}\left(\left|1-\mu\,\eta_x\right|\left(\eta-z\right)\right)^{n+1}=0,\tag{2.105}$$

after using the Frank–Katmeneskii approximation.

Moreover, in this model we have two possible boundary conditions at the base: one condition if the glacier is polar and another one if the glacier is polythermal.

In the case of polar glaciers, after the shallow ice scaling we deduce condition (2.83). Therefore neglecting the term of $\mathcal{O}\left(\varepsilon^2\right)$ we get the following basal boundary condition for the polar case:

$$-\frac{\partial T}{\partial z}=g_b.\tag{2.106}$$

Analogously, if we neglect $\mathcal{O}\left(\varepsilon^2\right)$ terms in condition (2.85) for polythermal glaciers, we get:

$$T\leq 0,\ T\left(\frac{\partial T}{\partial\vec{n}}-g_b\right)=0,\ 0\leq\frac{\partial T}{\partial\vec{n}}\leq g_b.\tag{2.107}$$

Chapter 3

Numerical Simulation of the Isothermal Glacier Profile Problem

3.1 Introduction

In the previous chapter the fully coupled *SIA* model has been deduced. As it has been already pointed out, it can be understood as the set of three coupled *SIA* submodels: profile, velocity and temperature submodels. In fact, in order to solve numerically the coupled *SIA* model, the most used strategy in the literature is to solve sequentially each submodel until convergence. In this framework, the main objective of the present chapter is solve the *SIA* profile model governed by equation (2.104) when the basal velocity and temperature are given data. For this purpose we first present an isothermal approximation of the model. Next, we solve this isothermal model by using a fixed domain formulation for the moving boundary problem of the *SIA* profile model combined with a set of appropriate numerical methods to deal with the main difficulties arising in the equations.

In a previous work [61] a front-tracking method that follows the unknown glacier geometry is proposed. In this region a semi explicit scheme posed on a finite differences discretization method is applied (see [55]). There exists a large literature concerning the numerical solution of ice sheet profile equation, some examples of recent references are [12, 53] or the summary of the first EISMINT workshop in [56].

Nevertheless, the profile equation in glaciers differs from the ice sheet case and has been not so treated in the literature. The here proposed fixed domain method allows the use a fixed mesh, with no need of updating at each time step. In this setting, the unknown basal extent of the glacier is implicitly obtained in terms of either the main solution or the multiplier associated to the nonnegative unilateral constraint on the profile. Moreover, the characteristics method for time discretization provides a well suited upwind scheme when solutions with regions of steep gradient are expected, as it is the case of the profile near the snout. The highly nonlinear diffusive term is treated by an appropriate explicit scheme and piecewise Lagrange linear finite elements are considered for spatial discretization.

This chapter is organized as follows: in Section 3.2 an isothermal uncoupled model for the glacier profile is stated. In Section 3.4 the fixed domain formulation for the moving boundary problem is posed in terms of a suitable complementarity problem. Section 3.5 is devoted to the description of the different numerical techniques involved in the proposed algorithm for the numerical solution of the model. Finally, in Section 3.6 various test examples illustrate the performance of the proposed methods.

3.2 Isothermal profile model for glaciers

In this section we consider just the profile model deduced in Chapter 2, assuming that sliding (or basal) velocity and temperature are known data functions. This problem setting naturally arises when solving the coupled problem with a global algorithm that sequentially computed temperature, velocity and profile until convergence. Notice that, in this chapter we consider an isothermal approach for the profile model, which seems a reasonable first step in the modelling process, where we mainly focus on the profile equation assuming a given temperature. Moreover, the variation of the Arrhenius' law, $A(T)$, with respect to real temperature is less important in glaciers than in ice sheets (in fact, the range of temperatures is lower).

In order to pose an isothermal approximation of the non-isothermal equation (2.103), we consider:

$$A(T) \approx e^{\gamma T_0}, \tag{3.1}$$

where T_0 is a prescribed constant temperature. In Section 3.6, which is devoted to numerical tests, the particular case with $T_0 = -1$ (so that $A(T) = e^{-\gamma}$) and the temperate one with $T_0 = 0$ (so that $A(T) = 1$) are considered.

In the isothermal setting here considered, we solve the integral in (2.103) and get the following basic equation for the glacier profile problem:

$$\begin{aligned} &\frac{\partial}{\partial t}(\eta - b) + \frac{\partial}{\partial x}\left[u_b(\eta - b)\right] + \\ &\quad + \frac{e^{\gamma T_0}}{n+2}\frac{\partial}{\partial x}\left[\left(1 - \mu\frac{\partial \eta}{\partial x}\right)\left|1 - \mu\frac{\partial \eta}{\partial x}\right|^{n-1}(\eta - b)^{n+2}\right] = a. \end{aligned} \tag{3.2}$$

Moreover, hereafter we will assume a flat bottom base for the glacier ($b = 0$) for simplicity, so that:

$$\frac{\partial \eta}{\partial t} + \frac{\partial}{\partial x}(u_b\,\eta) + \frac{e^{\gamma T_0}}{n+2}\frac{\partial}{\partial x}\left[\left(1 - \mu\frac{\partial}{\partial x}\eta\right)\left|1 - \mu\frac{\partial}{\partial x}\eta\right|^{n-1}\eta^{n+2}\right] = a. \tag{3.3}$$

3.3 Boundary conditions

The issue of boundary conditions for a valley glacier is an interesting one. The second order equation (3.3) requires two boundary conditions, upstream and downstream. At the snout of the glacier, assuming it terminates on land, we assume the homogeneous Dirichlet condition:

$$h = 0 \qquad \text{at} \qquad x = x_{front}, \tag{3.4}$$

where x_{front} is the position of the glacier front. The value of x_{front} is unknown (it is a free boundary), but the condition (3.4) is sufficient to determine it, since the equation is degenerate there (the diffusion coefficient is zero).

The condition at the upstream end of the glacier, x_{head}, is less clear. One first approximation might be:

$$h = 0 \qquad \text{at} \qquad x = x_{head}, \tag{3.5}$$

where x_{head} is the position of the glacier head. If we choose this condition, when $u_b = 0$ the flux:

$$\Upsilon = u_b \eta + \frac{e^{\gamma T_0}}{n+2}\left(1 - \mu \frac{\partial \eta}{\partial x}\right)\left|1 - \mu \frac{\partial \eta}{\partial x}\right|^{n-1} \eta^{n+2} \tag{3.6}$$

is then apparently zero unless $\partial\eta/\partial x$ is infinite. Indeed, the condition $\eta = 0$ then requires $\Upsilon \approx ax > 0$ near $x = x_{head}$, and this requires $\partial\eta/\partial x$ to be infinite and negative. Thus, when $u_b = 0$, the only way one can maintain $\eta = 0$ at the head is to have finite flux, and (since η must be positive in $x > x_{head}$), this must be a negative flux; that is to say, the glacier actually grows into an ice sheet with an ice divide downstream of the head.

Physically, we need to represent the bergschrund of the glacier. One way is to allow a variable basal slope, another option is applied a flux boundary condition:

$$\Upsilon = \Upsilon_0 \qquad \text{at} \qquad x = x_{head}. \tag{3.7}$$

In this problem we use both boundary conditions (3.5) and (3.7) at the head of the glacier and so we pose two problems: case without prescribed flux using (3.5) and case with prescribed flux using (3.7).

3.4 Moving boundary and complementarity problems

In this section we pose two moving boundary problems issued from different physical motivations. In the first case, the glacier profile evolution comes from the balance between accumulation-ablation phenomena plus the basal sliding. So, at each time the unknown positions of the head and the snout constitute the free boundary to be determined jointly with the profile function. In the second case, at a given position, x_{head}, the flux is prescribed so that the free boundary is just the snout position.

3.4.1 Case without prescribed flux

The equation (3.3) is valid for the function η that defines the glacier profile at those points x where $\eta\,(t,x) > 0$. Nevertheless, the set of those points is an additional unknown of the departure problem due to the fact that, a priori, the longitudinal extent of the ice layer is unknown (the same argument appears in [21, 27]). Therefore, this is a typical moving boundary problem which is appropriately formulated in the following paragraph.

Let $(0,t_A)$ be a large enough time interval and let $\Omega = (0, x_{\max})$ be a large enough bounded interval to be suitable fixed. Moreover, if a given accumulation-ablation function $a : (0,t_A) \times \Omega \to \mathbb{R}$ is considered and a positive initial glacier profile $\eta_0 : \Omega \to \mathbb{R}$ is prescribed, then the moving boundary formulation can be stated as follows:

For all $t \in [0,t_A]$, find the ice covered region $\Gamma\,(t) = (x_{head}\,(t)\,,\ x_{front}\,(t)) \subset \Omega$ and the profile function $\eta : \wp = \bigcup_{t\in[0,t_A]} (\{t\} \times \Gamma(t)) \to \mathbb{R}$ such that:

$$
\begin{aligned}
\frac{D\eta}{Dt} = -\frac{e^{\gamma T_0}}{(n+2)}\frac{\partial}{\partial x}\left[\left(1-\mu\frac{\partial \eta}{\partial x}\right)\left|1-\mu\,\frac{\partial \eta}{\partial x}\right|^{n-1}\eta^{n+2}\right] + a \qquad & \text{in} \quad \wp, \\
\eta > 0 \qquad & \text{in} \quad \wp, \\
\eta = 0 \quad \text{on} \quad \{x_{head}\,(t)\} \cup \{x_{front}\,(t)\}\,,\quad t \in (0,t_A)\,, & \\
\eta\,(0,x) = \eta_0\,(x) \qquad & \text{in} \quad \Omega,
\end{aligned}
\tag{3.8}
$$

where $\Gamma\,(t) = \{x/\eta(t,x) > 0\} = (x_{head}\,(t)\,, x_{front}\,(t))$ denotes the unknown basal longitudinal glacier extent and Ω is chosen such that $\Gamma\,(t) \subset \Omega$ for all t, a is a given time and space dependent accumulation-ablation rate function, and $\frac{D\eta}{Dt}$ denotes the total derivative with respect to the velocity field u_b in conservative form, that is:

$$
\frac{D\eta}{Dt} = \frac{\partial \eta}{\partial t} + \frac{\partial}{\partial x}\,(u_b \eta)\,. \tag{3.9}
$$

As it has been mentioned before, the set $\wp$ results to be an additional unknown. The technique of fixed domain methods for moving boundary problems involves a problem formulation in a given domain $\mathcal{Q} = (0,t_A) \times \Omega$, extending by zero the function $\eta\,(t,x)$ in the set $\mathcal{Q}\backslash\wp$, so that the *'extended'* glacier profile function verifies a nonlinear equation with multivalued operator (see [30], for example). For the sake of simplicity, we also denote by η the extent of the initial unknown to the fixed domain. Then, the function η satisfies the equations:

$$
\begin{aligned}
\frac{D\eta}{Dt}+\frac{e^{\gamma T_0}}{(n+2)}\frac{\partial}{\partial x}\left[\left(1-\mu\frac{\partial\eta}{\partial x}\right)\left|1-\mu\frac{\partial\eta}{\partial x}\right|^{n-1}\eta^{n+2}\right]-a\geq 0 \quad &\text{in} \quad \mathcal{Q},\\
\eta\geq 0 \quad &\text{in} \quad \mathcal{Q},\\
\left(\frac{D\eta}{Dt}+\frac{e^{\gamma T_0}}{(n+2)}\frac{\partial}{\partial x}\left[\left(1-\mu\frac{\partial\eta}{\partial x}\right)\left|1-\mu\frac{\partial\eta}{\partial x}\right|^{n-1}\eta^{n+2}\right]-a\right)\eta=0 \quad &\text{in} \quad \mathcal{Q},\\
\eta=0 \quad \text{on} \quad &(0,t_A)\times\partial\Omega,\\
\eta\left(0,x\right)=\eta_0\left(x\right) \quad \text{in} \quad &\Omega.
\end{aligned}
\tag{3.10}
$$

Notice that in the ice covered region, $\Gamma\left(t\right)$, the fact that $\eta\left(t,x\right)>0$ jointly with equation $(3.10)_3$ imply equation (3.3).

The above set of equations is classically known in moving boundary literature as a nonlinear parabolic complementarity formulation (see [30], for example).

3.4.2 Case with prescribed flux

In this case, for all $t\in[0,t_A]$, we have to find the ice covered region $\Gamma\left(t\right)=(0,\ x_{front}(t))\subset\Omega$ and the profile function $\eta:\wp=\bigcup_{t\in[0,t_A]}\left(\{t\}\times\Gamma(t)\right)\to\mathbb{R}$ such that equations $(3.8)_1$, $(3.8)_2$ and $(3.8)_4$ are verified. Moreover, equation $(3.8)_3$ is replaced by conditions:

$$\Upsilon=\Upsilon_0 \quad \text{on} \quad x=0,t\in\left(0,t_A\right), \tag{3.11}$$

$$\eta=0 \quad \text{on} \quad x=x_{front}\left(t\right),t\in\left(0,t_A\right), \tag{3.12}$$

where the flux is defined by:

$$\Upsilon=u_b\eta+\frac{e^{\gamma T_0}}{n+2}\left(1-\mu\frac{\partial\eta}{\partial x}\right)\left|1-\mu\frac{\partial\eta}{\partial x}\right|^{n-1}\eta^{n+2}, \tag{3.13}$$

and Υ_0 denotes the constant prescribed flux at the head of the glacier. So, the complementarity problem formulation is given by (3.10), but replacing boundary condition $(3.10)_4$ by (3.11) and:

$$\eta = 0 \quad \text{on} \quad (0, t_A) \times \{x_{\max}\}\,. \tag{3.14}$$

Notice that the unknown basal glacier extent is given in this case by the domain $\Gamma(t) = \{x/\eta(t,x) > 0\} = (0, x_{front}(t))$ and the free boundary just reduces to the point $x = x_{front}(t)$.

3.5 Numerical Methods

3.5.1 Case without prescribed flux

The set of equations (3.10) defines a nonlinear evolutive problem and the material derivative is involved in its formulation. In this section we describe different numerical methods for the approximation of the solution. The techniques are very close to those ones used for an analogous moving boundary model in ice sheets [21]. First, a characteristics method is proposed for time discretization. Next, a fixed point iteration is used for the nonlinear diffusive term at each time step. For the nonlinearity associated to the free boundary aspect (obstacle problem) a duality algorithm is proposed [5].

Time discretization

In order to discretize in time the nonlinear problem (3.10) an upwind characteristics scheme is chosen to approximate the material derivative, using the technique proposed in [2]. More precisely, let Δt be the time step and let us denote:

$$\eta^{m+1} = \eta\left((m+1)\,\Delta t, x\right), \qquad \forall x \in \Omega. \tag{3.15}$$

For $m = 0, 1, 2, ...$ Then, we introduce the approximation:

$$\frac{D\eta}{Dt}\big((m+1)\,\Delta t, x\big) \approx \frac{\eta^{m+1}(x) - J^m(x)\,\eta^m\big(\chi^m(x)\big)}{\Delta t}, \tag{3.16}$$

where $\chi^m(x) = \chi((m+1)\Delta t, x; m\Delta t)$ is obtained by solving the final value problem:

$$\begin{cases} \dfrac{d\chi(t,x;s)}{ds} & = u_b\big(\chi(t,x;s), s\big), \\ \chi(t,x;t) & = x, \end{cases} \tag{3.17}$$

and the function J^m is computed by numerical integration in the form:

$$J^m(x) = 1 - \int_{m\Delta t}^{(m+1)\Delta t} \frac{\partial u_b}{\partial x}\Big(\chi\big((m+1)\Delta t, x; \tau\big)\Big)\, d\tau. \tag{3.18}$$

More specifically, we denote $J^m(x) = J\big((m+1)\Delta t, x; m\Delta t\big)$, where the function J represents the jacobian of the change from eulerian coordinates to lagrangian coordinates defined by the function $x \to \chi(t,x;s)$, (see [2]).

Next, by replacing (3.16) in the problem (3.10), we obtain a sequence of nonlinear elliptic complementarity problems. More precisely, after initializing $\eta^0 = \eta(0,x)$, as indicated by equation (3.10), for each $m = 0, 1, 2, ...$, for a given function η^m, the following nonlinear problem is posed:

Find η^{m+1} such that:

$$\begin{aligned} &\frac{\eta^{m+1} - J^m(\eta^m \circ \chi^m)}{\Delta t} + \\ &+ \frac{e^{\gamma T_0}}{5} \frac{\partial}{\partial x}\left(\left(\eta^{m+1}\right)^5 \left| 1 - \mu \frac{\partial \eta}{\partial x}^{m+1} \right|^2 \left(1 - \mu \frac{\partial \eta}{\partial x}^{m+1} \right) \right) - a^{m+1} \geq 0 \text{ in } \Omega, \\ &\eta^{m+1} \geq 0 \text{ in } \Omega, \\ &\eta^{m+1} \left[\frac{\eta^{m+1} - J^m(\eta^m \circ \chi^m)}{\Delta t} + \right. \\ &\left. + \frac{e^{\gamma T_0}}{5} \frac{\partial}{\partial x}\left(\left(\eta^{m+1}\right)^5 \left| 1 - \mu \frac{\partial \eta}{\partial x}^{m+1} \right|^2 \left(1 - \mu \frac{\partial \eta}{\partial x}^{m+1} \right) \right) - a^{m+1} \right] = 0 \text{ in } \Omega, \\ &\eta^{m+1} = 0 \text{ on } \partial\Omega, \end{aligned} \tag{3.19}$$

where $a^{m+1}(x) = a\big((m+1)\Delta t, x\big)$ and $\circ$ denotes the composition symbol.

In order to solve the complementarity problems (3.19), an iterative fixed point technique is applied on the nonlinear diffusive term. In this way, a sequence of linear complementarity problems (indexed by k) is obtained.

More precisely, for each m, we initialize $\eta^{m+1,0}$, for example, $\eta^{m+1,0} = \eta^m$, and at step $k+1$ the following problem has to be solved:

Find $\eta^{m+1,k+1}$ *such that:*

$$\begin{aligned}
&\frac{\eta^{m+1,k+1} - J^m\left(\eta^m \circ \chi^m\right)}{\Delta t} + \\
&\qquad + \frac{e^{\gamma T_0}}{5}\frac{\partial}{\partial x}\left(f_1^{m+1,k}\left(1 - \mu\frac{\partial \eta}{\partial x}^{m+1,k+1}\right)\right) - a^{m+1} \geq 0 \quad \text{in} \quad \Omega, \\
&\qquad \eta^{m+1,k+1} \geq 0 \quad \text{in} \quad \Omega, \\
&\left[\frac{\eta^{m+1,k+1} - J^m\left(\eta^m \circ \chi^m\right)}{\Delta t} + \right. \\
&\left. + \frac{e^{\gamma T_0}}{5}\ \frac{\partial}{\partial x}\left(f_1^{m+1,k}\left(1 - \mu\frac{\partial \eta}{\partial x}^{m+1,k+1}\right)\right) - a^{m+1}\right]\eta^{m+1,k+1} = 0 \quad \text{in} \quad \Omega, \\
&\qquad \eta^{m+1,k+1} = 0 \quad \text{on} \quad \partial\Omega,
\end{aligned} \tag{3.20}$$

where

$$f_1^{m+1,k} = \left(\eta^{m+1,k}\right)^5 \left|1 - \mu\frac{\partial \eta}{\partial x}^{m+1,k}\right|^2.$$

Notice that problem (3.20) can be rewritten as follows:

Find $\eta^{m+1,k+1}$ *such that:*

$$\begin{aligned}
&\frac{\eta^{m+1,k+1} - J^m\left(\eta^m \circ \chi^m\right)}{\Delta t} - \\
&\qquad - \mu\frac{e^{\gamma T_0}}{5}\frac{\partial}{\partial x}\left(f_1^{m+1,k}\ \frac{\partial \eta}{\partial x}^{m+1,k+1}\right) + f_2^{m+1,k} - a^{m+1} \geq 0 \quad \text{in} \quad \Omega, \\
&\qquad \eta^{m+1,k+1} \geq 0 \quad \text{in} \quad \Omega, \\
&\left[\frac{\eta^{m+1,k+1} - J^m\left(\eta^m \circ \chi^m\right)}{\Delta t} - \right. \\
&\left. - \mu\frac{e^{\gamma T_0}}{5}\frac{\partial}{\partial x}\left(f_1^{m+1,k}\ \frac{\partial \eta}{\partial x}^{m+1,k+1}\right) + f_2^{m+1,k} - a^{m+1}\right]\eta^{m+1,k+1} = 0 \quad \text{in} \quad \Omega, \\
&\qquad \eta^{m+1,k+1} = 0 \quad \text{on} \quad \partial\Omega,
\end{aligned} \tag{3.21}$$

where

$$f_2^{m+1,k} = \frac{e^{\gamma T_0}}{5}\frac{\partial f_1}{\partial x}^{m+1,k} = \frac{e^{\gamma T_0}}{5}\frac{\partial}{\partial x}\left(\left(\eta^{m+1,k}\right)^5 \left|1 - \mu\frac{\partial \eta}{\partial x}^{m+1,k}\right|^2\right). \tag{3.22}$$

Spatial discretization and variational formulation

In order to pose the spatial discretization and the variational formulation, the following convex set is introduced:

$$K = \{\varphi \in H_0^1(\Omega) / \varphi \geq 0 \ \text{ a.e. in } \ \Omega\}. \tag{3.23}$$

Thus, for each value of m, $\eta^{m+1,0} \in K$ is initialized, for example $\eta^{m+1,0} = \eta^m$, and at the step $k+1$ the solution of the following variational inequality is posed:

Find $\eta^{m+1,k+1} \in K$ *such that:*

$$\begin{aligned}
&\frac{1}{\Delta t}\int_\Omega \eta^{m+1,k+1}\left(\varphi - \eta^{m+1,k+1}\right) d\Omega + \\
&+\mu\frac{e^{\gamma T_0}}{5}\int_\Omega f_1^{m+1,k}\,\frac{\partial\eta}{\partial x}^{m+1,k+1}\frac{\partial}{\partial x}\left(\varphi - \eta^{m+1,k+1}\right) d\Omega \ \geq \\
&\geq \frac{1}{\Delta t}\int_\Omega J^m\left(\eta^m \circ \chi^m\right)\left(\varphi - \eta^{m+1,k+1}\right) d\Omega - \\
&-\int_\Omega f_2^{m+1,k}\left(\varphi - \eta^{m+1,k+1}\right) d\Omega + \\
&+\int_\Omega a^{m+1}\left(\varphi - \eta^{m+1,k+1}\right) d\Omega, \qquad \forall \varphi \in K.
\end{aligned} \tag{3.24}$$

The relation between variational inequalities, complementarity problems and obstacle problems can be reviewed in [30], for example. In order to discretize (3.24) in space, a piecewise linear Lagrange finite elements space is used. Thus, for a positive given parameter l, a uniform finite elements mesh, τ_l, is built for the domain Ω with nodes $x_i = (i-1)l, \ i = 1, \ldots, N+1$. So, the following classical spaces and sets are introduced:

$$V_l = \{\varphi_l \in \mathcal{C}^0(\Omega) / \varphi_l|_E \in P_1, \forall E \in \tau_l\}, \tag{3.25}$$

$$V_{0l} = \{\varphi_l \in V_l / \varphi_l|_{\partial\Omega} = 0\}, \tag{3.26}$$

$$K_l = \{\varphi_l \in V_l / \varphi_l \geq 0, \ \text{a.e. in } \Omega, \varphi_l|_{\partial\Omega} = 0\}, \tag{3.27}$$

where E denotes a standard finite element. In this way, the discretized problem can be written as follows:

Find $\eta_l^{m+1,k+1} \in K_l$ *such that:*

$$\begin{aligned}
&\frac{1}{\Delta t}\int_\Omega \eta_l^{m+1,k+1}\left(\varphi_l - \eta_l^{m+1,k+1}\right) d\Omega + \\
&+\mu\frac{e^{\gamma T_0}}{5}\int_\Omega f_1^{m+1,k}\,\frac{\partial \eta_l}{\partial x}^{m+1,k+1}\frac{\partial}{\partial x}\left(\varphi_l - \eta_l^{m+1,k+1}\right) d\Omega \;\geq \\
&\geq \frac{1}{\Delta t}\int_\Omega J^m\left(\eta_l^m \circ \chi^m\right)\left(\varphi_l - \eta_l^{m+1,k+1}\right) d\Omega - \\
&-\int_\Omega f_2^{m+1,k}\left(\varphi_l - \eta_l^{m+1,k+1}\right) d\Omega + \\
&+\int_\Omega a^{m+1}\left(\varphi_l - \eta_l^{m+1,k+1}\right) d\Omega, \qquad \forall \varphi_l \in K_l. \quad (3.28)
\end{aligned}$$

In the following sections the subindex l has been suppressed for simplicity.

Duality algorithm

In order to solve the discretized nonlinear problem (3.28) several minimization algorithms applied to variational formulations of obstacle problems can be used [44]. In this work a duality method proposed in [5] to solve variational inequalities has been chosen. For this purpose, first we express the variational inequalities (3.24) in terms of the indicatrix function, I_K, of the convex K. So that we pose the problem:

Find $\eta^{m+1,k+1} \in V_{0l}(\Omega)$ *such that:*

$$\begin{aligned}
&\frac{1}{\Delta t}\int_\Omega \eta^{m+1,k+1}\left(\varphi - \eta^{m+1,k+1}\right) d\Omega + \\
&+\mu\frac{e^{\gamma T_0}}{5}\int_\Omega f_1^{m+1,k}\,\frac{\partial \eta}{\partial x}^{m+1,k+1}\frac{\partial}{\partial x}\left(\varphi - \eta^{m+1,k+1}\right) d\Omega + \\
&+I_K(\varphi) - I_K\left(\eta^{m+1,k+1}\right) \;\geq \\
&\geq \frac{1}{\Delta t}\int_\Omega J^m\left(\eta^m \circ \chi^m\right)\left(\varphi - \eta^{m+1,k+1}\right) d\Omega - \\
&-\int_\Omega f_2^{m+1,k}\left(\varphi - \eta^{m+1,k+1}\right) d\Omega + \\
&+\int_\Omega a^{m+1}\left(\varphi - \eta^{m+1,k+1}\right) d\Omega, \qquad \forall \varphi \in H_0^1(\Omega)\,(3.29)
\end{aligned}$$

where $(\partial I_K)_\lambda^\omega$ is the Yosida approximation of operator $(\partial I_K - \omega I)$ with parameter $\lambda > 0$.

Moreover, the results of subdifferential calculus for the convex function I_K allow to rewrite (3.29) in the following equivalent form:

$$\xi^{m+1,k+1} \;=\; -\left(\mathcal{A}\left(\eta^{m+1,k+1}\right) - g^{m+1,k}\right) \;\in\; \partial I_K\left(\eta^{m+1,k+1}\right), \tag{3.30}$$

where $\partial I_K(u)$ denotes the subdifferential of I_K at the point u, the operator $\mathcal{A}$: $H_0^1(\Omega) \to H^{-1}(\Omega)$ is defined by:

$$\left(\mathcal{A}(\varphi), \psi\right) \;=\; \frac{1}{\Delta t}\int_\Omega \varphi\,\psi\,d\Omega \;+\; \mu\frac{e^{\gamma T_0}}{5\,\nu}\int_\Omega f_1^{m+1,k}\,\frac{\partial\varphi}{\partial x}\,\frac{\partial\psi}{\partial x}\,d\Omega, \tag{3.31}$$

and the element $g^{m+1,k} \in H^{-1}(\Omega)$ is given by:

$$\left(g^{m+1,k}, \psi\right) \;=\; \frac{1}{\Delta t}\int_\Omega J^m\left(\eta^m \circ \chi^m\right)\psi\,d\Omega - \int_\Omega f_2^{m+1,k}\,\psi\,d\Omega + \int_\Omega a^{m+1}\,\psi\,d\Omega. \tag{3.32}$$

Therefore, equation (3.30) is equivalent to the following problem:

Find $\eta^{m+1,k+1} \in H_0^1(\Omega)$ such that:

$$\begin{aligned}
&\frac{1}{\Delta t}\int_\Omega \eta^{m+1,k+1}\,\psi\,d\Omega \;+\int_\Omega \xi^{m+1,k+1}\,\psi\,d\Omega \;+\\
&+\mu\,\frac{e^{\gamma T_0}}{5}\int_\Omega f_1^{m+1,k}\,\frac{\partial\eta}{\partial x}^{m+1,k+1}\,\frac{\partial\psi}{\partial x}\,d\Omega - \frac{1}{\Delta t}\int_\Omega J^m\,\left(\eta^m\circ\chi^m\right)\psi\,d\Omega \;=\\
&\quad= \int_\Omega a^{m+1}\,\psi\,d\Omega \;-\; \int_\Omega f_2^{m+1,k}\,\psi\,d\Omega, \qquad \forall\psi\in H_0^1(\Omega),
\end{aligned} \tag{3.33}$$

with

$$\xi^{m+1,k+1} \in \partial I_K\left[\eta^{m+1,k+1}\right]. \tag{3.34}$$

The method proposed in [5] to solve the nonlinear problem (3.33)–(3.34) introduces a new unknown, $q^{m+1,k+1}$, which works as multiplier, defined by:

$$q^{m+1,k+1} \in \partial I_K\left[\eta^{m+1,k+1}\right] - \omega\eta^{m+1,k+1}, \tag{3.35}$$

in terms of a positive parameter ω. Thus, equation (3.33) can be written as follows:

Find $\eta^{m+1,k+1} \in H_0^1(\Omega)$ such that:

$$\begin{aligned}
&\frac{1}{\Delta t}\int_\Omega \eta^{m+1,k+1}\,\psi\,d\Omega + \int_\Omega \left(q^{m+1,k+1} + \omega\,\eta^{m+1,k+1}\right)\psi\,d\Omega \;+\\
&+\mu\,\frac{e^{\gamma T_0}}{5}\int_\Omega f_1^{m+1,k}\,\frac{\partial\eta}{\partial x}^{m+1,k+1}\,\frac{\partial\psi}{\partial x}\,d\Omega = \frac{1}{\Delta t}\int_\Omega J^m\,\left(\eta^m\circ\chi^m\right)\psi\,d\Omega \;+\\
&\quad+\int_\Omega a^{m+1}\,\psi\,d\Omega - \int_\Omega f_2^{m+1,k}\,\psi\,d\Omega, \qquad \forall\psi\in H_0^1(\Omega),
\end{aligned} \tag{3.36}$$

where $q^{m+1,k+1}$ verifies (3.35).

As ∂I_K is a maximal monotone operator, the following conditions are equivalent (see proof in [5]):

$$q^{m+1,k+1} \in (\partial I_K - \omega I)\left(\eta^{m+1,k+1}\right), \tag{3.37}$$

$$q^{m+1,k+1} = (\partial I_K)^{\omega}_{\lambda}\left[\eta^{m+1,k+1} + \lambda q^{m+1,k+1}\right], \tag{3.38}$$

where $(\partial I_K)^{\omega}_{\lambda}$ is the Yosida approximation of operator $(\partial I_K - \omega I)$ with parameter $\lambda > 0$.

The duality formulation and the previous equivalence in the discretized problem are used to propose the following algorithm:

Step 0:

- Initialize $\left(\eta^{m+1,k+1}\right)^0$: $\left(\eta^{m+1,k+1}\right)^0 = \eta^{m+1,k}$ for example.

Step j: Given $\left(\eta^{m+1,k+1}\right)^j$:

- compute $\left(\eta^{m+1,k+1}\right)^{j+1} \in V_{0l}$ as the solution of the linear problem:

$$\begin{aligned}
&\left(\frac{1}{\Delta t} + \omega\right)\int_\Omega \eta^{m+1,k+1,j+1}\,\psi\, d\Omega + \\
&+ \mu\,\frac{e^{\gamma T_0}}{5}\int_\Omega f_1^{m+1,k}\,\frac{\partial \eta}{\partial x}^{m+1,k+1,j+1}\frac{\partial \psi}{\partial x}\, d\Omega \;= \\
&= -\int_\Omega q^{m+1,k+1,j}\,\psi\, d\Omega + \frac{1}{\Delta t}\int_\Omega J^m\left(\eta^m \circ \chi^m\right)\,\psi\, d\Omega + \\
&+ \int_\Omega a^{m+1}\,\psi\, d\Omega - \int_\Omega f_2^{m+1,k}\,\psi\, d\Omega, \qquad \forall \psi \in V_{0l},
\end{aligned} \tag{3.39}$$

- update the multiplier by:

$$\left(q^{m+1,k+1}\right)^{j+1} = (\partial I_K)^{\omega}_{\lambda}\left[\left(\eta^{m+1,k+1}\right)^{j+1} + \lambda\left(q^{m+1,k+1}\right)^{j}\right].$$

The duality method convergence is obtained in [5] when $\lambda\omega \le 0.5$. The case of constant parameters corresponds to the classical case. Further extensions using functional parameters had been consider in [68] for specific problems. For the particular choice of the parameters $\lambda\omega = 0.5$, the Yosida approximation is given by:

$$(\partial I_K)^{\omega}_{\frac{1}{2\omega}}(r) = -2\omega\,|r|\,.$$

3.5.2 Case with prescribed flux

In this case, the departure point for the variational formulation replaces the Sobolev space $H_0^1(\Omega)$ by $V = \{\varphi \in H^1(\Omega)/\varphi(x_{\max}) = 0\}$ in the definition of convex K at equation (3.23). Then, formulation (3.24) is replaced by:

Find $\eta^{m+1,k+1} \in K$ *such that:*

$$\begin{aligned}
&\frac{1}{\Delta t}\int_\Omega \eta^{m+1,k+1}\left(\varphi - \eta^{m+1,k+1}\right) d\Omega + \\
&+\mu\frac{e^{\gamma T_0}}{5}\int_\Omega f_1^{m+1,k}\,\frac{\partial\eta}{\partial x}^{m+1,k+1}\frac{\partial}{\partial x}\left(\varphi - \eta^{m+1,k+1}\right) d\Omega \geq \\
&\geq \frac{1}{\Delta t}\int_\Omega J^m\left(\eta^m\circ\chi^m\right)\left(\varphi - \eta^{m+1,k+1}\right) d\Omega - \int_\Omega f_2^{m+1,k}\left(\varphi - \eta^{m+1,k+1}\right) d\Omega + \\
&+\int_\Omega a^{m+1}\left(\varphi - \eta^{m+1,k+1}\right) d\Omega \;+\; \widehat{\Upsilon}_0\left(\varphi(0) - \eta^{m+1,k+1}(0)\right), \qquad \forall\varphi\in K, \qquad (3.40)
\end{aligned}$$

where we have replaced condition $\eta^{m+1,k+1}(0) = 0$ by:

$$u_b\eta^{m+1,k}(0) + \frac{e^{\gamma T_0}}{5}f_1^{m+1,k}(0)\left(1 - \mu\frac{\partial\eta}{\partial x}^{m+1,k+1}\right)(0) = \Upsilon_0,$$

which corresponds to a linearization of the initially prescribed nonlinear flux. Thus, in (3.40) we use the notation:

$$\widehat{\Upsilon}_0 = \Upsilon_0 - u_b\eta^{m+1,k}(0) - \frac{e^{\gamma T_0}}{5}f_1^{m+1,k}(0). \qquad (3.41)$$

Following similar procedures to the ones in the case without imposed flux and defining:

$$V_{0l} \;=\; \{\varphi_l \in V_l/\varphi_l(x_{\max}) = 0\}, \qquad (3.42)$$

we achieve the following linear problem:

$$\begin{aligned}
&\left(\frac{1}{\Delta t} + \omega\right)\int_\Omega \eta^{m+1,k+1,j+1}\,\psi\, d\Omega + \\
&+\;\mu\,\frac{e^{\gamma T_0}}{5}\int_\Omega f_1^{m+1,k}\left(\frac{\partial\eta}{\partial x}\right)^{m+1,k+1,j+1}\frac{\partial\psi}{\partial x}\, d\Omega = \\
&= -\int_\Omega q^{m+1,k+1,j}\,\psi\, d\Omega + \frac{1}{\Delta t}\int_\Omega J^m\left(\eta^m\circ\chi^m\right)\,\psi\, d\Omega + \\
&+\int_\Omega a^{m+1}\psi d\Omega - \int_\Omega f_2^{m+1,k}\psi d\Omega + \widehat{\Upsilon}_0\,\psi(0), \qquad \forall\psi\in V_{0l}, \qquad (3.43)
\end{aligned}$$

which replaces (3.39).

3.6 Numerical Tests

In this section, we present numerical results corresponding to analytical and non–analytical test solutions. The results have been obtained by implementing in FORTRAN90 the numerical methods previously described in this chapter.

3.6.1 Test examples with analytical solution

This analytical test is an academic example developed to validate the correct performance of the algorithm proposed in this chapter.

Case without prescribed flux

In this section we have chosen several examples corresponding to the case without prescribed flux and for which the exact time dependent solution is:

$$\eta_e\,(t,x) = 0.86025\,(1-0.1t)\left(1-(x-1)^2\right)^{1/2}. \tag{3.44}$$

For this purpose, the following accumulation ablation function has been chosen:

$$a_e(t,x) = \frac{\partial \eta_e}{\partial t} + \frac{\partial}{\partial x}\left(u_b\eta_e\right) + \frac{e^{\gamma T_0}}{5}\frac{\partial}{\partial x}\left[\left(1-\mu\frac{\partial \eta_e}{\partial x}\right)^3 \eta_e^5\right], \tag{3.45}$$

and the parameters selected for this example are:

$$\gamma = 4.52,\ \delta = 10^{\mathrm{o}},\ \mu = 0.4 \text{ and } T_0 = -1.$$

Moreover, a first example without basal velocity, $u_b = 0$, and a second one with constant basal velocity, $u_b = 10^{-3}$, have been tested.

For the numerical solution, we have chosen several uniform finite element meshes (with $N = 1000,\ 2000,\ 4000$ and 8000 nodes) and time steps ($\Delta t = 10^{-4},\ 10^{-5}$ and 10^{-6}). Moreover, we have chosen the value of 10^{-20} as stopping test for the fixed point iteration and duality algorithms.

The exact solution in expression (3.44) and the correspond exact accumulation-ablation function (3.45) are plotted in Figure 3.1 and Figure 3.2 respectively. Tables

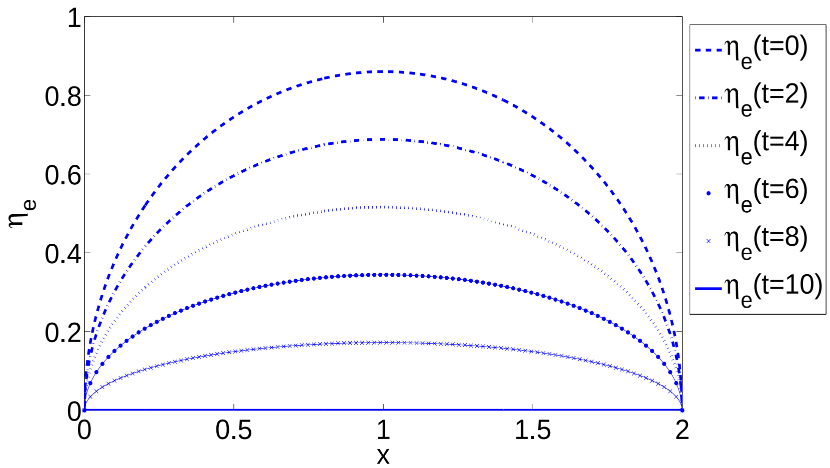

Figure 3.1: Exact solution for the analytical test without prescribed flux

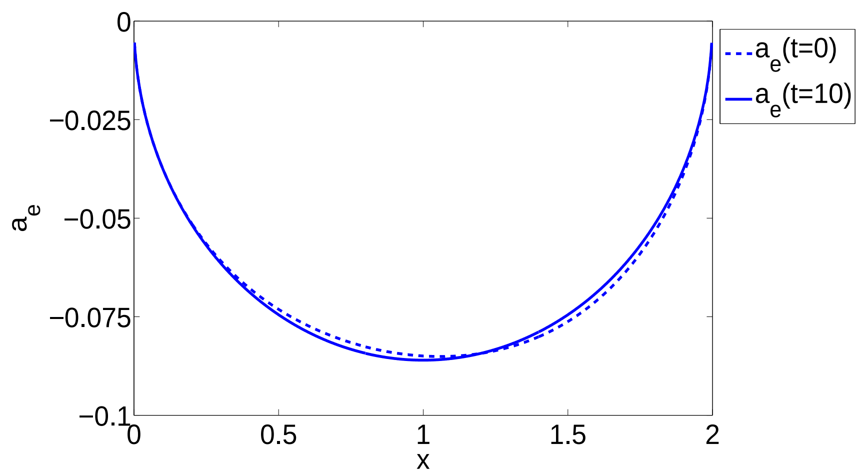

Figure 3.2: Exact accumulation-ablation function for the analytical test without prescribed flux

Δt	N = 100	N = 1000	N = 10000
1.e-4	1.2876e-4	9.0814e-5	———
1.e-5	1.2974e-4	9.0689e-5	8.6606e-5
1.e-6	1.2922e-4	9.0676e-5	8.6602e-5

Table 3.1: Errors in infinity norm at time $t = 7$ for the analytical test example without prescribed flux. Domain [0, 2] and no sliding velocity ($u_b = 0$).

Δt	N = 100	N = 1000	N = 10000
1.e-4	1.6103e-2	1.5981e-2	———
1.e-5	1.6102e-2	1.5981e-2	8.8129e-3
1.e-6	1.6119e-2	1.5981e-2	8.8128e-3

Table 3.2: Errors in infinity norm at time $t = 7$ for the analytical test example without prescribed flux. Domain [0, 2] and sliding velocity $u_b = 10^{-3}$.

3.1 to 3.6 show the infinity norm of the obtained error for $\eta(t, .)$ with $t = 7$ for different meshes and time steps. That is, they show the value $\|\eta_e(t, x_i) - \eta_c(t, x_i)\|_\infty$, where η_c denotes the computed solution. First, Table 3.1 corresponds to zero basal velocity and Table 3.2 corresponds to the constant basal velocity $u_b = 10^{-3}$. The problem domain in both tables is [0, 2]. For the same domain, but just considering the errors on the nodes in [0.1, 1.9], analogous Tables 3.3 and 3.4 are shown. If we compare these new tables with the previous ones, we can conclude that most of the errors are concentrated at the domain margins. The main cause is due to the accumulation-ablation function (3.45) associated to the exact solution (3.44) that presents infinite slope at the margins. For this reason, we have also considered another test example where the profile problem is posed in [0.1, 1.9], and the corresponding errors of these new tests are presented in Tables 3.5 and 3.6. Notice that the convergence results are better illustrated in this last tests than in the previous ones, and moreover errors for zero sliding velocity are smaller than for nonzero sliding velocity case. Note also that in all previous examples the free boundary does not appear and the solution corresponds to a fully ice covered domain.

As a general conclusion about the previous results we can state the good convergence results obtained when refining both the time and spatial mesh steps. Although

Δt	N = 100	N = 1000	N = 10000
1.e-4	5.1363e-6	2.2556e-6	———
1.e-5	6.0288e-6	2.2900e-7	2.2914e-7
1.e-6	6.1180e-6	5.0555e-8	2.6120e-8

Table 3.3: Errors in infinity norm measured only in $[0.1, 1.9]$ at time $t = 7$ for the analytical test example without prescribed flux. Domain [0, 2] and no sliding velocity ($u_b = 0$).

Δt	N = 100	N = 1000	N = 10000
1.e-4	4.2611e-4	5.1859e-5	———
1.e-5	4.2506e-4	5.0874e-5	4.4088e-6
1.e-6	4.2495e-4	5.0775e-5	4.3060e-6

Table 3.4: Errors in infinity norm measured only in $[0.1, 1.9]$ at time $t = 7$ for the analytical test example without prescribed flux. Domain [0, 2] and sliding velocity $u_b = 10^{-3}$.

Δt	N = 100	N = 1000	N = 10000
1.e-4	9.9581e-6	7.4474e-8	———
1.e-5	1.0892e-5	6.4142e-8	2.9143e-8
1.e-6	1.0986e-5	6.7154e-8	2.6299e-8

Table 3.5: Errors in infinity norm at time $t = 7$ for the analytical test example without prescribed flux. Domain [0.1, 1.9] and no sliding velocity ($u_b = 0$).

Δt	N = 100	N = 1000	N = 10000
1.e-4	2.9899e-4	3.6353e-5	———
1.e-5	2.9791e-4	3.6260e-5	3.8513e-6
1.e-6	2.9780e-4	3.6247e-5	3.7497e-6

Table 3.6: Errors in infinity norm at time $t = 7$ for the analytical test example without prescribed flux. Domain [0.1, 1.9] and sliding velocity $u_b = 10^{-3}$.

several numerical methods dealing with the involved nonlinearities, we remember that the characteristics method for time discretizations presents an order of convergence $\mathcal{O}(\Delta t + h + h^2/\Delta t)$ (see [3]) leading to a first order convergence for $\Delta t = h$.

Case with prescribed flux

In this section we present the same methodology to check the algorithm but now by choosing different data, because in this case we have different boundary condition on the head of the glacier.

We have chosen a flat sloped based as the base of the glacier, but in this case we want to test a fixed flow as boundary condition at the head of the glacier for which the exact time dependent solution is given by:

$$\eta_f\,(t,x) = (1-0.1t)\left(1-\left(\frac{x}{2}\right)^2\right)^{1/2}, \tag{3.46}$$

and the accumulation-ablation function applied in this academic example is:

$$a_f(t,x) = \frac{\partial \eta_f}{\partial t} + \frac{\partial}{\partial x}\,(u_b\eta_f) + \frac{e^{\gamma\, T_0}}{5}\frac{\partial}{\partial x}\left[\left(1-\mu\frac{\partial \eta_f}{\partial x}\right)^3 \eta_f^5\right], \tag{3.47}$$

which it is plotted in Figure 3.4. The selected parameters for this example are:

$$\gamma = 2.5,\ \delta = 10,\ \mu = 0.4 \ \text{ and } \ T_0 = -1.$$

Moreover, examples without basal velocity, $u_b = 0$, and with constant basal velocity, $u_b = 10^{-3}$, have been tested.

The value of the flux is given by:

$$\Upsilon_f = u_b\eta_f + \frac{e^{\gamma\, T_0}}{5}\left(1-\mu\frac{\partial \eta_f}{\partial x}\right)^3 \eta_f^5,$$

so that the boundary condition (3.11) remains as follows:

$$\Upsilon = \Upsilon_0 = u_b\,(1-0.1t) + \frac{e^{\gamma\, T_0}}{5}(1-0.1t)^5 \qquad \text{at} \qquad x=0, \quad t>0. \tag{3.48}$$

Tables 3.7 to 3.10 show the infinity norm of the obtained error for $\eta(.,t)$ with $t = 7$ for the different meshes and time steps. The value $\|\eta_f\,(t,x) - \eta_c\,(t,x)\|_\infty$ is

Δt	N = 100	N = 1000	N = 2000	N = 4000	N = 8000
1.e-4	5.2681e-2	1.1571e-2	6.0962e-3	———	———
1.e-5	5.2679e-2	1.1571e-2	6.0962e-3	3.1382e-3	———
1.e-6	5.2678e-2	1.1571e-2	6.0962e-3	3.1382e-3	1.5936e-3
1.e-7	———	1.1571e-2	6.0962e-3	3.1382e-3	1.5936e-3

Table 3.7: Errors in infinity norm at time $t = 7$ for the analytical test example with prescribed flux. Domain [0, 2] and no sliding velocity ($u_b = 0$).

Δt	N = 100	N = 1000	N = 2000	N = 4000	N = 8000
1.e-4	4.5393e-2	9.6712e-3	5.0270e-3	———	———
1.e-5	4.5392e-2	9.6712e-3	5.0207e-3	2.5674e-3	1.4590e-3
1.e-6	4.5392e-2	9.6712e-3	5.0207e-3	2.5674e-3	1.4590e-3
1.e-7	———	9.6712e-3	5.0207e-3	2.5674e-3	1.4590e-3

Table 3.8: Errors in infinity norm at time $t = 7$ for the analytical test example with prescribed flux. Domain [0, 2] and sliding velocity $u_b = 10^{-3}$.

Δt	N = 100	N = 1000	N = 2000	N = 4000	N = 8000
1.e-4	5.0670e-2	1.0977e-3	5.4767e-4	———	———
1.e-5	5.0669e-2	1.0977e-3	5.4764e-4	2.7354e-4	———
1.e-6	5.0669e-2	1.0977e-3	5.4770e-4	2.7358e-4	1.3672e-4
1.e-7	———	1.0977e-3	5.4767e-4	2.7355e-4	1.3670e-4

Table 3.9: Errors in infinity norm at time $t = 7$ for the analytical test example with prescribed flux. Domain [0, 1.9] and no sliding velocity ($u_b = 0$).

Δt	N = 100	N = 1000	N = 2000	N = 4000	N = 8000
1.e-4	4.3569e-2	1.3219e-3	4.7798e-4	———	———
1.e-5	4.3569e-2	1.3219e-3	4.7797e-4	2.4420e-4	1.2359e-4
1.e-6	4.3568e-2	1.3219e-3	4.7800e-4	2.4425e-4	1.2357e-4
1.e-7	———	1.3219e-3	4.7797e-4	2.4420e-4	1.2359e-4

Table 3.10: Errors in infinity norm at time $t = 7$ for the analytical test example with prescribed flux. Domain [0, 1.9] and sliding velocity $u_b = 10^{-3}$.

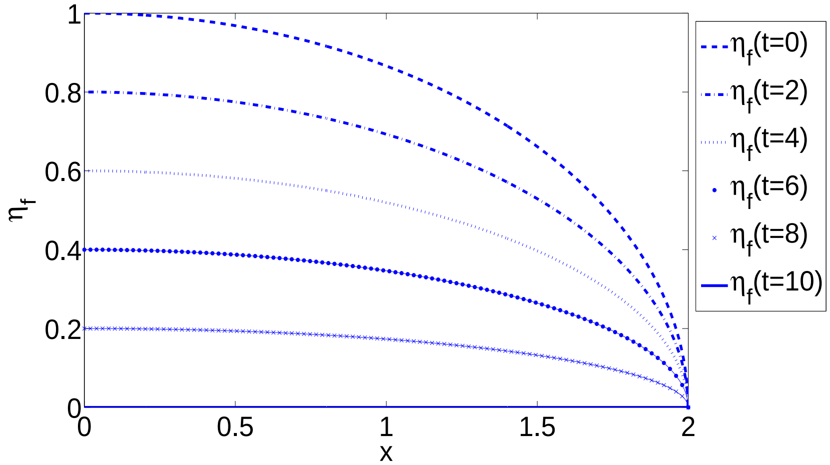

Figure 3.3: Exact solution for analytical test example with prescribed flux

shown, where η_c denotes the computed solution, as we have indicated in the previous example.

First, Table 3.7 corresponds to zero basal velocity and Table 3.8 corresponds to the constant basal velocity $u_b = 10^{-3}$. The problem domain in both tables is [0, 2]. Considering the domain in [0, 1.9] analogous Tables 3.9 and 3.10 are shown.

Note that in all previous examples of this analytical test the free boundary does not appear and the solution corresponds to a fully ice covered domain.

3.6.2 Test without closed form solution

In this section we have considered several examples without analytical solution, some of them corresponding to the case without imposed flux and others to the case of prescribed flux at the head.

Case without prescribed flux

In this setting we first consider an example corresponding to an isothermal temperate regime, defined by constant temperature $T_0 = 0$ (so that $A(T) = 1$) and different sliding velocities. More precisely, the values $u_b = 1$ and $u_b = 5$ have been chosen. The domain $\Omega = (0, 5)$ has been taken. We have considered the dimensionless

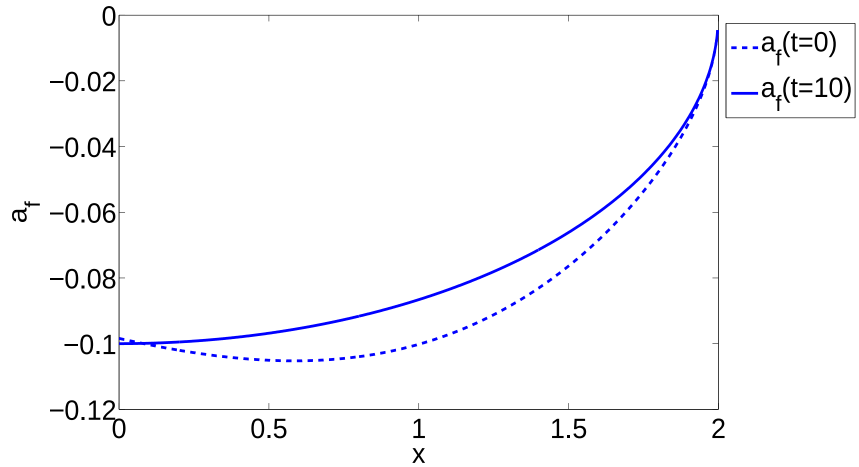

Figure 3.4: Exact accumulation-ablation function for analytical test with prescribed flux

accumulation-ablation given by:

$$a(t, x) = c(1 - x), \tag{3.49}$$

with $c = 1$ or $c = 2$. This accumulation-ablation function is $\mathcal{O}(1)$ and assumes accumulation taking place on the left part (upper glacier region) and ablation occurring on the right part (lower glacier region). As initial conditions we have considered either a zero initial profile or the following flattened half-sphere on a sloping ground:

$$\eta(0, x) = \begin{cases} 0.1\,(1 - (x-1)^2)^{1/2} & \text{if} \quad | x - 1 | \leq 1 \\ 0 & \text{if} \quad | x - 1 | > 1, \end{cases} \tag{3.50}$$

which is very close to the one already used in [61]. Moreover, from this example we have also taken the following parameters to simulate the glacier behavior:

$$d_1 = 1\text{km},\ d_2 = 132\text{m},\ \delta = 10^o \text{ and } \varepsilon = 0.13.$$

The resulting profiles when $u_b = 1$ are shown in Fig. 3.5 for different times until steady state is achieved. The two upper pictures in this figure show the case $c = 1$ with the initial condition defined in (3.50) and zero initial condition, respectively.

Thus illustrating that the same steady state is achieved from both initial conditions. The bottom part of Fig. 3.5 shows the expected behavior when both accumulation and ablation increase at the left and right regions, respectively. Next, in Fig. 3.6 the analogous results are shown for $u_b = 5$.

The second example corresponds to a polar regime when $T_0 = -1$ (so that $A(T) = e^{-\gamma}$, with $\gamma = 5$) and no sliding ($u_b = 0$) are considered. The resulting profiles are shown in Fig. 3.7. Notice that while in the temperate case a finite slope is observed at the head, in the polar one an infinite slope seems to appear. Thus, in this second case we think that the homogeneous Dirichlet boundary condition at the head leads to a negative flux at that point, so that it is more realistic to impose the flux. This is the main reason why we consider the second case with prescribed flux.

The parameters associated to time and space discretizations have been taken to $\Delta t = 10^{-6}$ and $\Delta x = 10^{-3}$, respectively. The stopping test parameter for the nonlinear algorithms have been taken to 10^{-9}.

Case with prescribed flux

In this second set of tests we have considered a prescribed flux at the head of the glacier. Unless specifically pointed out, the common data are the same as in the previous example. As initial condition we just consider a zero profile function, but in all tests the same steady state results are obtained with initial condition (3.50).

The first tests correspond to the polar case, by taking $T_0 = -1$, $u_b = 0$, $c = 1$ and different flux values Υ_0. The obtained profiles are shown in Fig. 3.8 and illustrate the behavior with respect to Υ_0. Notice that finite slopes appear at the head. Analogous results for the case $c = 2$ (thus increasing the accumulation-ablation) are shown in Fig. 3.9.

The rest of the tests correspond to the temperate case with $T_0 = 0$ and $\Upsilon_0 = 0.5$ as fixed parameters, and different values of u_b and c. The obtained profiles are shown in Figs. 3.10 and 3.11.

Notice that we can deduce further information about the position of the free

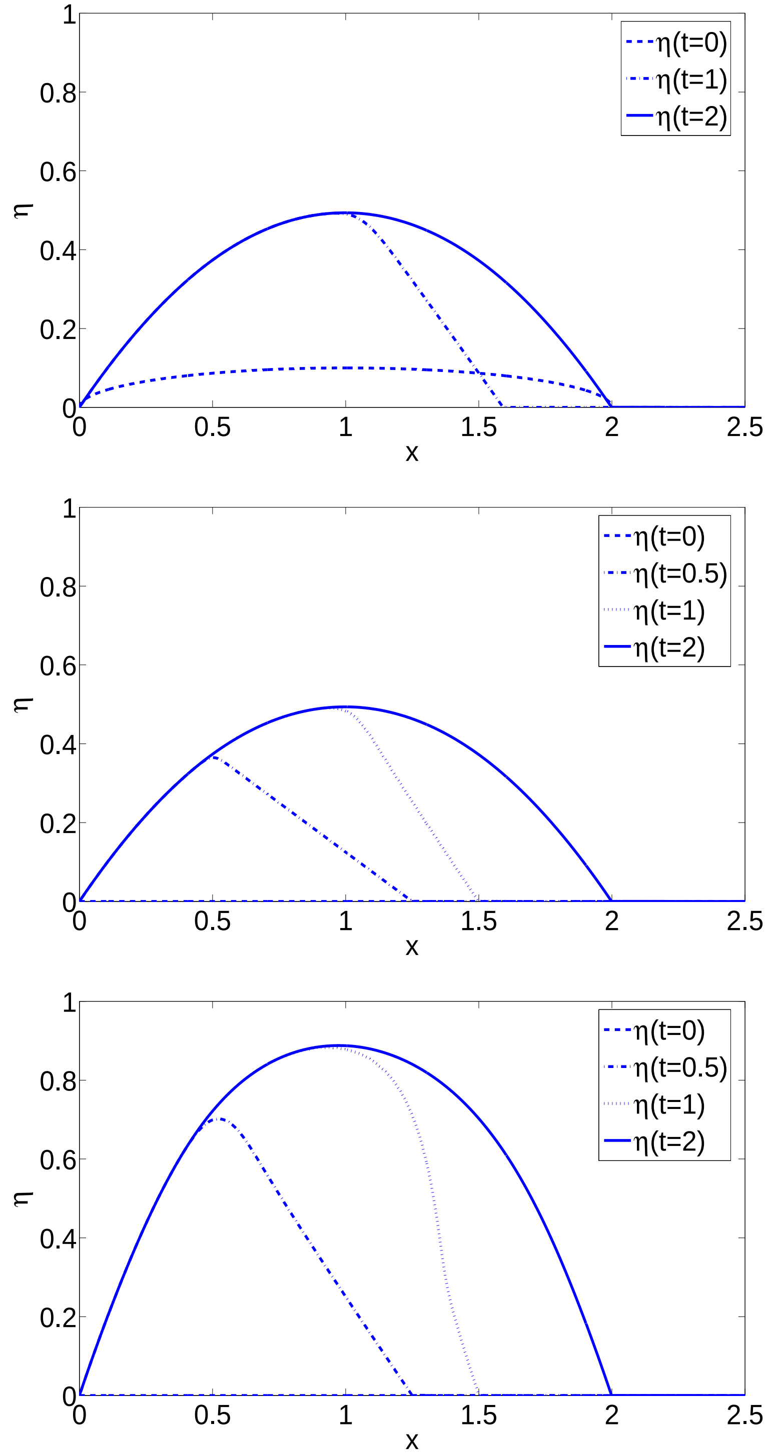

Figure 3.5: Computed profiles for the temperate case ($T_0 = 0$) without prescribed flux and with $u_b = 1$. From top to bottom: case $c = 1$ and flat bottom initial condition, case $c = 1$ and zero initial condition and case $c = 2$ and zero initial condition.

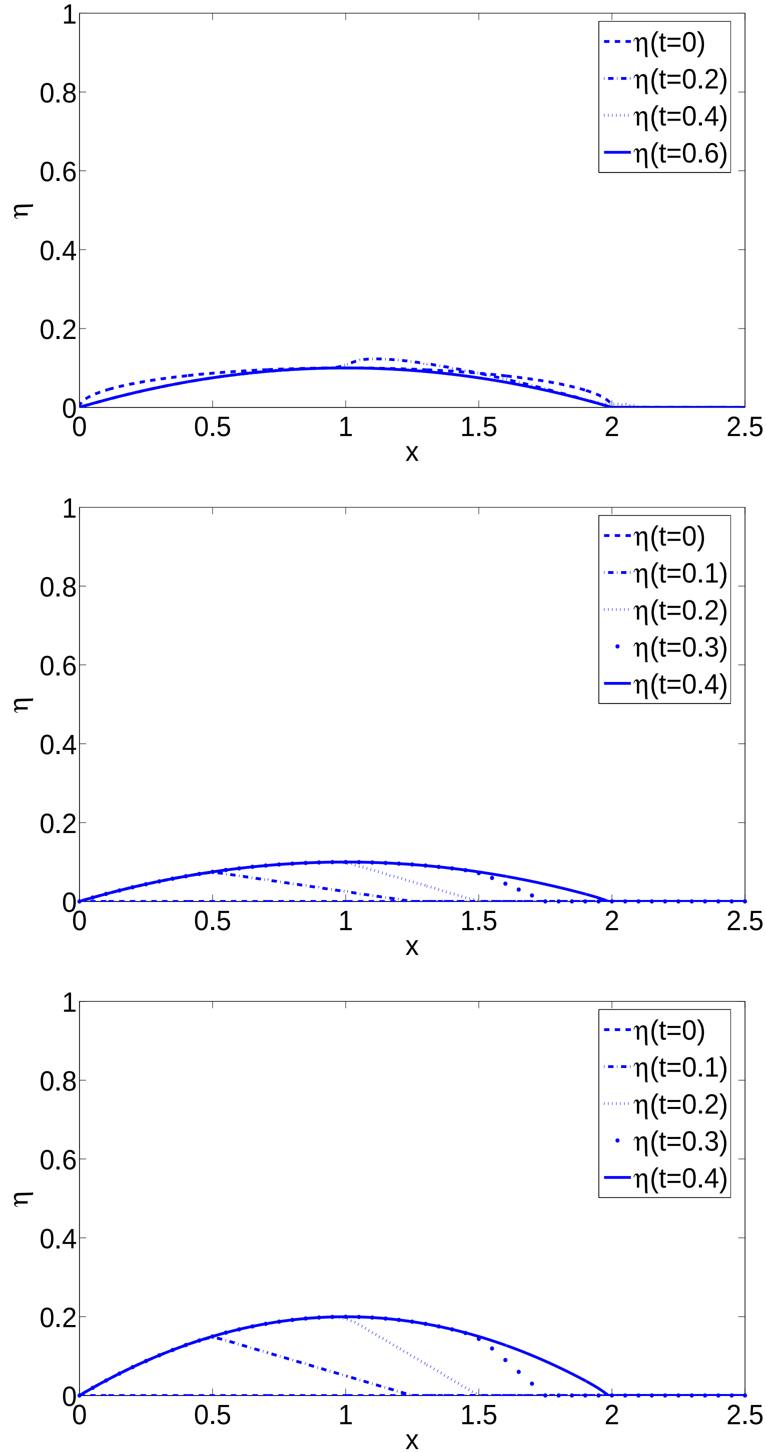

Figure 3.6: Computed profiles for the temperate case ($T_0 = 0$) without prescribed flux and with $u_b = 5$. From top to bottom: case $c = 1$ and flat bottom initial condition, case $c = 1$ and zero initial condition and case $c = 2$ and zero initial condition.

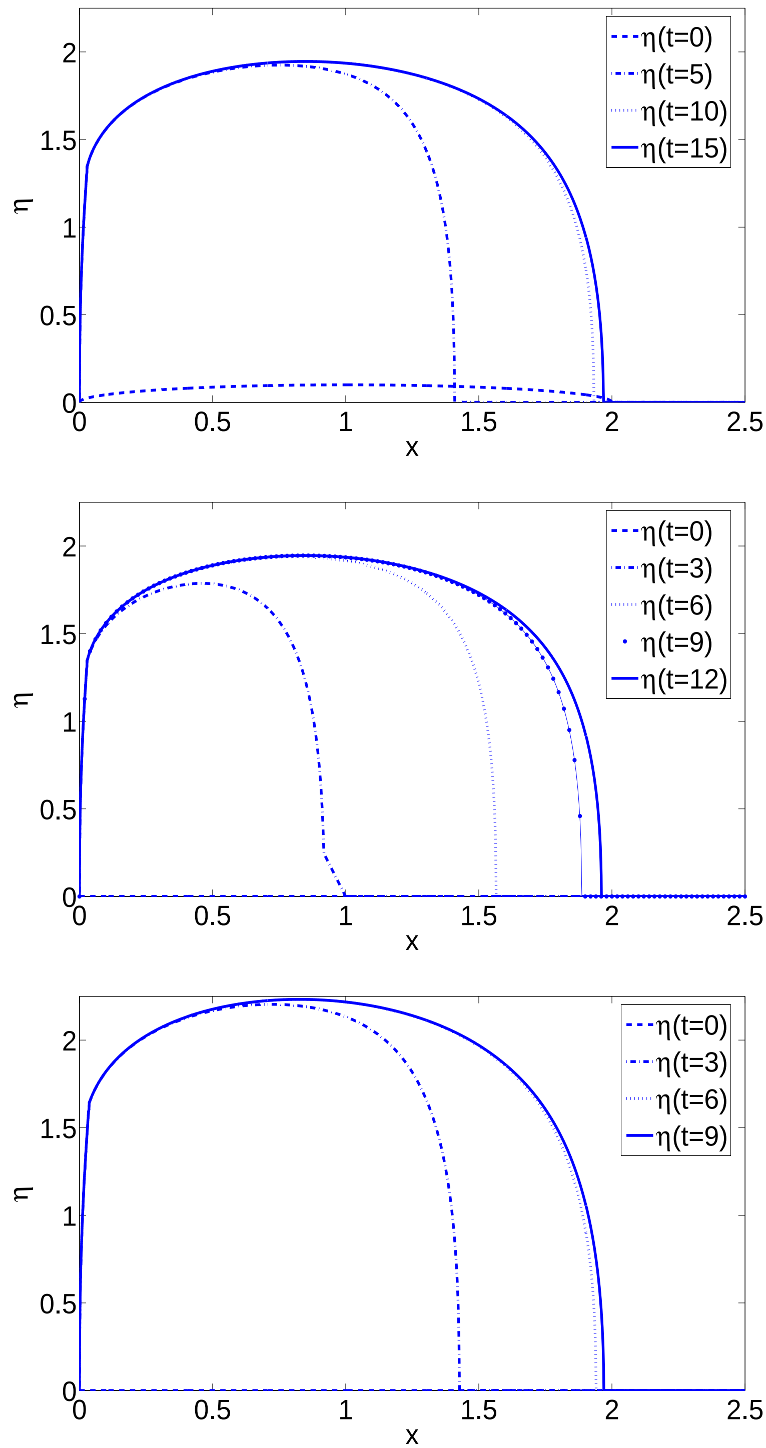

Figure 3.7: Computed profiles for the polar case ($T_0 = -1$) without prescribed flux and with $u_b = 0$. From top to bottom: case $c = 1$ and flat bottom initial condition, case $c = 1$ and zero initial condition and case $c = 2$ and zero initial condition.

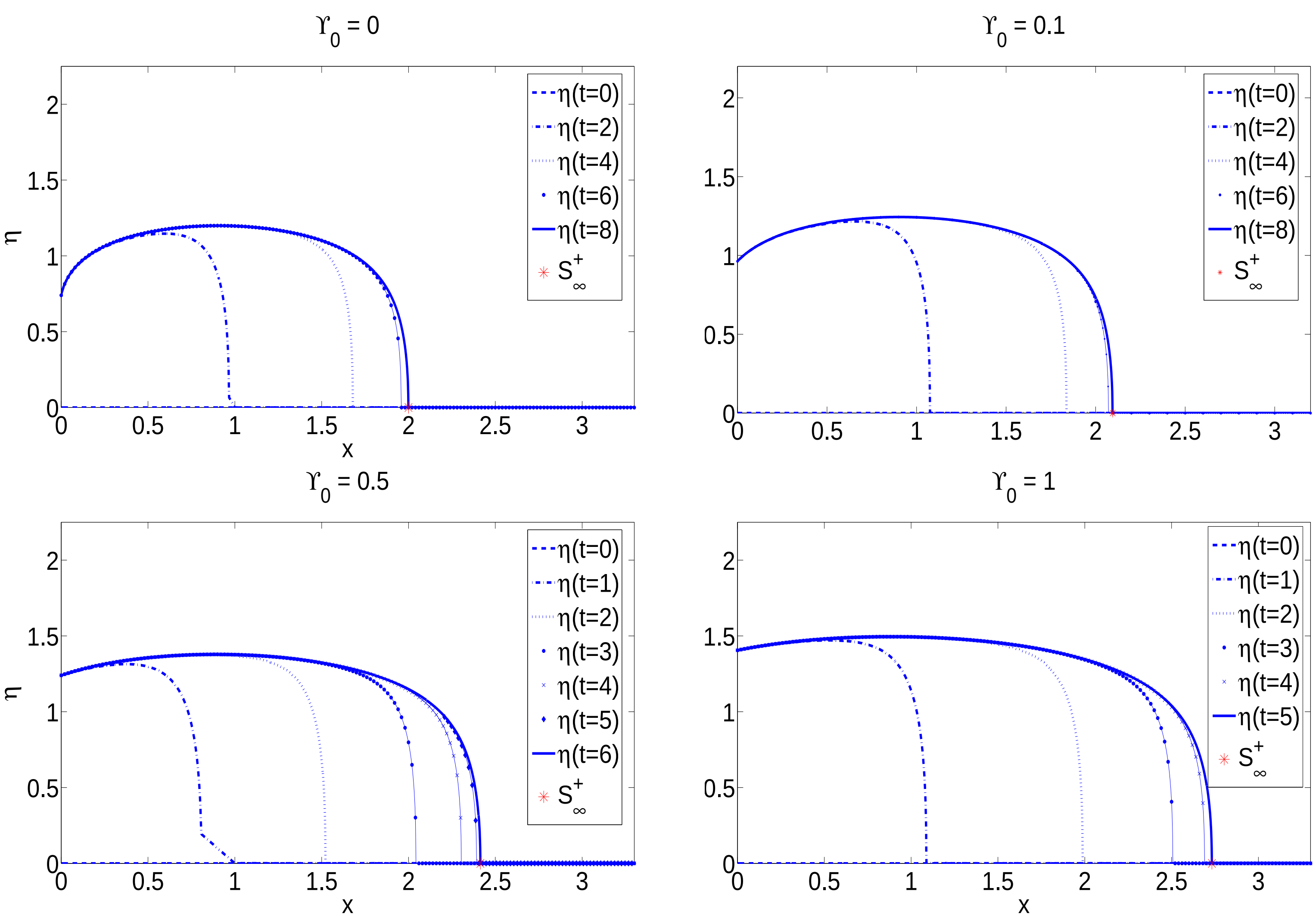

Figure 3.8: Computed profiles for the polar case ($T_0 = -1$), $u_b = 0$, $c = 1$ and with different prescribed fluxes: $\Upsilon_0 = 0$, $\Upsilon_0 = 0.1$, $\Upsilon_0 = 0.5$ and $\Upsilon_0 = 1$.

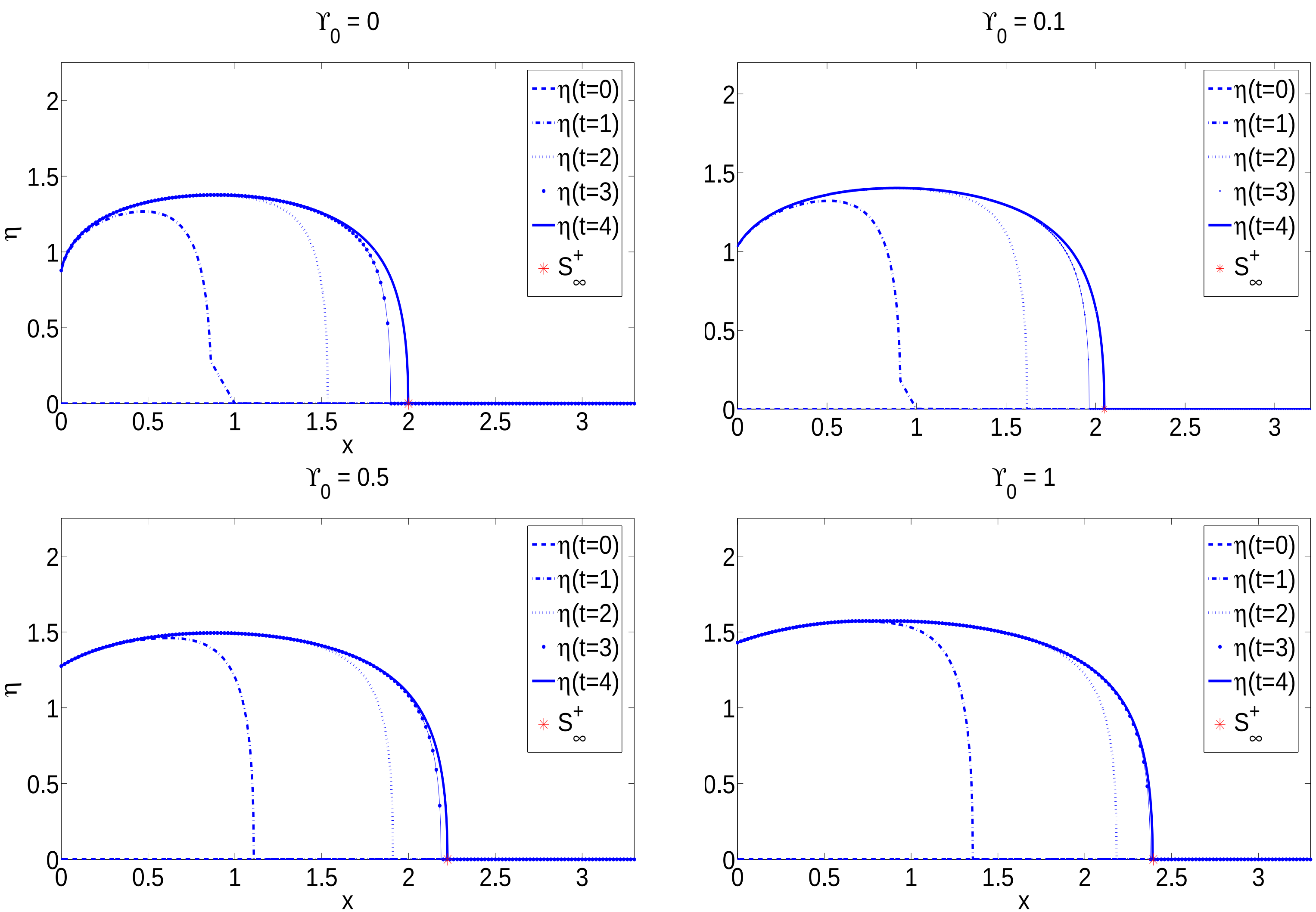

Figure 3.9: Computed profiles for the polar case ($T_0 = -1$), $u_b = 0$, $c = 2$ and with different prescribed fluxes: $\Upsilon_0 = 0$, $\Upsilon_0 = 0.1$, $\Upsilon_0 = 0.5$ and $\Upsilon_0 = 1$.

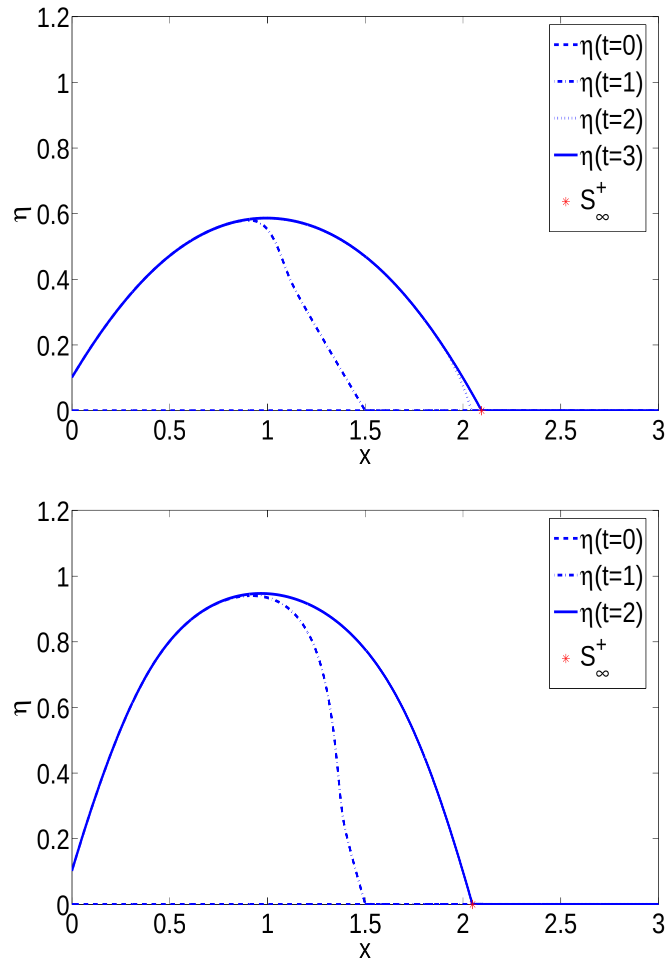

Figure 3.10: Computed profiles for the temperate case ($T_0 = 0$) with prescribed flux $\Upsilon_0 = 0.1$ and $u_b = 1$. From top to bottom: case $c = 1$ and case $c = 2$.

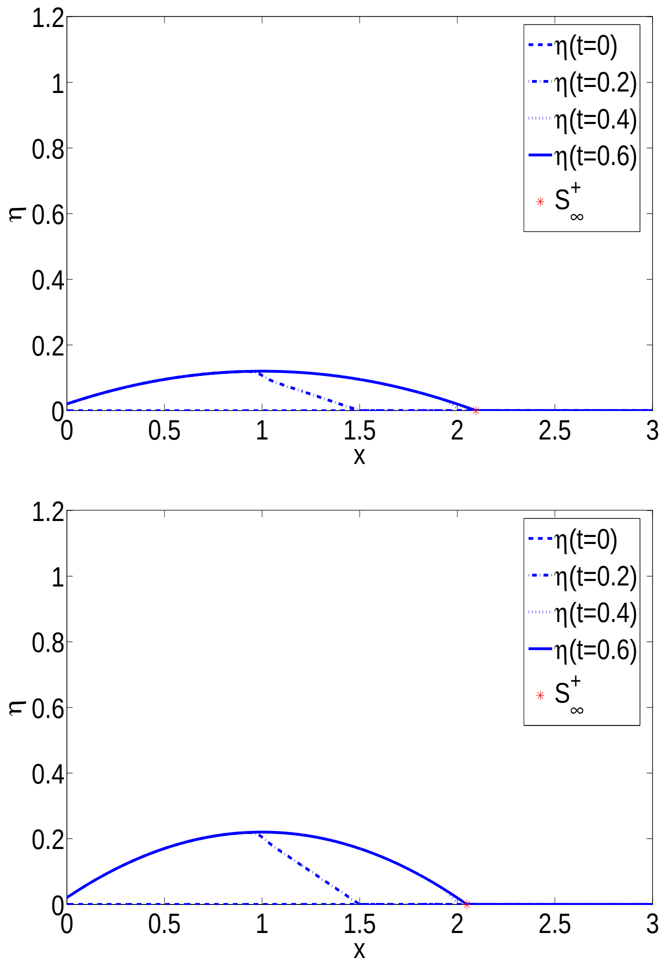

Figure 3.11: Computed profiles for the temperate case ($T_0 = 0$) with prescribed flux $\Upsilon_0 = 0.1$ and $u_b = 5$. From top to bottom: case $c = 1$ and case $c = 2$.

boundary at the steady state solution:

$$x_{front}^{\infty} = \lim_{t\to\infty} x_{front}(t).$$

More precisely, if we define the function η^{∞} by:

$$\eta^{\infty}(x) = \lim_{t\to\infty} \eta(t,x),$$

then, for a time independent accumulation-ablation function, a, we have:

$$a = \frac{\partial \Upsilon^{\infty}}{\partial x},$$

where Υ^{∞} denotes the flux associated to η^{∞}. Next, if we integrate the previous equation between the head and the front of the glacier we get:

$$\int_0^{x_{front}^{\infty}} a(x)\, dx = -\Upsilon_0, \tag{3.51}$$

just by using that $\eta^{\infty}(x_{front}^{\infty}) = \Upsilon(x_{front}^{\infty}) = 0$ and $\Upsilon(0) = \Upsilon_0$.

Now, if the accumulation-ablation function is given by (3.49), then (3.51) leads to equation:

$$c\left(x_{front}^{\infty} - \frac{(x_{front}^{\infty})^2}{2}\right) = -\Upsilon_0,$$

and therefore (the negative root does not correspond to a real situation):

$$x_{front}^{\infty} = 1 + \sqrt{1 + \frac{2\ \Upsilon_0}{c}}. \tag{3.52}$$

From the previous expression, notice that for a given accumulation-ablation function the steady state free boundary x_{front}^{∞} moves to the right when increasing the prescribed flux, Υ_0. Conversely, for fixed values of Υ_0, the free boundary moves to the left when increasing c (we are increasing ablation at the snout region). Moreover, we can compute the value of x_{front} for a given c and Υ_0 values. We compare this exact value of x_{front}^{∞} with the computed value in the polar case in Table 3.11 and for the temperate case in Table 3.12. Notice that the values of the velocity does not affect the position of the free-boundary as expected from expression (3.52), although it modifies the solution.

Υ_0	c=1		c=2	
	exact value	*computed value*	exact value	*computed value*
0	2	*2*	2	*2*
0.1	2.0954	*2.096*	2.0488	*2.049*
0.5	2.4142	*2.414*	2.2247	*2.224*
1	2.7321	*2.732*	2.4142	*2.414*

Table 3.11: Exact and computed values of the free boundary in the polar case with prescribed flux boundary condition and $u_b = 0$.

u_b	c=1		c=2	
	exact value	*computed value*	exact value	*computed value*
1	2.0954	*2.096*	2.0488	*2.049*
5	2.0954	*2.096*	2.0488	*2.049*

Table 3.12: Exact and computed values of the free boundary in the temperate case with prescribed flux $\Upsilon_0 = 0.1$ and with different nonzero basal velocities: $u_b = 1$ and $u_b = 5$.

As argued in [61], the joint consideration in previous examples of small aspect ratio and small slope bedrock justifies the applicability of the SIA approximation. The fixed domain formulation here proposed prevents from using different meshes associated to the basal glacier extent that appears for different time steps.

3.7 Conclusions

In the present chapter, first we have described isothermal SIA models for a valley glacier profile computation. One main novelty relies on their formulation in terms of a new obstacle problem associated to a highly nonlinear convection-diffusion equation. More precisely, we use fixed domain formulations where the unknown moving boundary between the ice covered and ice free regions is implicitly obtained. The modelling of prescribed profile and prescribed flux at the glacier head leads to two different fixed domain formulations, the second one being the more innovative in view of the existing literature. The main advantage with respect to some possible front-tracking alternatives (posing the nonlinear equation in the unknown ice covered domain) comes from our use of a fixed domain and a fixed mesh instead of updating the mesh associated to the ice covered domain at each time step. For the numerical solution, a combination of characteristics method for time discretization, a duality method for the nonlinear obstacle formulation and an appropriate explicit treatment of the nonlinear diffusive term have been considered. Moreover, piecewise linear Lagrange finite elements for the spatial discretization have been used.

Numerical results illustrate the performance of the proposed numerical algorithm and techniques when applied to an academic example with closed form analytical solution. When addressing problems with not know analytical solution, in polar regimes the results show the presence of an infinite slope when a zero profile condition at the head is prescribed. This is motivated by the appearance of unrealistic negative fluxes at the head in this formulation. Therefore, an original and more realistic formulation with prescribed flux at the head is proposed and numerical methods are suitably adapted.

Chapter 4

Numerical Simulation of the Non-Isothermal Coupled Glacier Problems

4.1 Introduction

An original model for the simulation of a valley glacier behavior in the framework of non-isothermal shallow ice approximation models is proposed in this chapter. More precisely, we use the shallow ice approximation already described in Chapter 2 to get a simplified coupled model for the profile, velocity and temperature. As in Chapter 3, the glacier profile is an additional unknown of the problem, thus giving rise to a free boundary feature. Nevertheless, in the thermomechanical model developed in this chapter, the use of an isothermal approximation in the term $A(T)$ to compute the longitudinal velocity is not realistic. The non-isothermal approach is addressed by maintaining a non constant temperature in this term in order to couple the profile, velocity and temperature equations.

In this non-isothermal setting, for a given temperature function and a basal velocity, the profile model is posed as a free boundary obstacle problem associated to a nonlinear parabolic integro-differential equation which governs the profile above the ice covered region. Moreover, for prescribed profile and temperature, the velocity field inside the ice domain can be obtained. Also, from the ice velocity field, the profile, the surface temperature and the basal magnitudes (tension and velocity), a Stefan model with a Signorini boundary condition at the base provides the temperature distribution in the ice region. Finally, from a rheology law, the basal velocity and tension are expressed in terms of the basal temperature.

The previous paragraph summarizes a possible way to uncouple the different involved coupled phenomena. In fact, this idea is used for the numerical solution of the coupled problem which essentially consists of sequentially solving the various uncoupled problems until convergence. This idea has been already used in the case of ice sheets in Calvo–Durany–Vázquez [22].

An additional aspect comes from the use of suitable fixed domain formulations. More precisely, the ice domain is assumed to be contained in a fixed domain which contains not only the ice glacier region but also the atmosphere region around it.

This chapter is organized as follows: In Section 4.2 a non-isothermal coupled model for the glacier evolution is stated, and the corresponding boundary conditions of this coupled model are explained in Section 4.3. Then, in Section 4.4 the fixed domain formulation for the coupled model is posed. Section 4.5 is devoted to the description of the different numerical techniques involved in the proposed algorithm for the numerical solution of the model. Finally, in Section 4.6 several test examples illustrate the performance of the numerical methods.

4.2 Non-isothermal coupled model on the cold ice region

In Chapter 2 we have deduced the main equations defining a *SIA* approximation model to obtain the profile, velocity and temperature in a valley glacier. Notice the coupled feature of the *SIA* model. In Chapter 3 we have used an isothermal approximation to get an uncoupled profile problem, so that the upper profile and the longitudinal extent of the glacier are obtained in terms of a given basal velocity and a prescribed constant ice temperature.

Notice that the isothermal approach relies on the use of a constant temperature in the Frank–Katmeneskii's approximation of the Arrhenius' law. In the present thermocoupled problem we maintain the law (2.87) with non constant temperature in order to get a non-isothermal fully coupled model:

$$A\left(T\left(x,z\right)\right)=e^{\gamma T(x,z)}.$$

More precisely, in the ice region we recover (2.104) as the basic profile equation, which is more complex than the non-linear one treated in the isothermal model of Chapter 3. Moreover, we consider (2.105) as the basic temperature equation in the cold ice region, while the horizontal and vertical components of the velocity field verify equations (2.99) and (2.101), respectively.

Thus, in the cold ice region occupied by ice below melting point, the set of governing equations can be written as follows for the case $b=0$:

$$\frac{\partial \eta}{\partial t}+\frac{\partial}{\partial x}\left(u_b\eta\right)+\frac{\partial}{\partial x}\left[\left(1-\mu\,\frac{\partial \eta}{\partial x}\right)\left|1-\mu\,\frac{\partial \eta}{\partial x}\right|^{n-1}\int_0^{\eta} e^{\gamma T(s)}(\eta-s)^{n+1}ds\right]=a \tag{4.1}$$

$$\frac{\partial T}{\partial t}+\overrightarrow{v}\cdot\nabla T-\beta\frac{\partial^2 T}{\partial z^2}-\alpha e^{\gamma T}\left(\left|1-\mu\,\frac{\partial \eta}{\partial x}\right|(\eta-z)\right)^{n+1}=0 \tag{4.2}$$

$$u=u_b+\left(1-\mu\,\frac{\partial \eta}{\partial x}\right)\left|1-\mu\,\frac{\partial \eta}{\partial x}\right|^{n-1}\int_0^{z} e^{\gamma T(s)}\left(\eta-s\right)^{n}ds \tag{4.3}$$

$$v=-\frac{\partial}{\partial x}\int_0^{\eta} u\;dz. \tag{4.4}$$

4.3 Boundary conditions

The issue of boundary conditions for the profile problem of a valley glacier has been already widely discussed in Section 3.3 for the isothermal setting, so here we just enumerate them.

At the snout of the glacier we assume that it terminates on land, so we have the following Dirichlet homogeneous boundary condition:

$$\eta = 0 \qquad \text{at} \qquad x = x_{front} \tag{4.5}$$

where x_{front} is the snout of the glacier.

At the upstream end of the glacier two alternative conditions on the profile have been analyzed in Chapter 3. Thus, a first condition is:

$$\eta = 0 \qquad \text{at} \qquad x = x_{head}, \tag{4.6}$$

where x_{head} is the head of the glacier. The second possible condition, as discussed in previous chapter, is a more realistic boundary condition, specially if $b = 0$. This alternative boundary condition is to prescribe the flux at the given head of the glacier, as follows:

$$\Upsilon = \Upsilon_0 \qquad \text{at} \qquad x = x_{head}. \tag{4.7}$$

where

$$\Upsilon = u_b \eta + \left(1 - \mu \frac{\partial \eta}{\partial x}\right) \left|1 - \mu \frac{\partial \eta}{\partial x}\right|^{n-1} \int_0^\eta e^{\gamma T(s)} (\eta - s)^{n+1} ds.$$

Regarding the boundary conditions of the thermal problem, we are considering a polythermal glacier regime so that cold ice regions (with ice below melting point) and temperate regions (with ice at melting point) coexist. In any case, we must prescribe thermal boundary conditions at the basal and upper boundaries.

The possible basal boundary conditions for temperature corresponding to both the polar case and the polythermal one are described in Chapter 2. We are interested in a realistic model that includes the presence of temperate ice (ice at melting point). So, we use the following basal condition for polythermal glaciers in our model:

$$T \leq 0, \quad T\left(\frac{\partial T}{\partial \vec{n}} - g_b - \tau_b u_b\right) = 0, \quad 0 \leq \frac{\partial T}{\partial \vec{n}} \leq g_b + \tau_b u_b, \tag{4.8}$$

where g_b and τ_b represent the geothermal flux and the basal shear stress, respectively.

Moreover, this polythermal boundary condition can be expressed as the following Signorini condition at the basal boundary:

$$\begin{aligned} -\frac{\partial T}{\partial z} &= g_b + \tau_b u_b \quad \text{if} \quad T < 0, \\ -\frac{\partial T}{\partial z} &= 0 \quad \text{if} \quad T > 0, \\ 0 < -\frac{\partial T}{\partial z} &< g_b + \tau_b u_b \quad \text{if} \quad T = 0. \end{aligned} \tag{4.9}$$

Theoretically, the ice begins to slide at the base when the basal temperature reaches the melting point and, consequently, basal melt water is produced. But, sliding processes have also been experimentally observed on sub-temperate regions ($T = -4.6\,C$, approximately). So, keeping this in mind and following the work of Blatter and Hutter [6], the basal shear stress, τ_b, and the basal velocity, u_b are modeled by the following expressions:

$$\tau_b = \eta \left(1 - \mu \frac{\partial \eta}{\partial x}\right), \qquad u_b = c_b \left|\tau_b\right| \tau_b e^{T/\delta_b}, \tag{4.10}$$

where $c_b \in (0.1, 10)$ and $\delta_b \ll 1$ are given parameters (see the work of Fowler [32], for example).

As pointed out in Chapter 2, a modelling approach similar to the one proposed in Boukrouche–Saidi [8] for non isothermal lubrication problems results to be far more complex due to the non-Newtonian and phase change features.

The temperature at the glacier surface coincides with the atmospheric temperature. In the case of ice sheet several models have been considered in the literature. Thus, for example in Bueler–Brown–Linge [12], Huybrecht–Payne [56] and Saito–Abe–Ouchi–Blatter [73] a surface temperature depending on the distance to the ice sheet divide is considered. More recently, in Calvo–Durany–Vázquez [23] an atmospheric temperature provided by an Energy Balance Model corrected by the altitude effect is proposed.

In the case of the valley glacier here treated, we keep in mind the troposphere temperature for the glacier surface temperature. The troposphere is the lowest layer of the atmosphere. It extends from the Earth surface to an altitude of 7 kilometers at the poles or 17 kilometers at the equator, with some minor variations due to weather. Notice that the troposphere is mostly heated by energy transfer from the surface, so on average the lowest part of the troposphere is warmest and temperature decreases with altitude. The rate of temperature decrease is known as the temperature lapse rate and it is around 6K per kilometer. Thus, by considering the previous arguments and taking into account that the coordinate system is rotated from the horizontal by the angle δ, we impose that the dimensionless temperature:

$$T_A = T_{A0} - \frac{6}{\Delta T}\left(-x\, d_1 \sin\delta + z\, d_2 \cos\delta\right), \tag{4.11}$$

where $z \geq \eta(t,x)$ and T_{A0} denotes the dimensionless atmospheric temperature at the ground that surrounds the front of the valley glacier.

4.4 Thermocoupled problem over fixed domains

In this section we describe the different subproblems involved in the thermocoupled problem, when it is posed on a fixed domain. The segregation in different subproblems allows us to use a fixed point iteration which splits the solution of the coupled problem into the sequential solution of the three uncoupled problems determining: ice profile, velocity and temperature evolutions.

As in the previous chapter, the profile evolution problem is posed over a $1D$ fixed domain in terms of the accumulation-ablation rate, sliding velocity and temperature. The velocity field problem is posed over a fixed $2D$ domain in terms of the profile, temperature and basal velocity. Next, the temperature problem is posed in terms of profile and velocity over the same $2D$ domain.

Notice that both fixed $1D$ and $2D$ domains contain not only the glacier but also the atmosphere surrounding the glacier. In the subsequent sections we explain how to solve numerically these three problems which are posed over fixed domains.

Let us consider a longitudinal section of a linear valley glacier as shown in Figure 2.1. We assume that shallow ice scaling has been applied so that x is the dimensionless coordinate pointing to the downslope direction while z coordinate points upward in the normal direction to x. As the region occupied by the ice is not known *a priori*, a fixed larger rectangular domain, Ω_G, including not only the longitudinal section of the glacier, $\Omega_I(t)$, but also the atmosphere domain, $\Omega_A(t)$, that surrounds the ice mass, is considered. More precisely, we define the following domains:

$$\Omega_G = \{(x,z)\,/\,0 \leq x \leq x_{\max}, 0 \leq z \leq z_{\max}\}\,, \tag{4.12}$$

$$\Omega_I(t) = \{(x,z)\,/\,x_{head}(t) \leq x \leq x_{front}(t)\,,\ 0 \leq z \leq \eta(t,x)\}, \tag{4.13}$$

$$\Omega_A(t) = \{(x,z)\,/\,(x,z) \in \Omega_G, (x,z) \notin \Omega_I(t)\}, \tag{4.14}$$

where $(x_{head}(t)\,,\ x_{front}(t)) \subset (0,\ x_{\max})$ denotes the unknown basal longitudinal extent of glacier section and η is the dimensionless upper profile function depending on time t and longitudinal coordinate x.

Moreover, in order to impose the boundary conditions we divide the boundary of the glacier into two parts $\partial\Omega_I(t) = \Gamma_0(t) \cup \Gamma_1(t)$, where $\Gamma_0(t)$ corresponds to the lower flat boundary which is in contact with the Earth surface:

$$\Gamma_0(t) = \{(x,z)\,/\,x_{head}(t) \leq x \leq x_{front}(t),\ z = 0\},$$

and $\Gamma_1(t)$ corresponds to the upper boundary that is contact with the atmosphere:

$$\Gamma_1(t) = \{(x,z)\,/\,x_{head}(t) \leq x \leq x_{front}(t),\ z = \eta(t,x)\}.$$

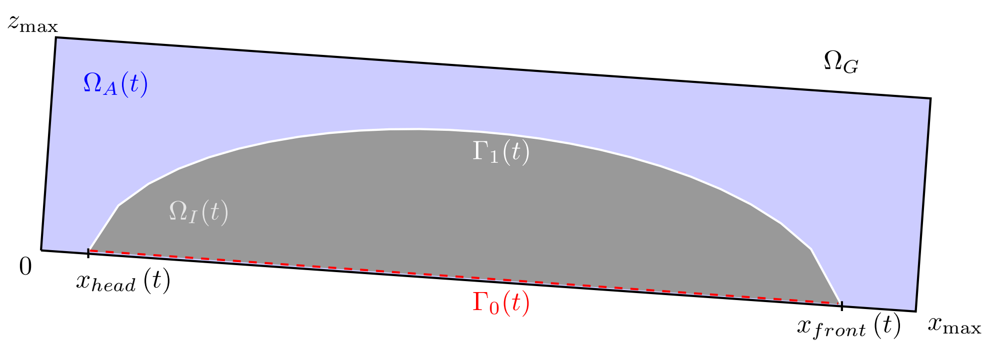

Figure 4.1: Fixed domain and time-dependent subdomains and boundaries at time t

The fixed domain Ω_G and the time-dependent subdomains and boundaries, $\Omega_I(t)$, $\Omega_A(t)$, $\Gamma_0(t)$ and $\Gamma_1(t)$, are illustrated in Figure 4.1.

4.4.1 Non-isothermal profile problem

Equation (4.1) is the basic model for the glacier profile. It consists of an integro-differential equation which is more complex than the non-linear equation (3.3) appearing in Chapter 3, where an isothermal approach has been considered.

Notice that, as in Chapter 3, equation (4.1) is only valid at the points x where $\eta(t,x) > 0$. Also, as in Chapter 3, the set of those points x is an additional unknown of the departure problem because the basal extent of the glacier is unknown. Therefore, these are the typical features of moving boundary problems. So, we pose the analogous appropriate fixed domain formulation in the following paragraph:

Let $(0, t_A)$ be a large enough time interval and let $\Omega = (0,\ x_{\max})$ be also a large enough bounded interval. Notice that Ω is the bottom boundary of the global fixed domain Ω_G. Moreover, if we consider a given accumulation-ablation rate function $a : (0, t_A) \times \Omega \to \mathbb{R}$ and an initial glacier profile $\eta_0 : \Omega \to \mathbb{R}$, then the moving boundary formulation can be stated as follows:

Find the ice covered region $\Gamma(t) = (x_{head}(t), x_{front}(t)) \subset \Omega, \forall t \in [0, t_A]$, *and the profile function* $\eta : \mathcal{P} = U_{t\in[0,t_A]} (\{t\} \times \Gamma(t)) \to \mathbb{R}$, *such that:*

$$\begin{aligned}
\frac{D\eta}{Dt} + \frac{\partial}{\partial x}\left[f_1\left(1 - \mu\frac{\partial\eta}{\partial x}\right)\right] = a \ \ &\text{in } \mathcal{P},\\
\eta > 0 \ \ &\text{in } \mathcal{P},\\
\eta = 0 \ \ &\text{on } (0, t_A) \times \{x_{front}(t)\},\\
\eta = 0 \ \ &\text{on } (0, t_A) \times \{x_{head}(t)\},\\
\eta = \eta_0 \ &\text{in } \{0\} \times (x_{head}(0), x_{front}(0)),
\end{aligned} \tag{4.15}$$

where

$$f_1 = \left|1 - \mu\frac{\partial\eta}{\partial x}\right|^{n-1} \int_0^\eta e^{\gamma T(s)} (\eta - s)^{n+1} d\, s, \tag{4.16}$$

and we use again the notation of material derivative in classical formulation:

$$\frac{D\eta}{Dt} = \frac{\partial\eta}{\partial t} + \frac{\partial}{\partial x}(u_b\eta).$$

In the previous formulation we have chosen the homogeneous Dirichlet boundary condition (4.6) at the unknown upper margin of the glacier. If we had chosen the flux boundary condition (4.7), where $x_{head} = 0$ is the given head of the glacier, the only difference with respect to previous formulation consists of replacing $(4.15)_4$ by the following condition:

$$\Upsilon = \Upsilon_0 \text{ on } (0, t_A) \times \{0\}. \tag{4.17}$$

where Υ_0 is the prescribed flux at the head. Note that with the prescribed flux boundary condition the ice covered region is $\Gamma(t) = (0, x_{front}(t))$, so that the unknown free boundary is the point x_{front}.

With both boundary conditions, the set $\mathcal{P}$ is an additional unknown of the problems. So, as in Chapter 3, we apply fixed domain methods for moving boundary problems. These methods are based on the problem formulation in a fixed given domain $\mathcal{Q} = (0, t_A) \times \Omega$, extending by zero the function η to the points of the set $\mathcal{Q}/\ \mathcal{P}$. So, the 'extended' glacier profile function verifies a nonlinear equation with multivalued operator.

Again, as in Chapter 3, for the sake of simplicity, we also denote by η the unknown associated to the fixed domain. Then, the function η satisfies the equations:

$$\begin{aligned}
\frac{D\eta}{Dt} + \frac{\partial}{\partial x}\left[f_1\left(1 - \mu\frac{\partial\eta}{\partial x}\right)\right] &\geq a \text{ in } \mathcal{Q}, \\
\eta &\geq 0 \text{ in } \mathcal{Q}, \\
\left(\frac{D\eta}{Dt} + \frac{\partial}{\partial x}\left[f_1\left(1 - \mu\frac{\partial\eta}{\partial x}\right)\right]\right)\eta &= a \text{ in } \mathcal{Q}, \\
\eta &= 0 \text{ on } (0, t_A) \times \{x_{\max}\}, \\
\eta &= 0 \text{ on } (0, t_A) \times \{0\}, \\
\eta &= \eta_0 \text{ in } \{0\} \times \Omega.
\end{aligned} \tag{4.18}$$

Notice that in the ice covered region, $\Gamma(t)$, the fact that $\eta(t, x) > 0$ jointly with equation $(4.18)_4$ imply equation $(4.15)_1$. Once again, if we choose the flux boundary condition (4.17) instead of the Dirichlet one, the only difference remains on the substitution of $(4.18)_5$ by (4.17).

Problem (4.18) is classically known in moving boundary literature as a nonlinear parabolic complementarity problem. The mathematical analysis of this complementarity problem (4.18) is an open question. However in the case of ice sheets the theoretical analysis has been studied in [13].

The solution of the previous complementarity problem also provides, for each time t, the glacier boundaries. That is, the necessary geometrical data $\Gamma_0(t)$ and $\Gamma_1(t)$ for the other subproblems.

4.4.2 Velocity field problem

Equations (4.3)–(4.4) are the basic ones to compute the velocity field in the valley glacier. These equations are not valid in the whole domain, Ω_G, because they are just valid in the ice region, $\Omega_I(t)$.

So, we propose the stream function associated to the ice velocity field but now extended to the whole domain in the form:

$$\Upsilon(t,x,z) = \begin{cases} \displaystyle\int_0^z u(t,x,s)\,ds & \text{if} \quad z \le \eta \\ \displaystyle\int_0^\eta u(t,x,s)\,ds & \text{if} \quad z > \eta. \end{cases} \tag{4.19}$$

Therefore, the vertical velocity, v, can be obtained as follows:

$$v(t,x,z) = \begin{cases} -\dfrac{\partial}{\partial x}\Upsilon(t,x,z) & \text{if} \quad z \le \eta \\ 0 & \text{if} \quad z > \eta. \end{cases} \tag{4.20}$$

Notice that once the profile and the temperature functions are known, the velocity field components can be obtained from expressions (4.3) and (4.4) by using numerical differentiation and quadrature formulae.

4.4.3 Thermal problem

In order to pose a thermomechanical coupled problem, the temperature distribution within the glacier has to be obtained from the *SIA*-approximation of the energy equation appearing in the departure continuum mechanics model of Chapter 2 (see equation (2.105)).

Moreover, as we are dealing with polythermal glaciers, which include the presence of temperate ice (i.e. ice at melting point, $T = 0$), and following previous works in ice-sheets (see [20], for example), an appropriate two phase Stefan model is proposed.

Therefore, for each time t, the behavior of polythermal glacier temperature is obtained by solving the following equations:

$$\begin{aligned} \frac{\partial T}{\partial t} + \overrightarrow{v} \cdot \nabla T - \beta \frac{\partial^2 T}{\partial z^2} + \alpha e^{\gamma T} \left(\left| 1 - \mu \frac{\partial \eta}{\partial x} \right| (\eta - z) \right)^{n+1} &= 0 \qquad \text{in } \Omega_C(t), \\ T &\geq 0 \qquad \text{in } \Omega_T(t), \\ \beta \frac{\partial T}{\partial \vec{n}(t)} &= L_c \frac{\partial s}{\partial t} \qquad \text{on } \Sigma(t), \end{aligned} \tag{4.21}$$

where $s = (s_1(t), s_2(t))$ is the parameterization of the moving boundary

$$\Sigma(t) = \{(s_1(t), s_2(t)) / t \in [0, t_A]\},$$

separating the cold and temperate regions:

$$\Omega_C(t) = \{(x, z) \in \Omega_I(t) / T(t, x, z) < 0\},$$

$$\Omega_T(t) = \{(x, z) \in \Omega_I(t) / T(t, x, z) \geq 0\}.$$

Moreover, $\vec{n}(t)$ denotes the unitary normal vector to $\Sigma(t)$ pointing towards $\Omega_C(t)$, and L_c is the dimensionless latent heat.

The nonlinear viscous dissipation term is given by:

$$F_1 = \alpha e^{\gamma T} \left(\left| 1 - \mu \frac{\partial \eta}{\partial x} \right| (\eta - z) \right)^{n+1}. \tag{4.22}$$

The previous set of equations is completed with the boundary conditions defined by equation (4.11) at the glacier surface, and the basal condition (4.9). Moreover, as we are dealing with an evolutive problem an initial temperature has to be considered.

As we will explain later, in fact the enthalpy formulation of the thermal problem only use actually one phase Stefan model (cold region) while the temperate region is provided by the mushy region.

4.5 Numerical methods for the non-isothermal coupled problem

In this section we describe the numerical techniques for the thermomechanical problem. Thus, we propose a fixed point technique which splits the solution of the coupled problem in the sequential solution of several uncoupled problems. These uncoupled problems can be summarized as follows:

1. **Ice profile evolution** in terms of accumulation-ablation rate, sliding velocity and temperature.

2. **Surface temperature** in terms of profile.

3. **Velocity field** in terms of profile and temperature.

4. **Temperature** in terms of profile, velocity field and surface temperature.

4.5.1 Numerical solution of the profile problem

In this section we describe the numerical techniques for the solution of problem (4.18) for given functions a, T and u_b.

Notice that the main difference between the non-isothermal profile problem and the isothermal one is the integral term appearing in the function f_1 in (4.16). In the isothermal problem the result of this integral appears explicitly because we have an isothermal approximation of the Arrhenius's law, and so we can solve the integral analytically.

As we mainly use the same numerical techniques than in the isothermal problem described in Chapter 3, we just describe the numerical solution with Dirichlet boundary conditions starting from the time discretization by the method of characteristics:

For $m = 0, 1, 2, \dots,$ *find* η^{m+1} *such that:*

$$\frac{\eta^{m+1} - J^m\left(\eta^m \circ \chi^m\right)}{\Delta t} + \frac{\partial}{\partial x}\left(\left|1 - \mu \frac{\partial \eta}{\partial x}^{m+1}\right|^2 \left(1 - \mu \frac{\partial \eta}{\partial x}^{m+1}\right) \times \right.$$

$$\left. \times \int_0^{\eta^m} e^{\gamma T(x,s)} \left(\eta^m - s\right)^4 ds\right) - a^{m+1} \geq 0 \text{ in } \Omega,$$

$$\eta^{m+1} \geq 0 \text{ in } \Omega,$$

$$\left[\frac{\eta^{m+1} - J^m\left(\eta^m \circ \chi^m\right)}{\Delta t} + \frac{\partial}{\partial x}\left(\left|1 - \mu \frac{\partial \eta}{\partial x}^{m+1}\right|^2 \left(1 - \mu \frac{\partial \eta}{\partial x}^{m+1}\right) \times \right.\right.$$

$$\left.\left. \times \int_0^{\eta^m} e^{\gamma T(x,s)} \left(\eta^m - s\right)^4 ds\right) - a^{m+1}\right] \eta^{m+1} \geq 0 \text{ in } \Omega,$$

$$\eta^{m+1} = 0 \text{ on } \partial\Omega,$$

$$\eta^0 = \eta_0(x) \text{ in } \Omega, \qquad (4.23)$$

where $a^{m+1} = a((m+1)\Delta t, \cdot)$, and $\circ$ denotes the composition symbol.

In order to solve (4.23), an iterative fixed point technique is applied on the nonlinear diffusive term. In this way, a sequence of linear complementarity problems (indexed by k) is obtained. More precisely, for each m, we initialize $\eta^{m+1,0}$, for example, $\eta^{m+1,0} = \eta^m$, and the following problem has to be solved at each time step $k+1$:

Find $\eta^{m+1,k+1}$ *such that:*

$$\frac{\eta^{m+1,k+1} - J^m\left(\eta^m \circ \chi^m\right)}{\Delta t} +$$

$$+ \frac{\partial}{\partial x}\left(f_1^{m+1,k}\left(1 - \mu \frac{\partial \eta}{\partial x}^{m+1,k+1}\right)\right) - a^{m+1} \geq 0 \quad \text{in} \quad \Omega,$$

$$\eta^{m+1,k+1} \geq 0 \quad \text{in} \quad \Omega,$$

$$\left[\frac{\eta^{m+1,k+1} - J^m\left(\eta^m \circ \chi^m\right)}{\Delta t} + \right.$$

$$\left. + \frac{\partial}{\partial x}\left(f_1^{m+1,k}\left(1 - \mu \frac{\partial \eta}{\partial x}^{m+1,k+1}\right)\right) - a^{m+1}\right] \eta^{m+1,k+1} = 0 \quad \text{in} \quad \Omega,$$

$$\eta^{m+1,k+1} = 0 \quad \text{on} \quad \partial\Omega, \quad (4.24)$$

where

$$f_1^{m+1,k} = \left|1 - \mu \frac{\partial \eta}{\partial x}^{m+1,k}\right|^2 \int_0^{\eta^m} e^{\gamma T(x,s)} \left(\eta^m - s\right)^4 .$$

Notice that problem (4.24) can be rewritten as follows:

Find $\eta^{m+1,k+1}$ such that:

$$\begin{aligned}
&\frac{\eta^{m+1,k+1} - J^m\left(\eta^m \circ \chi^m\right)}{\Delta t} + \\
&\qquad + \mu \frac{\partial}{\partial x}\left(f_1^{m+1,k} \frac{\partial \eta}{\partial x}^{m+1,k+1}\right) + f_2^{m+1,k} - a^{m+1} \geq 0 \quad \text{in} \quad \Omega, \\
&\qquad \eta^{m+1,k+1} \geq 0 \quad \text{in} \quad \Omega, \\
&\Bigg[\frac{\eta^{m+1,k+1} - J^m\left(\eta^m \circ \chi^m\right)}{\Delta t} + \\
&\qquad + \mu \frac{\partial}{\partial x}\left(f_1^{m+1,k} \frac{\partial \eta}{\partial x}^{m+1,k+1}\right) + f_2^{m+1,k} - a^{m+1}\Bigg] \eta^{m+1,k+1} = 0 \quad \text{in} \quad \Omega, \\
&\qquad \eta^{m+1,k+1} = 0 \quad \text{on} \quad \partial\Omega, \qquad (4.25)
\end{aligned}$$

where

$$f_2^{m+1,k} = \frac{\partial f_1}{\partial x}^{m+1,k} = \frac{\partial}{\partial x}\left(\left|1 - \mu \frac{\partial \eta}{\partial x}^{m+1,k}\right|^2 \int_0^{\eta^m} e^{\gamma T(x,s)} \left(\eta^m - s\right)^4 ds\right).$$

Now, to solve (4.25), we use the equivalent variational inequality formulation:

Find $\eta^{m+1,k+1} \in K$ such that:

$$\begin{aligned}
&\frac{1}{\Delta t} \int_\Omega \eta^{m+1,k+1} \left(\varphi - \eta^{m+1,k+1}\right) d\Omega + \\
&+\mu \int_\Omega f_1^{m+1,k} \frac{\partial \eta}{\partial x}^{m+1,k+1} \frac{\partial}{\partial x} \left(\varphi - \eta^{m+1,k+1}\right) d\Omega \geq \\
&\geq \frac{1}{\Delta t} \int_\Omega J^m\left(\eta^m \circ \chi^m\right)\left(\varphi - \eta^{m+1,k+1}\right) d\Omega - \\
&- \int_\Omega f_2^{m+1,k} \left(\varphi - \eta^{m+1,k+1}\right) d\Omega + \\
&+ \int_\Omega a^{m+1} \left(\varphi - \eta^{m+1,k+1}\right) d\Omega, \qquad \forall \varphi \in K, \qquad (4.26)
\end{aligned}$$

where $K = \{\varphi \in H_0^1(\Omega) / \varphi \geq 0 \text{ a.e. in } \Omega\}$.

For the classical relation between the variational inequality, the linear complementarity problem and the obstacle problem we direct the reader to Elliot–Ockendon [30], for example. Notice that the nonlinear diffusive term in (4.26) is analogous to the one appearing in the isothermal problem in (3.24). So, the duality algorithm proposed in [5] is also applied to this variational inequality formulation. For this purpose, inequality (4.26) is expressed in terms of the indicatrix function I_K, of the convex K, in the form:

Find $\eta^{m+1} \in K$ such that:

$$\begin{aligned}
&\frac{1}{\Delta t}\int_\Omega \eta^{m+1,k+1}\left(\varphi - \eta^{m+1,k+1}\right) d\Omega + \\
&+\mu \int_\Omega f_1^{m+1,k}\,\frac{\partial \eta}{\partial x}^{m+1,k+1}\frac{\partial}{\partial x}\left(\varphi - \eta^{m+1,k+1}\right) d\Omega + \\
&+I_K\left(\varphi\right) - I_K\left(\eta^{m+1,k+1}\right) \geq \\
&\geq \frac{1}{\Delta t}\int_\Omega J^m\left(\eta^m \circ \chi^m\right)\left(\varphi - \eta^{m+1,k+1}\right) d\Omega - \\
&-\int_\Omega f_2^{m+1,k}\left(\varphi - \eta^{m+1,k+1}\right) d\Omega + \\
&+\int_\Omega a^{m+1}\left(\varphi - \eta^{m+1,k+1}\right) d\Omega, \qquad \forall \varphi \in K,
\end{aligned} \tag{4.27}$$

where

$$I_K\left(\varphi\right) = \begin{cases} 0 & \text{if } \varphi \in K \\ \infty & \text{otherwise.} \end{cases} \tag{4.28}$$

The subdifferential calculus leads to the equivalent formulation:

$$\xi^{m+1,k+1} \;=\; -\left(\mathcal{A}\left(\eta^{m+1,k+1}\right) - g^{m+1,k}\right) \;\in\; \partial I_K\left(\eta^{m+1,k+1}\right), \tag{4.29}$$

where $\partial I_K\left(u\right)$ denotes the subdifferential of I_K at the point u, the operator $\mathcal{A}$: $H_0^1\left(\Omega\right) \rightarrow H^{-1}\left(\Omega\right)$ is defined by:

$$\left(\mathcal{A}\left(\varphi\right), \psi\right) \;=\; \frac{1}{\Delta t}\int_\Omega \varphi\,\psi\,d\Omega \;+\; \mu\int_\Omega f_1^{m+1,k}\,\frac{\partial \varphi}{\partial x}\,\frac{\partial \psi}{\partial x}\,d\Omega, \tag{4.30}$$

and the element $g^{m+1,k} \in H^{-1}\left(\Omega\right)$ is given by:

$$\left(g^{m+1,k}, \psi\right) \;=\; \frac{1}{\Delta t}\int_\Omega J^m\left(\eta^m \circ \chi^m\right)\,\psi\,d\Omega - \int_\Omega f_2^{m+1,k}\,\psi\,d\Omega + \int_\Omega a^{m+1}\,\psi\,d\Omega. \tag{4.31}$$

Therefore, equation (4.29) is equivalent to the following problem:

Find $\eta^{m+1,k+1} \in H_0^1(\Omega)$ *such that:*

$$\frac{1}{\Delta t}\int_\Omega \eta^{m+1,k+1}\,\psi\,d\Omega\ + \int_\Omega \xi^{m+1,k+1}\,\psi\,d\Omega\ +$$
$$\mu\,\frac{e^{\gamma T_0}}{5\nu}\int_\Omega f_1^{m+1,k}\,\frac{\partial\eta}{\partial x}^{m+1,k+1}\frac{\partial\psi}{\partial x}\,d\Omega - \frac{1}{\Delta t}\int_\Omega J^m\left(\eta^m\circ\chi^m\right)\psi\,d\Omega\ =$$
$$= \int_\Omega a^{m+1}\,\psi\,d\Omega\ -\ \int_\Omega f_2^{m+1,k}\,\psi\,d\Omega, \qquad \forall\psi\in H_0^1(\Omega)\,, \tag{4.32}$$

with

$$\xi^{m+1,k+1} \in \partial I_K\left[\eta^{m+1,k+1}\right] \tag{4.33}$$

The method proposed in [5] to solve the nonlinear problem (4.32)–(4.33) introduces a new unknown, $q^{m+1,k+1}$, (multiplier) defined by:

$$q^{m+1,k+1} \in \partial I_K\left[\eta^{m+1,k+1}\right] - \omega\eta^{m+1,k+1}, \tag{4.34}$$

in terms of a positive parameter ω. Thus, equation (4.32) can be written as follows:

Find $\eta^{m+1,k+1} \in H_0^1(\Omega)$ *such that:*

$$\frac{1}{\Delta t}\int_\Omega \eta^{m+1,k+1}\,\psi\,d\Omega + \int_\Omega \left(q^{m+1,k+1} + \omega\,\eta^{m+1,k+1}\right)\psi\,d\Omega +$$
$$+\,\mu\,\frac{e^{\gamma T_0}}{5\nu}\int_\Omega f_1^{m+1,k}\,\frac{\partial\eta}{\partial x}^{m+1,k+1}\frac{\partial\psi}{\partial x}\,d\Omega = \frac{1}{\Delta t}\int_\Omega J^m\left(\eta^m\circ\chi^m\right)\psi\,d\Omega +$$
$$+ \int_\Omega a^{m+1}\,\psi\,d\Omega - \int_\Omega f_2^{m+1,k}\,\psi\,d\Omega, \qquad \forall\psi\in H_0^1(\Omega)\,, \tag{4.35}$$

where $q^{m+1,k+1}$ verifies (4.34).

As ∂I_K is an maximal monotone operator, in [5] it is proved that the following conditions are equivalent

$$q^{m+1,k+1} \in \left(\partial I_K - \omega I\right)\left(\eta^{m+1,k+1}\right), \tag{4.36}$$
$$q^{m+1,k+1} = \left(\partial I_K\right)_\lambda^\omega\left[\eta^{m+1,k+1} + \lambda q^{m+1,k+1}\right], \tag{4.37}$$

where $\left(\partial I_K\right)_\lambda^\omega$ is the Yosida approximation of operator $\left(\partial I_K - \omega I\right)$ with parameter $\lambda > 0$.

The duality algorithm proposed for the non-isothermal case is the same that the algorithm proposed for the isothermal one, the only difference with respect to the isothermal case remains in the expression of $f_1^{m+1,k}$. Next, in order to discretize in space equations (4.35)–(4.37) we take the same mesh, finite elements spaces and sets used for the isothermal problem (3.25)–(3.27). Then, the fully discretized profile problem can be posed as follows:

Find $\eta_l^{m+1} \in V_{0l}$ *such that:*

$$\left(\frac{1}{\Delta t}+\omega\right)\int_\Omega \eta_l^{m+1,k+1}\,\psi_l\,d\Omega + \mu\int_\Omega f_{1l}^{m+1,k}\,\frac{\partial \eta_l}{\partial x}^{m+1,k+1}\,\frac{\partial \psi_l}{\partial x}\,d\Omega = \\ = -\int_\Omega q_l^{m+1,k+1}\,\psi\,d\Omega + \frac{1}{\Delta t}\int_\Omega J^m\left(\eta_l^m \circ \chi^m\right)\,\psi_l\,d\Omega + \\ + \int_\Omega a_l^{m+1}\,\psi_l\,d\Omega - \int_\Omega f_{2l}^{m+1,k}\,\psi_l\,d\Omega, \quad \forall \psi_l \in V_{0l} \tag{4.38}$$

To compute the nonlinear diffusive coefficient, $f_1^{m+1,k}$, we use a quadrature trapezoidal rule in expression (4.16). More precisely, in the proposed time stepping algorithm for the coupled problem explained in Section 4.5.5, we take the temperature in the expression (4.16) as the corresponding to the previous time step, i.e. $T = T^m$. Notice that T^m has been previously approximated in the thermal problem on the $2D$ mesh nodes.

Therefore, in practice, the procedure to compute f_1^m by numerical integration requires some technical skills to handle the appropriate quadrature nodes. More precisely, first for each node x_i in the $1D$-mesh, the intersection points between the triangle edges in the $2D$ ice domain mesh and the straight line from x_i to $\eta(x_i)$ must to be computed to define these points as quadrature nodes for the numerical integration procedure. Moreover, the integrand values at the quadrature nodes are obtained by using their barycentric coordinates and the associated piecewise linear interpolation from the values at the corresponding triangle vertices.

Notice that the solution of the nonlinear problem (4.38)–(4.37) is obtained by a fixed point iteration as in the isothermal case (see Chapter 3)

4.5.2 Computation of the velocity field

In order to obtain the velocity field, we use appropriate numerical integration in expressions (4.3) and (4.19) to approximate the horizontal velocity and the stream functions, and numerical derivation in (4.20) to compute the vertical component of the velocity. As the integrands appearing in (4.3) and (4.19) are known at the $2-D$ mesh nodes, the technical skills in the numerical integration procedure are analogous to the ones described for expression f_1^m.

4.5.3 Numerical computation of the glacier surface temperature and atmosphere temperature

Both glacier surface and atmosphere temperature are obtained from expression (4.11). More precisely, the value of this expression is prescribed in the thermal problem at each 2D mesh node verifying $z_i \geq \eta(x_i)$ (in the same way as Dirichlet boundary conditions are presented in finite element methods).

4.5.4 Numerical solution of the thermal problem

In this section we describe the numerical methods to obtain the ice temperature from the profile function and velocity field.

For this purpose, following the ideas developed in [20] for the case of ice sheets, we introduce the variational formulation of the thermal problem as a previous step to build an appropriate numerical algorithm to simulate the temperature inside the glacier.

In a first step to obtain the variational formulation, we introduce the Heaviside multivalued operator:

$$H(s) = \begin{cases} 1 & if \quad s > 0 \\ [0,\ 1] & if \quad s = 0 \\ 0 & if \quad s < 0 \end{cases}$$

to express the Signorini type basal boundary condition (4.9) on $\Gamma_0(t)$ by means of this multivalued operator in the form:

$$\frac{\partial T}{\partial \vec{n}} \in (g_b + \tau_b u_b)\,(1 - H\,(T)) \quad \Leftrightarrow \quad \frac{\partial T}{\partial \vec{n}} - (g_b + \tau_b u_b) \in -(g_b + \tau_b u_b)\; H\,(T)\,. \tag{4.39}$$

Related to this boundary condition, the convex, lower semicontinuous functional J:

$$J\,(\varphi) = \int_{\Gamma_0} (g_b + \tau_b u_b)\,\varphi^+ \,d\sigma, \qquad \forall \varphi \in H^1\,(\Omega)$$

is introduced, where symbol + denotes $(\cdot) = \max\,(\cdot,\ 0)$. So, we obtain the identity:

$$(g_b + \tau_b u_b) - \frac{\partial T}{\partial \vec{n}} \in \partial J\,(T) \;\text{ at } \Gamma_0, \tag{4.40}$$

following classical subdifferential calculus (see [44], for example).

On the other hand, we shall consider the enthalpy formulation for a particular two phase Stefan problem (see [30], for example). Thus, we introduce the enthalpy operator in terms of the reference temperature and the dimensionless latent heat as follows:

$$E\,(T) = \begin{cases} T & \text{if} \quad T < 0, \\ [0, L_c] & \text{if} \quad T = 0, \\ L_c & \text{if} \quad T > 0. \end{cases}$$

Thus, in practice the computed temperature results to be nonpositive and only the cold ice phase and the mushy region (temperate ice) appear [29]. As indicated in [23], in the work of Aschwanden and Blatter [1] a different enthalpy formulation is applied. More precisely, in [1] an enthalpy function is defined in terms of temperature in cold ice region and the water content in the temperate region, associated to a diffusion equation with discontinuous coefficients. Moreover, a regularization of the enthalpy function based on sea ice modelling is chosen. In the present approach, the multivalued enthalpy expression is exactly solved by a duality method, and not by a regularization procedure. Computationally, enthalpy methods represent a clear advantage with respect to front tracking ones.

So, we can write the variational formulation of the Stefan–Signorini problem as follows:

Find $y(t,\cdot) \in V_A(t)$ *such that:*

$$\int_{\Omega_G} \frac{De}{Dt}(\varphi - y)\, d\Omega + \int_{\Omega_G} \frac{\partial y}{\partial z}\frac{\partial}{\partial z}(\varphi - y)\, d\Omega + \delta \int_{\Omega_G} \frac{\partial y}{\partial x}\frac{\partial}{\partial x}(\varphi - y)\, d\Omega +$$
$$+ \int_{\Omega_G} \left(F_1 \circ \Lambda^{-1}\right)(y)(\varphi - y)\, d\Omega - \int_{\Gamma_0(t)} g(\varphi - y)\, d\Gamma +$$
$$+ \beta J(\varphi) - \beta J(y) \geq 0, \quad \forall \varphi \in V_0(t) \tag{4.41}$$
$$e \in \left(E \circ \Lambda^{-1}\right)(y), \tag{4.42}$$

with the notation for the total derivative:

$$\frac{De}{Dt} = \frac{\partial e}{\partial t} + \vec{v} \cdot \nabla e,$$

the classical Kirchoff change of variable:

$$y = \Lambda(T) = \int_0^T \beta\, ds = \beta T, \tag{4.43}$$

and a horizontal diffusion term controlled by the regularization parameter δ. Moreover, β represents the dimensionless thermal conductivity (2.53), and we use the notation $g = \beta g_b$. The Kirchoff change of variable (4.43) generalizes the case where the thermal conductivity is not a constant. However, if we assume that β is a constant, identity (4.43) gives a linear relation between the temperature and the new variable y which makes the numerical computations easier.

The functional sets appearing in (4.41)–(4.42) are defined by the following expressions:

$$V_0 = \left\{ v \in H^1(\Omega) / v = 0 \text{ on } \Gamma_1 \right\},$$

$$V_A = \left\{ v \in H^1(\Omega) / v = \Lambda(T_A) \text{ on } \Gamma_1 \right\}.$$

In order to apply a duality method for the numerical approximation, we use the relations (4.39) and (4.40) between the functional J and the Heaviside operator H to pose the problem (4.41)–(4.42) as follows:

Find $y(t,\cdot) \in V_A$ *such that:*

$$\int_{\Omega_G} \frac{De}{Dt}(\varphi - y)\, d\Omega + \int_{\Omega_G} \frac{\partial y}{\partial z}\frac{\partial}{\partial z}(\varphi - y)\, d\Omega + \delta \int_{\Omega_G} \frac{\partial y}{\partial x}\frac{\partial}{\partial x}(\varphi - y)\, d\Omega +$$
$$+ \int_{\Omega_G} \left(F_1 \circ \Lambda^{-1}\right)(y)(\varphi - y)\, d\Omega - \int_{\Gamma_0(t)} g(\varphi - y)\, d\Gamma +$$
$$+ \int_{\Gamma_0} g\,\theta(\varphi - y)\, d\Gamma = 0, \quad \forall \varphi \in V_0(t), \tag{4.44}$$
$$e \in \left(E \circ \Lambda^{-1}\right)(y), \tag{4.45}$$
$$\theta \in \left(H \circ \Lambda^{-1}\right)(y). \tag{4.46}$$

For the semidiscretization in time of the problem (4.44)–(4.46), we have chosen the particular upwind scheme of characteristics. Pironneau [2, 71] and Douglas–Russell [28] introduced this idea for convection-diffusion equations and Navier–Stokes equations. This method is based on the approximation of the material derivative in the convection term by an upwind quotient in the direction of the integral paths of the velocity field.

Denoting by Δt the time step, the total derivative of the nonlinear enthalpy operator is approximated as follows:

$$\frac{De}{Dt}((m+1)\Delta t, x, z) \approx \frac{e^{m+1} - e^m \circ \chi^m}{\Delta t}, \tag{4.47}$$

where

$$e^{m+1} = e((m+1)\Delta t, x, z),$$

and χ^m is defined by:

$$\chi^m(x,z) = S((m+1)\Delta t, x, z; m\Delta t),$$

with S the trajectory of the velocity field, being solution of the following final value problem:

$$\begin{cases} \frac{dS(t,x,z;s)}{ds} & = & \vec{v}\left(S(t,x,z;s), s\right), \\ s(t,x,z;t) & = & (x,z). \end{cases} \tag{4.48}$$

In practice, the previous o.d.e. problem needs to be numerically solved for a general velocity field. Then the substitution of the approximation (4.47) in (4.44) allow us to pose the following sequence of problems:

Find $y^{m+1} \in V_A$ *such that:*

$$\frac{1}{\Delta t}\int_{\Omega_G} e^{m+1}\,\psi\,d\Omega - \frac{1}{\Delta t}\int_{\Omega_G}\left(e^m \circ \chi^m\right)\psi\,d\Omega + \int_{\Omega_G}\frac{\partial y}{\partial z}^{m+1}\frac{\partial \psi}{\partial z}d\Omega +$$
$$+\,\delta\int_{\Omega_G}\frac{\partial y}{\partial x}^{m+1}\frac{\partial \psi}{\partial x}d\Omega + \int_{\Omega_G}\left(F_1\circ\Lambda^{-1}\right)\left(y^{m+1}\right)\psi\,d\Omega - \int_{\Gamma_0(t)} g\,\psi\,d\Gamma +$$
$$+\int_{\Gamma_0} g\,\theta^{m+1}\,\psi\,d\Gamma = 0, \quad \forall\psi\in V_0\,(t)\,, \tag{4.49}$$

$$e^{m+1} \in \left(E\circ\Lambda^{-1}\right)\left(y^{m+1}\right), \tag{4.50}$$

$$\theta^{m+1} \in \left(H\circ\Lambda^{-1}\right)\left(y^{m+1}\right). \tag{4.51}$$

Once the semidiscretization in time has been applied, the highly nonlinear problem (4.49)–(4.51) must be solved. In fact, we can distinguish three nonlinear aspects: the Signorini type boundary condition on $\Gamma_0\,(t)$, the enthalpy operator and the Frank-Katmeneskii term that appears in the reaction function F_1. Due to the fact that the first two nonlinearities can be associated to a maximal monotone operator we will treat them by means of duality methods. In the following paragraph we detail this technique.

First, in order to apply the Bermudez–Moreno algorithm [5] to (4.51), as in Chapter 3, we introduce a new unknown r^{m+1} and a positive parameter ω_1 such that

$$r^{m+1} \in \left(H\circ\Lambda^{-1}\right)\left(y^{m+1}\right) - \omega_1\,y^{m+1},$$

and then we can rewrite the problem (4.49)–(4.51) in the following equivalent form:

$$\frac{1}{\Delta t}\int_{\Omega_G} e^{m+1}\,\psi\,d\Omega + \int_{\Omega_G}\frac{\partial y}{\partial z}^{m+1}\frac{\partial \psi}{\partial z}d\Omega + \delta\int_{\Omega_G}\frac{\partial y}{\partial x}^{m+1}\frac{\partial \psi}{\partial x}d\Omega +$$
$$+\int_{\Omega_G}\left(F_1\circ\Lambda^{-1}\right)\left(y^{m+1}\right)\psi\,d\Omega + \int_{\Gamma_0(t)} g\,\omega_1\,y^{m+1}\,\psi\,d\Gamma =$$
$$= \frac{1}{\Delta t}\int_{\Omega_G}\left(e^m\circ\chi^m\right)\psi\,d\Omega - \int_{\Gamma_0} g\,r^{m+1}\,\psi\,d\Gamma + \int_{\Gamma_0} g\,\psi\,d\Gamma, \quad \forall\psi\in V_0\,(t)\,, \tag{4.52}$$

$$e^{m+1} \in \left(E\circ\Lambda^{-1}\right)\left(y^{m+1}\right). \tag{4.53}$$

As the operator $H \circ \Lambda^{-1}$ is maximal monotone, we can apply a Bermúdez–Moreno Lemma [5] and get the following equivalence:

$$r^{m+1} \in \left(H \circ \Lambda^{-1} - \omega I\right)\left(y^{m+1}\right) \quad \Leftrightarrow \quad r^{m+1} = \left(H \circ \Lambda^{-1}\right)_{\lambda_1}^{\omega_1}\left(y^{m+1} + \lambda_1\, r^{m+1}\right),$$

where the expression $(H \circ \Lambda^{-1})_{\lambda_1}^{\omega_1}$ denotes the Yosida approximation of the operator $((H \circ \Lambda^{-1}) - \omega_1 I)$ with parameter $\lambda_1 > 0$.

In a second step the same strategy can be use with the maximal monotone enthalpy operator $E \circ \Lambda^{-1}$ by introducing a new variable:

$$s^{m+1} \in \left(E \circ \Lambda^{-1}\right)\left(y^{m+1}\right) - \omega_2\, y^{m+1}$$

in terms of the positive real parameter ω_2, and rewriting the problem (4.49)–(4.51) as follows:

Find $y^{m+1} \in V_A$ such that:

$$\begin{aligned}
&\frac{\omega_2}{\Delta t}\int_{\Omega_G} y^{m+1}\,\psi\, d\Omega + \int_{\Omega_G} \frac{\partial y}{\partial z}^{m+1}\frac{\partial \psi}{\partial z} d\Omega + \delta \int_{\Omega_G} \frac{\partial y}{\partial x}^{m+1}\frac{\partial \psi}{\partial x} d\Omega + \\
&+ \int_{\Omega_G} \left(F_1 \circ \Lambda^{-1}\right)\left(y^{m+1}\right)\,\psi\, d\Omega + \int_{\Gamma_0(t)} g\,\omega_1\, y^{m+1}\,\psi\, d\Gamma = \\
&= \frac{1}{\Delta t}\int_{\Omega_G} \left[\left(E \circ \Lambda^{-1}\right)\left(y^{m+1}\right)\right] \circ \chi^m\,\psi\, d\Omega - \int_{\Gamma_0} g\, r^{m+1}\,\psi\, d\Gamma + \\
&+ \int_{\Gamma_0} g\,\psi\, d\Gamma - \frac{1}{\Delta t}\int_{\Omega_G} s^{m+1}\,\psi\, d\Omega, \quad \forall \psi \in V_0\,(t)\,, \qquad (4.54)\\
&r^{m+1} = \left(H \circ \Lambda^{-1}\right)_{\lambda_1}^{\omega_1}\left(y^{m+1} + \lambda_1\, r^{m+1}\right), \qquad (4.55)\\
&s^{m+1} = \left(E \circ \Lambda^{-1}\right)_{\lambda_2}^{\omega_2}\left(y^{m+1} + \lambda_2\, s^{m+1}\right), \qquad (4.56)
\end{aligned}$$

where the notation $(E \circ \Lambda^{-1})_{\lambda_2}^{\omega_2}$ represents the Yosida approximation of operator $((E \circ \Lambda^{-1}) - \omega_2\, I)$ with parameter $\lambda_2 > 0$.

The problem (4.54)–(4.56) is still nonlinear due to presence of the function F_1. For the treatment of this last nonlinear term we follow the work of Bermúdez–Durany–Posse–Vázquez [4] about convection-diffusion-reaction equations in the context of hypersonic flows. The technique is based on the Newton method to linearize the problem and keeping in mind the finite element product approximations. In the spatial discretization of (4.54) we use piecewise linear Lagrange finite elements (see Ciarlet [24], for example).

For each positive real parameter l, let be τ_l a triangular finite elements mesh of the domain $\overline{\Omega_G}$. The functional space to approximate the formulation (4.54) is the classical finite elements space V_l, and the subsets V_{0l} and V_{Al} are defined by:

$$V_l = \left\{ v_l \in \mathcal{C}^0 \left(\overline{\Omega_G} \right) / v_{l|P} \in P_1, P \in \tau_l \right\},$$

$$V_{0l} = \left\{ v_l \in V_l / v_{l|\Gamma_1} = 0 \right\},$$

$$V_{Al} = \left\{ v_l \in V_l / v_{l|\Gamma_1} = \Lambda \left(T_A \right) \right\}.$$

We denote by N the dimension of V_l, which is equal to the number of nodes of the finite elements mesh. Let $\{w_1, \ldots, w_N\}$ be the base of V_l such that the function w_i is determined by the conditions

$$w_i \left(p_j \right) = \delta_{ij}, \quad j = 1, 2, \ldots, N$$

where $\{p_j, j = 1, \ldots, N\}$ is the set of nodes of the finite elements mesh. So we can pose the discretized problem associated with (4.54)–(4.56) in the following form:

Find $y_l^{m+1} \in V_{Al}$ *such that:*

$$\begin{aligned}
&\frac{\omega_2}{\Delta t} \int_{\Omega_G} y_l^{m+1} \psi_l \, d\Omega + \int_{\Omega_G} \frac{\partial y_l}{\partial z}^{m+1} \frac{\partial \psi_l}{\partial z} d\Omega + \delta \int_{\Omega_G} \frac{\partial y_l}{\partial x}^{m+1} \frac{\partial \psi_l}{\partial x} d\Omega + \\
&+ \int_{\Omega_G} \left(F_1 \circ \Lambda^{-1} \right) \left(y_l^{m+1} \right) \psi_l \, d\Omega + \int_{\Gamma_0(t)} g \, \omega_1 \, y_l^{m+1} \psi_l \, d\Gamma = \\
&= \frac{1}{\Delta t} \int_{\Omega_G} \left[\left(E \circ \Lambda^{-1} \right) \left(y_l^m \right) \right] \circ \chi^m \, \psi_l \, d\Omega - \int_{\Gamma_0} g \, r^{m+1} \, \psi_l \, d\Gamma + \\
&+ \int_{\Gamma_0} g \, \psi_l \, d\Gamma - \frac{1}{\Delta t} \int_{\Omega_G} s^{m+1} \, \psi_l \, d\Omega, \quad \forall \psi \in V_0 \left(t \right),
\end{aligned} \tag{4.57}$$

$$r^{m+1} \left(p_i \right) = \left(H \circ \Lambda^{-1} \right)_{\lambda_1}^{\omega_1} \left(y_l^{m+1} + \lambda_1 \, r^{m+1} \right) \left(p_i \right), \tag{4.58}$$

$$s^{m+1} \left(p_i \right) = \left(E \circ \Lambda^{-1} \right)_{\lambda_2}^{\omega_2} \left(y^{m+1} + \lambda_2 \, s^{m+1} \right) \left(p_i \right). \tag{4.59}$$

In order to approximate the integral of the nonlinear reaction term associated to F_1 we propose the following finite elements product approximation:

$$\int_{\Omega_G} \left(F_1 \circ \Lambda^{-1} \right) \left(y_l^{m+1} \right) \psi_l \, d\Omega \approx \sum_{j=1}^{N} \int_{\Omega_G} \left(F_1 \circ \Lambda^{-1} \right) \left(y_l^{m+1} \left(p_j \right) \right) w_j \, \psi_l \, d\Omega,$$

which is based on the following approximation of F_1:

$$\left(F_1 \circ \Lambda^{-1}\right)\left(y_l^{m+1}\right) \approx \sum_{j=1}^{N} \left(F_1 \circ \Lambda^{-1}\right)\left(y_l^{m+1}\left(p_j\right)\right)\, w_j.$$

So, equation (4.57) is equivalent to the nonlinear system:

$$\begin{aligned}&\left(\frac{\omega_2}{\Delta t} M_l + K_l^{\delta}\right) Y_l^{m+1} + M_l\, G\left(Y_l^{m+1}\right) + N_l\, G_B\left(Y_l^{m+1}\right) = \\ &= \frac{1}{\Delta t} B_l\, Y_l^{m} - b_r^{m+1} - b_g - \frac{1}{\Delta t} b_s^{m+1},\end{aligned} \tag{4.60}$$

where the expressions of the different matrices and vectors are given by:

$$\left(M_l\right)_{ij} = \int_{\Omega_G} w_j\, w_i\, d\Omega, \tag{4.61}$$

$$\left(K_l^{\delta}\right)_{ij} = \int_{\Omega} \frac{\partial w_j}{\partial z}\, \frac{\partial w_i}{\partial z}\, d\Omega + \delta \int_{\Omega} \frac{\partial w_j}{\partial x}\, \frac{\partial w_i}{\partial x}\, d\Omega, \tag{4.62}$$

$$\left(N_l\right)_{ij} = \int_{\Gamma_0} w_j\, w_i\, d\Gamma, \tag{4.63}$$

$$\left(B_l\right)_{ij} = \int_{\Omega_G} w_j \circ \chi_l^{m}\, w_i\, d\Omega \tag{4.64}$$

$$\left(b_r^{m+1}\right)_i = \int_{\Gamma_0} g\, r^{m+1}\, w_i\, d\Gamma, \tag{4.65}$$

$$\left(b_g\right)_i = \int_{\Gamma_0} g\, w_i\, d\Gamma, \tag{4.66}$$

$$\left(b_s^{m+1}\right)_i = \int_{\Omega_G} s^{m+1}\, w_i\, d\Omega, \tag{4.67}$$

and removing dependence of m for the sake of simplicity. The following notation has been used:

$$Y_l = \begin{pmatrix} y_l\left(p_1\right) \\ \vdots \\ y_l\left(p_N\right) \end{pmatrix},\; G\left(Y_l\right) = \begin{pmatrix} \left(F_1 \circ \Lambda^{-1}\right)\left(y_l\left(p_1\right)\right) \\ \vdots \\ \left(F_1 \circ \Lambda^{-1}\right)\left(y_l\left(p_N\right)\right) \end{pmatrix},\; G_B\left(Y_l\right) = \begin{pmatrix} \omega_1\; g\; y_l\left(p_1\right) \\ \vdots \\ \omega_1\; g\; y_l\left(p_N\right) \end{pmatrix}$$

Notice that the matrix B_l, associated with characteristics discretization, cannot be computed exactly. So we propose a numerical approximation of the coefficients based in the following quadrature formula:

$$(B_l)_{ij} = \sum_{P\in\tau_l} \sum_{r=1}^{N_q} \xi_r^P \, w_j \left(\chi^m \left(q_r^P\right)\right) \, w_i \left(q_r^P\right),$$

where N_q is the number of quadrature nodes per triangle, q_r^P is the r-th quadrature node of the triangle P, and ξ_r^P is the weight associated to the r-th quadrature node q_r^P. Vertex, edge mid-points and the Gauss–Lobato formula (see Zienkiewicz–Taylor [78], for example) constitute possible choices.

Moreover, for the same reason, the vectors b_r^{m+1} and b_s^{m+1} need to be numerically approximated. A trapezoidal rule with one degree of precision seems to be adequate.

Now, we explain the numerical simulation algorithm for the fully discretized problem (4.60). First, equations (4.58) and (4.59) let us solve (4.60) at time-iteration $m+1$ using a sort of fixed point technique as follows:

Step 0**:**

- Initialize $b_r^{m+1,0}$ and $b_s^{m+1,0}$, for example to b_r^m and b_p^m, respectively. Those values have been computed in the previous iteration m.

Step j**:**

- Compute $Y_l^{m+1,j}$ solving the following nonlinear system:

$$\left(\frac{\omega_2}{\Delta t} M_l + K_l^\delta\right) Y_l^{m+1,j} + M_l \, G\left(Y_l^{m+1,j}\right) + N_l \, G_B \left(Y_l^{m+1,j}\right) =$$
$$= \frac{1}{\Delta t} B_l \, Y_l^M - b_r^{m+1,j-1} - b_g - \frac{1}{\Delta t} b_s^{m+1,j-1}, \tag{4.68}$$

- Update $(b_r^{m+1})^j$ and $(b_r^{m+1})^j$ using the formulae:

$$r^{m+1,j} = \left(H \circ \Lambda^{-1}\right)_{\lambda_1}^{\omega_1} \left(Y_l^{m+1,j} + \lambda_1 \, r^{m+1,j-1}\right), \tag{4.69}$$
$$s^{m+1,j} = \left(E \circ \Lambda^{-1}\right)_{\lambda_2}^{\omega_2} \left(Y_l^{m+1,j} + \lambda_2 \, s^{m+1,j-1}\right), \tag{4.70}$$

  detailed in the Appendix A.

- Test the convergence of the iterations indexed by j

Several theoretical lemmas about convergence of this algorithm under hypotheses of $\lambda_1\,\omega_1 \leq 0.5$ and $\lambda_2\,\omega_2 \leq 0.5$ are given in [5].

Notice that in the previous algorithm, at each step j we have to solve the nonlinear system (4.68). So, we propose the classical Newton's method. That is, we introduce the vectorial function $\vec{f}$ and we suppress just for simplicity the dependence of l to write the following nonlinear vectorial function:

$$\begin{aligned}\vec{f}\left(Y^{m+1,j}\right) = &\left(\frac{\omega_2}{\Delta t}\,M + K^{\delta}\right)\left(Y^{m+1,j}\right) + N\,G_B\left(Y^{m+1,j}\right) + \\ &+ \sigma\,M\,G\left(Y^{m+1,j}\right) + (1-\sigma)\;M\,G\left(Y^{m+1,j-1}\right) - \\ &- \frac{1}{\Delta t}\,B\,Y^{m} + b_r^{m+1,j-1} - b_g + \frac{1}{\Delta t}\,b_s^{m+1,j-1},\end{aligned} \tag{4.71}$$

with σ a real relaxation parameter such that $0 \leq \sigma \leq 1$. So, if we choose $\sigma = 1$ we get an implicit scheme, and for $\sigma = 0$ an explicit one. Moreover, the system (4.68) can be written at each step j as follows:

$$\vec{f}\left(Y^{m+1,j}\right) = \vec{0},$$

so that Newton's iterations leads to the following algorithm:

Step 0**:** Initialize $Y^{m+1,j,0}$ to $Y^{m+1,j-1}$, for example

Step $k+1$**:** Compute $Y^{m+1,j,k+1}$ by solving the linear system:

$$D\vec{f}\left(Y^{m+1,j,k}\right)\,Y^{m+1,j,k+1} = D\vec{f}\left(Y^{m+1,j,k}\right)\,Y^{m+1,j,k} - \vec{f}\left(Y^{m+1,j,k}\right), \tag{4.72}$$

where $D\vec{f}\left(Y^{k}\right)$ denotes the jacobian matrix of the vectorial function $\vec{f}$ at Y^{k}, given

by

$$D\vec{f}\left(Y^{k}\right) = \left(\frac{\omega_2}{\Delta t}\,M + K^{\delta}\right)\left(Y^{k}\right) + N\,DG_B\left(Y^{k}\right) + \sigma\,M\,DG\left(Y^{k}\right)$$

with the diagonal jacobian matrices $DG\left(Y^{k}\right)$ and $DG_B\left(Y^{k}\right)$ defined by:

$$DG\left(Y^{k}\right) = \left[D\left(F \circ \Lambda^{-1}\right)\right]\left(Y^{k}\right), \qquad DG_B\left(Y^{k}\right) = w_1 g I_N$$

being I_N the identity matrix of order N, and the vector $\vec{f}\left(Y^{m+1,j,k}\right)$ defined by the following expression:

$$\begin{aligned}\vec{f}\left(Y^{m+1,j,k}\right) = &\left(\frac{\omega_2}{\Delta t}\, M + K^{\delta}\right)\left(Y^{m+1,j,k}\right) + N\, G_B\left(Y^{m+1,j,k}\right) + \\ &+ \sigma\, M\, G\left(Y^{m+1,j,k}\right) + (1-\sigma)\ M\, G\left(Y^{m+1,j-1}\right) - \\ &- \frac{1}{\Delta t}\, B\, Y^m + b_r^{m+1,j-1} - b_g + \frac{1}{\Delta t}\, b_s^{m+1,j-1}. \end{aligned} \tag{4.73}$$

Finally, at each step j, we have to solve the linear system (4.72) using the method of preconditioned bi-conjugate stabilized gradient method (see [76] for details). The use of this technique is due to the fact that the coefficient matrix is not always well conditioned nor positive definite.

4.5.5 Algorithm for the fully coupled problem

The final objective is to compute the profile, the surface temperature, the velocity and the temperature distribution of the valley glacier as well as the corresponding basal magnitudes.

For this purpose, we sequentially solve the specific equations by using the previously described numerical strategies.

In fact, the pseudocode of the algorithm remains as follows:

Step 0**:**

- Fixed domains meshing: $[0, x_{\max}]$ for profile problem and Ω_G for velocity and temperature problems.
- Initialize temperature ($T^0 = T_0$), surface temperature (T_A^0), and profile ($\eta^0 = \eta_0$).

Step $m+1$**:** Compute the unknowns at time $t^{m+1} = (m+1)\Delta t$.

- From u_b^m and T^m, computation of $\eta^{m+1}(x)$, $x_{head}(t^{m+1})$, $x_{front}(t^{m+1})$, by solving (4.38).
- Identification of the sets $\Omega_I(t^{m+1})$, $\Omega_A(t^{m+1})$, $\Gamma_0(t^{m+1})$ and $\Gamma_1(t^{m+1})$.

- Computation of the velocities, u^{m+1} and v^{m+1}, with the appropriate numerical approximation of expressions (4.3) and (4.20).
- Obtain the surface temperature T_A^{m+1} from (4.11).
- Obtain T^{m+1}, by numerically solving (4.21) at step $m+1$.
- Update basal velocity and shear stress, u_b^{m+1} and τ_b^{m+1}, with the expressions (4.10).

4.6 Numerical tests

In this section several numerical examples based on typical data for polar and temperate glaciers are presented to illustrate the performance of the algorithm described in the previous sections to solve the problem (4.1)–(4.4).

In our examples, the values of length and height are $d_1 = 10$km and $d_2 = 132$m, respectively. Moreover, a slope of $\delta = 10°$ has been considered.

Thus, we always consider the reference domain Ω_G defined by (4.12) with the particular values of $x_{\max} = 3$ and $z_{\max} = 4$:

$$\Omega_G = \{(x, z)\,/0 \le x \le 3, 0 \le z \le 4\}\,.$$

As in the isothermal profile model, we have considered an accumulation-ablation function of order $\mathcal{O}\,(1)$, with accumulation taking place on the left part (upper glacier region) and ablation occurring on the right part (lower glacier region). More precisely, we take expression (3.49) with $c = 1$:

$$a\,(t, x) = 1 - x. \tag{4.74}$$

Moreover, also as in the case of isothermal glaciers, we have considered the zero profile as initial condition. Besides, we select 271K as atmospheric temperature at the bottom-right of the domain.

For the numerical simulation in the profile problem, a uniform finite element mesh with 2001 nodes for the interval [0, 3] is considered. Moreover, for the domain Ω_G

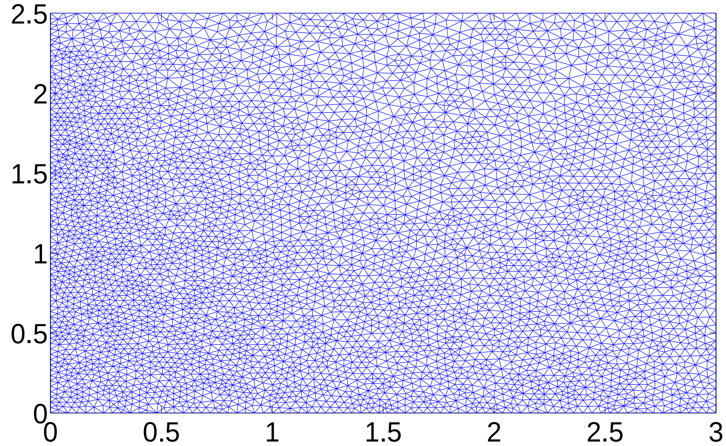

Figure 4.2: Mesh over the fixed domain

we use the unstructured and locally refined triangular finite elements mesh which is plotted in Fig. 4.2, with 9098 triangular finite elements and 4675 vertex. The mesh has been generated from the software toolbox EMC^2 (*Edition de Maillages et de Contours en 2 Dimensions*) which is a portable, interactive and graphic software for edition of two dimensional geometries and meshes [51].

In the profile problem, a time step of $\Delta t = 10^{-6}$, which represents 1.3158×10^{-4} years (about 70 minutes), has been chosen, and the parameter $\omega = 1$ in the duality method has been considered. For the thermal problem, the analogous involved parameters are $\Delta t = 10^{-4}$, which represents 0.0132 years (about 4.8 days), and $\omega_1 = 100$ and $\omega_2 = 10$ in the duality method.

4.6.1 Example 1. Cold-based ice without prescribed flux

The first example corresponds to a glacier with polar regime at the base, so that the geothermal heat must be small enough. The parameters used in this test are:

$$\Delta T = 40,\ \gamma = 5,\ g_b = 0.2,\ \alpha = 0.125,\ \beta = 2.9,\ \text{and}\ \varepsilon = 0.13.$$

Fig. 4.3 shows the time evolution of the glacier profile and velocity field. More precisely, their behaviour at $t = 1$, 5, 15 and 20 are presented. Notice that the computed solutions for $t = 20$ correspond to the steady state. Moreover, the right hand side free boundary point in the obstacle problem (which separates the ice-covered and ice-free regions) is placed at $x = 1$ since almost the beginning of the time evolution until it starts moving monotonically to the right once the slope of the profile function reaches a large enough value. This kind of *waiting time property* has been also observed in [13] for the case of ice sheets and also appears in all the following examples. Fig. 4.4 shows the basal temperature which is everywhere below melting point, as expected in the cold-based case. Moreover, in the ice free region the temperature linearly decreases with altitude as assumed for the atmosphere temperature. Fig. 4.5 shows the basal stress. Notice that the computed basal velocity results to be equal to zero, as expected for a polar basis. Finally, Fig. 4.6 shows the temperature distribution in the glacier and the surrounding atmosphere for $t = 5$, $t = 15$ and $t = 20$.

4.6.2 Example 2. Temperate-based ice without prescribed flux

The second example corresponds to a glacier with temperate regime at the base. Here the geothermal heat flux is considered to be greater than for the polar case. So, the chosen parameters are the typical values for temperate-based glaciers:

$$\Delta T = 20,\ \gamma = 2.5,\ g_b = 2.9,\ \alpha = 0.25,\ \beta = 0.29,\ \text{and}\ \varepsilon = 0.13.$$

In this example, Fig. 4.7 shows the profile and velocity field evolution for $t = 1$, 5, 9 and 10 (steady state). Fig. 4.8 to 4.10 show the evolution of basal magnitudes (temperature, stress and velocity) for the same dimensionless time values. Notice the nonzero basal velocity in the region at meting point temperature. Figure 4.11 shows the temperature distribution at $t = 10$.

4.6.3 Example 3. Cold-based ice with prescribed flux

The third example corresponds to a glacier with polar regime at the base as in Example 1, but with an imposed flux boundary condition at the given head position

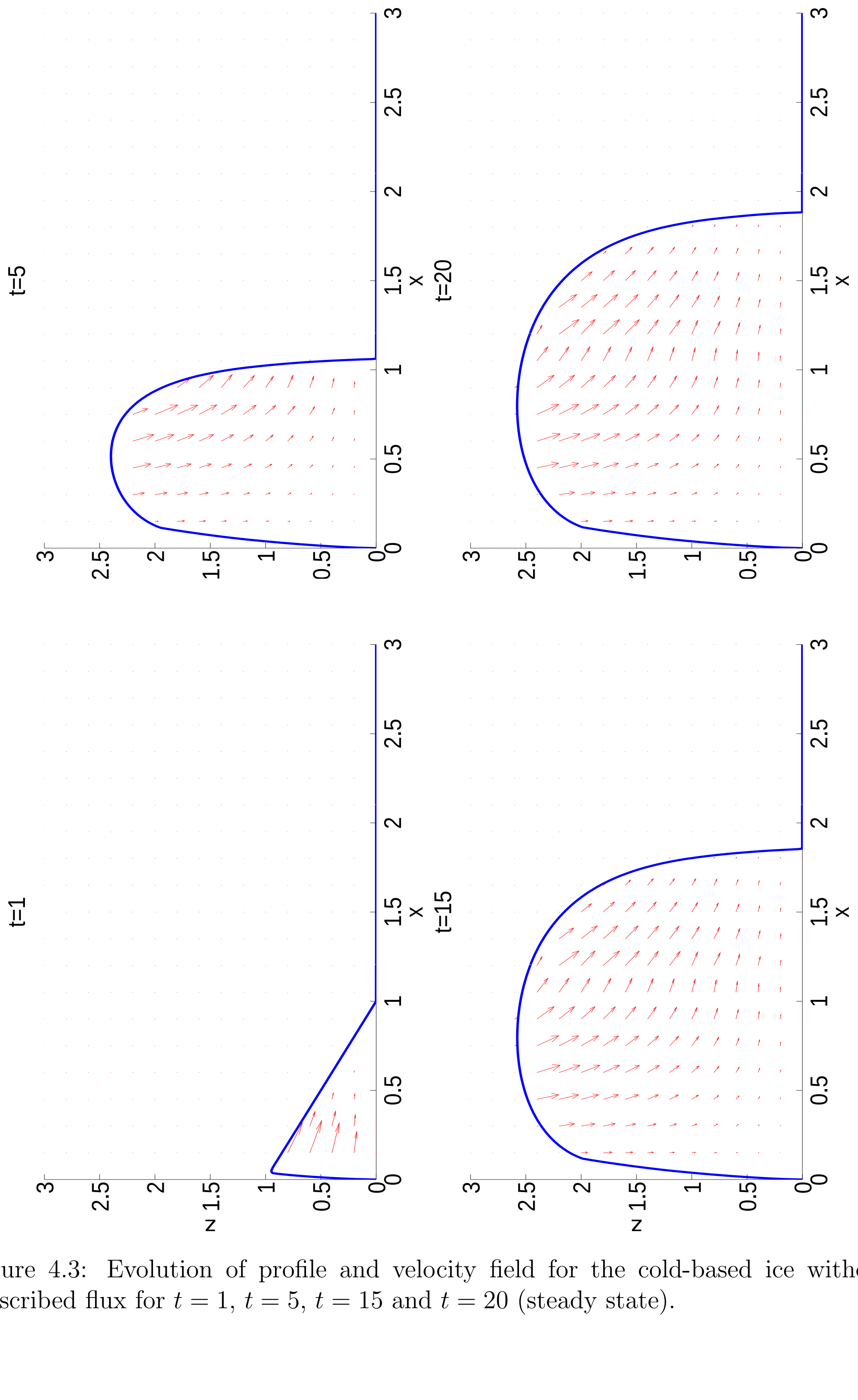

Figure 4.3: Evolution of profile and velocity field for the cold-based ice without prescribed flux for $t = 1$, $t = 5$, $t = 15$ and $t = 20$ (steady state).

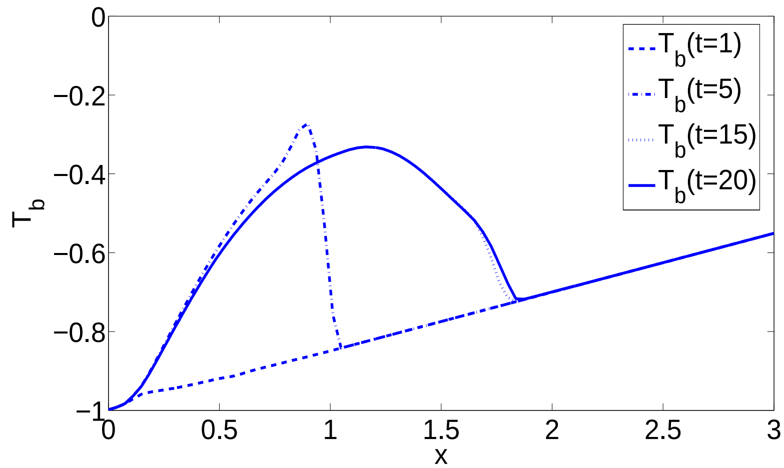

Figure 4.4: Basal temperature for the cold-based ice without prescribed flux.

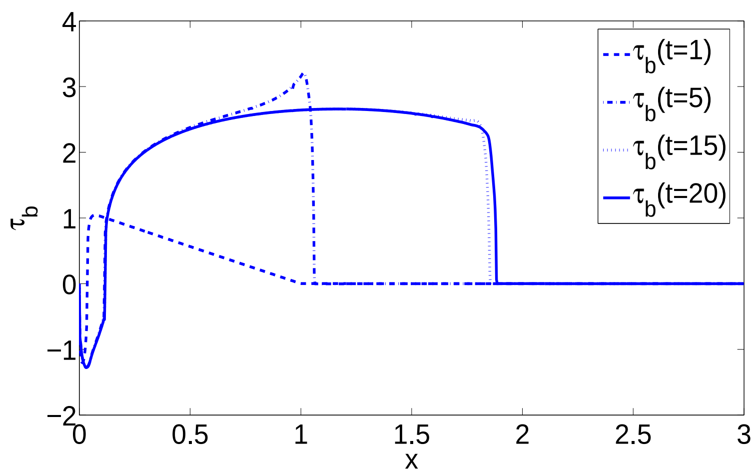

Figure 4.5: Basal stress for the cold-based ice without prescribed flux.

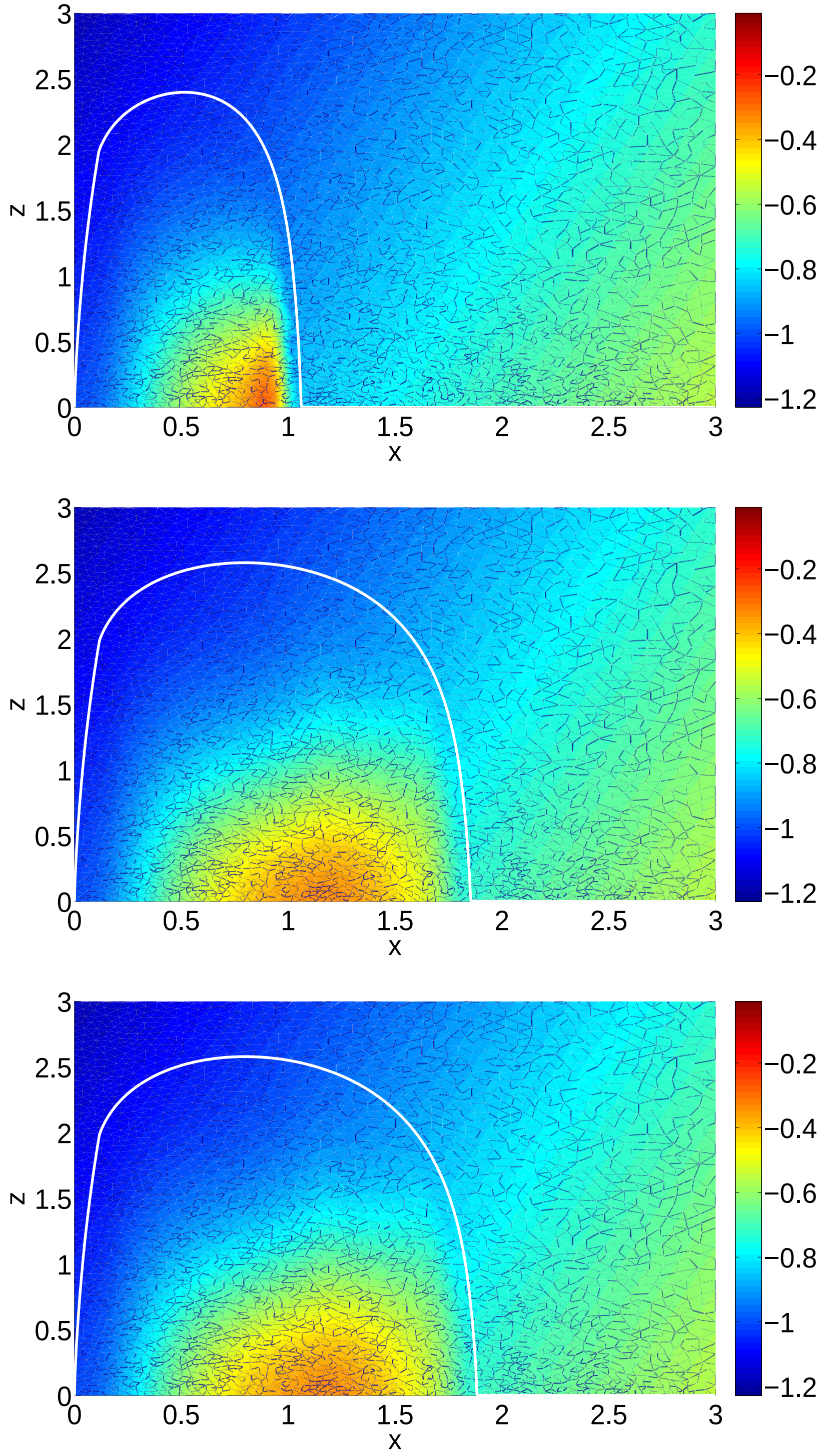

Figure 4.6: Evolution of temperature for the cold-based ice without prescribed flux. From top to bottom: $t = 5$, $t = 15$ and $t = 20$.

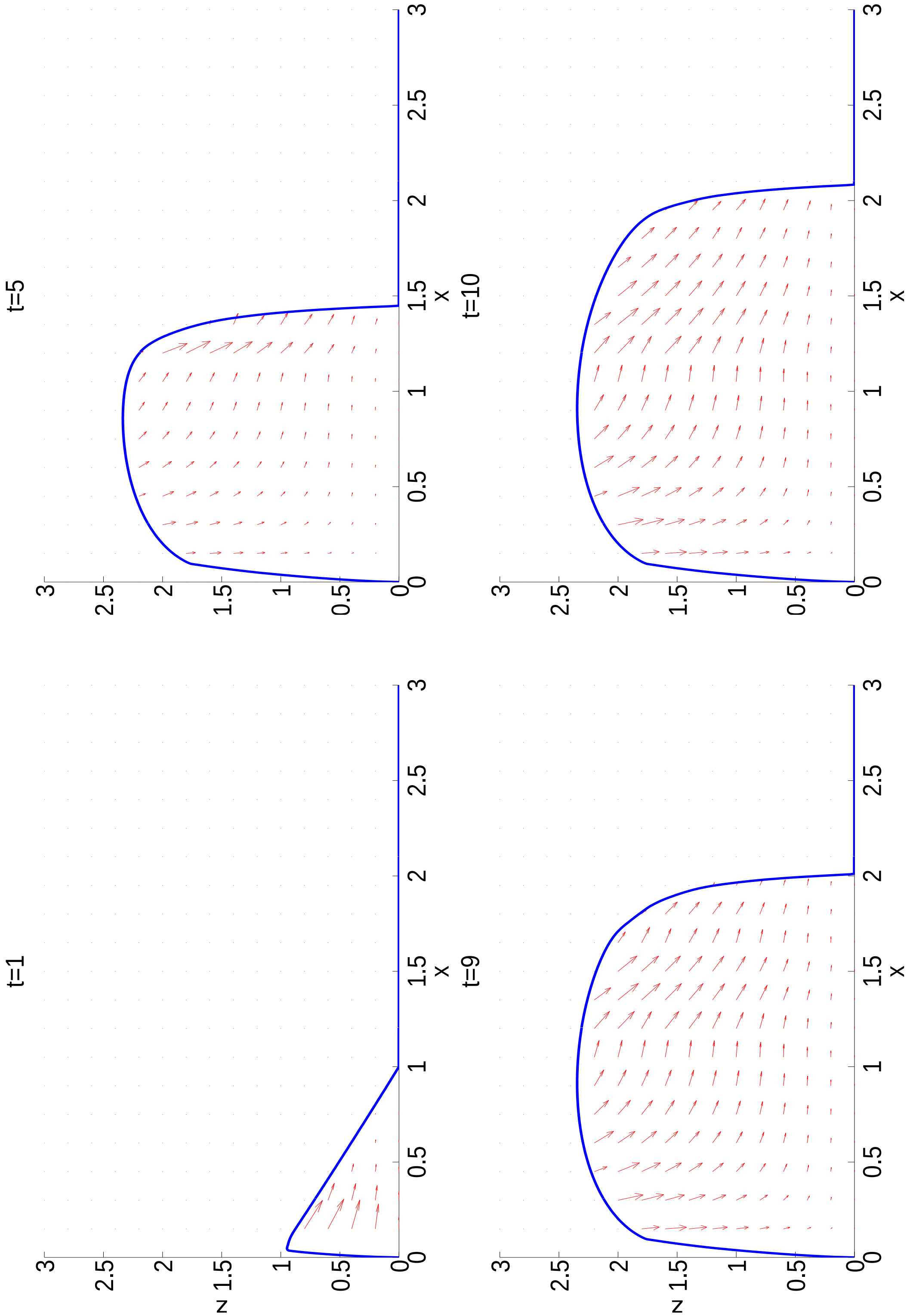

Figure 4.7: Evolution of profile and velocity field for the temperate-based ice without prescribed flux for $t = 1$, $t = 5$, $t = 9$ and $t = 10$ (steady state).

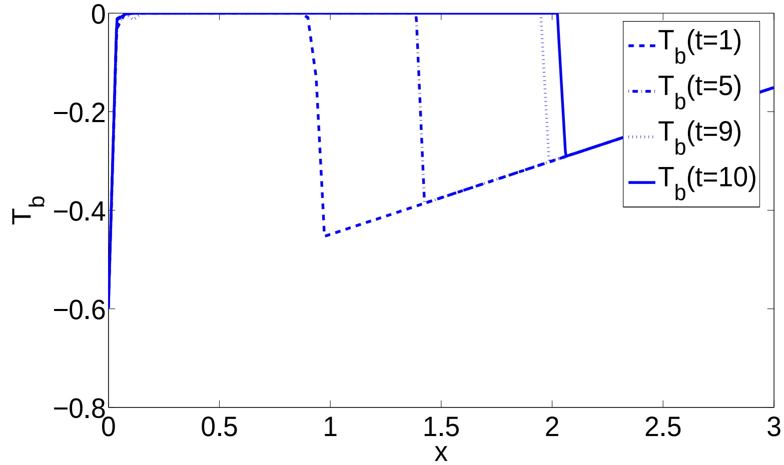

Figure 4.8: Basal temperature for the temperate-based ice without prescribed flux.

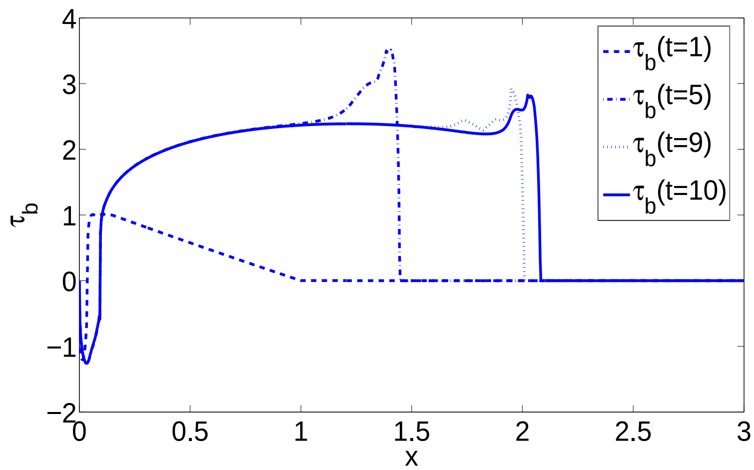

Figure 4.9: Basal stress for the temperate-based ice without prescribed flux.

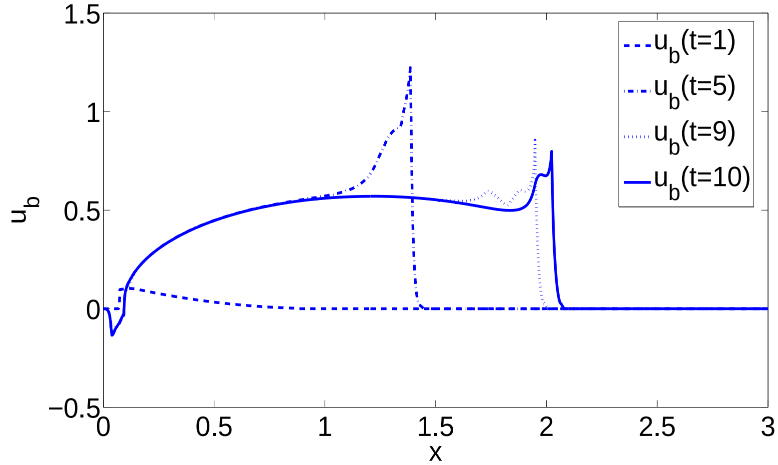

Figure 4.10: Basal velocity for the temperate-based ice without prescribed flux.

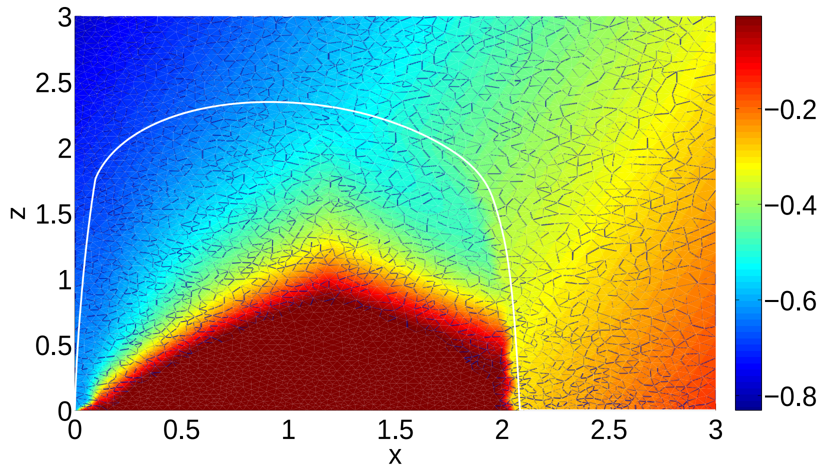

Figure 4.11: Temperature for the temperate-based ice without prescribed flux at $t = 10$.

($x = 0$). In this example we expect to find a cold based region. The parameters used here are the same than in Example 1 and the prescribed flux on the head is $\Upsilon_0 = 0.1$.

Fig. 4.12 shows the time evolution of the glacier profile and velocity field. More precisely, their behaviour at $t = 1$, 5, 15 and 29 (steady state) are presented. Fig. 4.13 shows the basal temperature which is everywhere below melting point as expected in the polar based case. Moreover, in the ice free region the temperature linearly decreases with altitude as assumed for the atmosphere temperature. Fig. 4.14 shows the basal stress. Notice that the computed basal velocity results to be equal to zero, as expected for a polar basis. Finally, Fig. 4.15 shows the temperature distribution in the glacier and the surrounding atmosphere for $t = 5$, $t = 15$ and $t = 29$.

4.6.4 Example 4. Temperate-based ice with prescribed flux

This example corresponds to a glacier with temperate base as in Example 2, but with imposed flux boundary condition at the given head position ($x = 0$), as in Example 3.

In this example, Fig. 4.16 shows the profile and velocity field evolution for $t = 1$, 5, 8 and 9 (steady state). Fig. 4.17 to 4.19 show the evolution of basal magnitudes (temperature, stress and velocity) for the same dimensionless time values. Notice the nonzero basal velocity in the region at meting point temperature. Fig. 4.20 shows the temperature distribution at $t = 9$.

4.7 Conclusions

In this chapter we have presented a new thermomechanical SIA model for glaciers evolution. The main innovative aspect is the consideration of a non isothermal model for the profile equation, thus fully coupled with the shallow ice approximation for the velocity and the temperature equation. This new profile model is posed in terms of a new obstacle problem associated to an integro-differential equation, the numerical solution of which is addressed by the same techniques that in the isothermal model jointly with numerical integration for the nonlocal diffusion coefficient function.

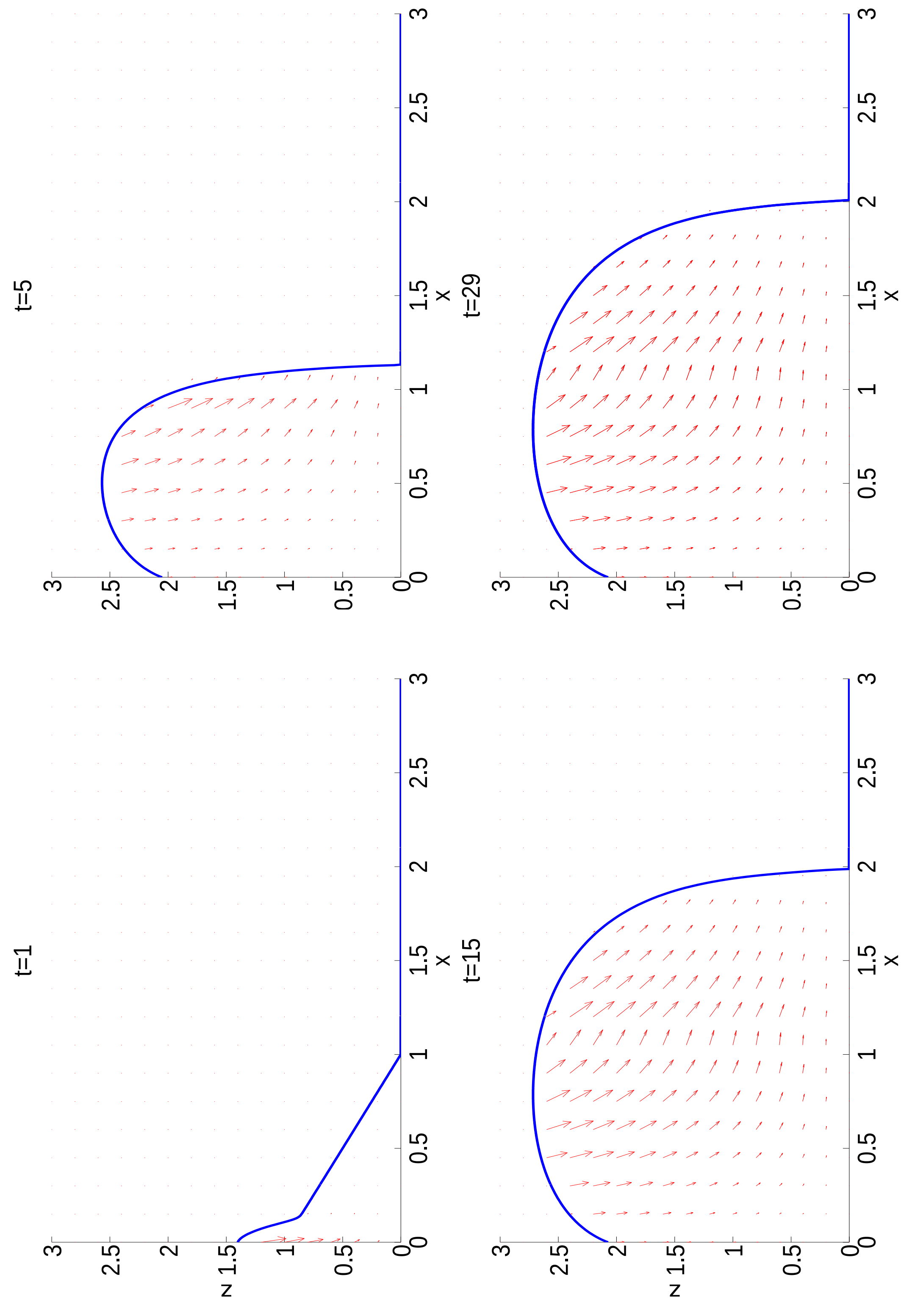

Figure 4.12: Evolution of profile and velocity field for the cold-based ice with prescribed flux for $t = 1$, $t = 5$, $t = 15$ and $t = 29$ (steady state).

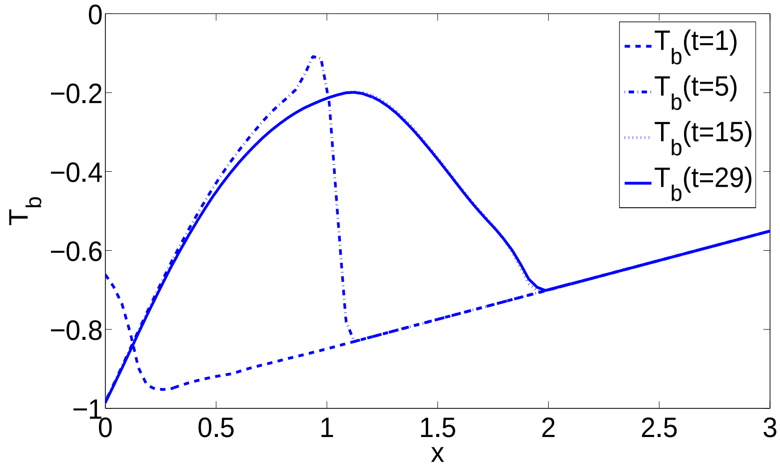

Figure 4.13: Basal temperature for the cold-based ice with prescribed flux.

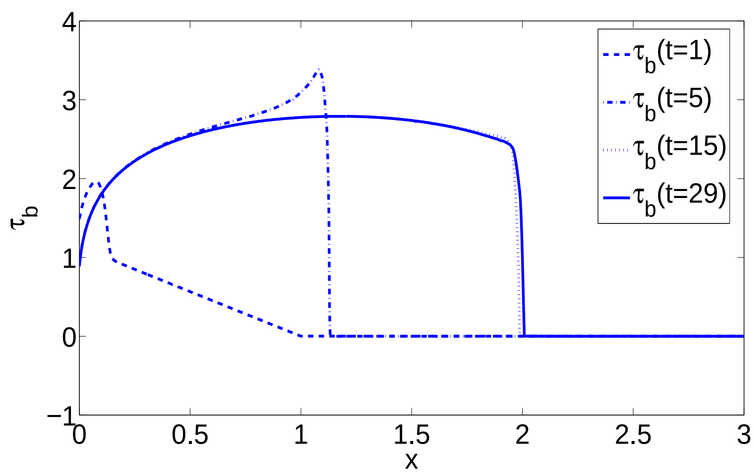

Figure 4.14: Basal stress for the cold-based ice with prescribed flux.

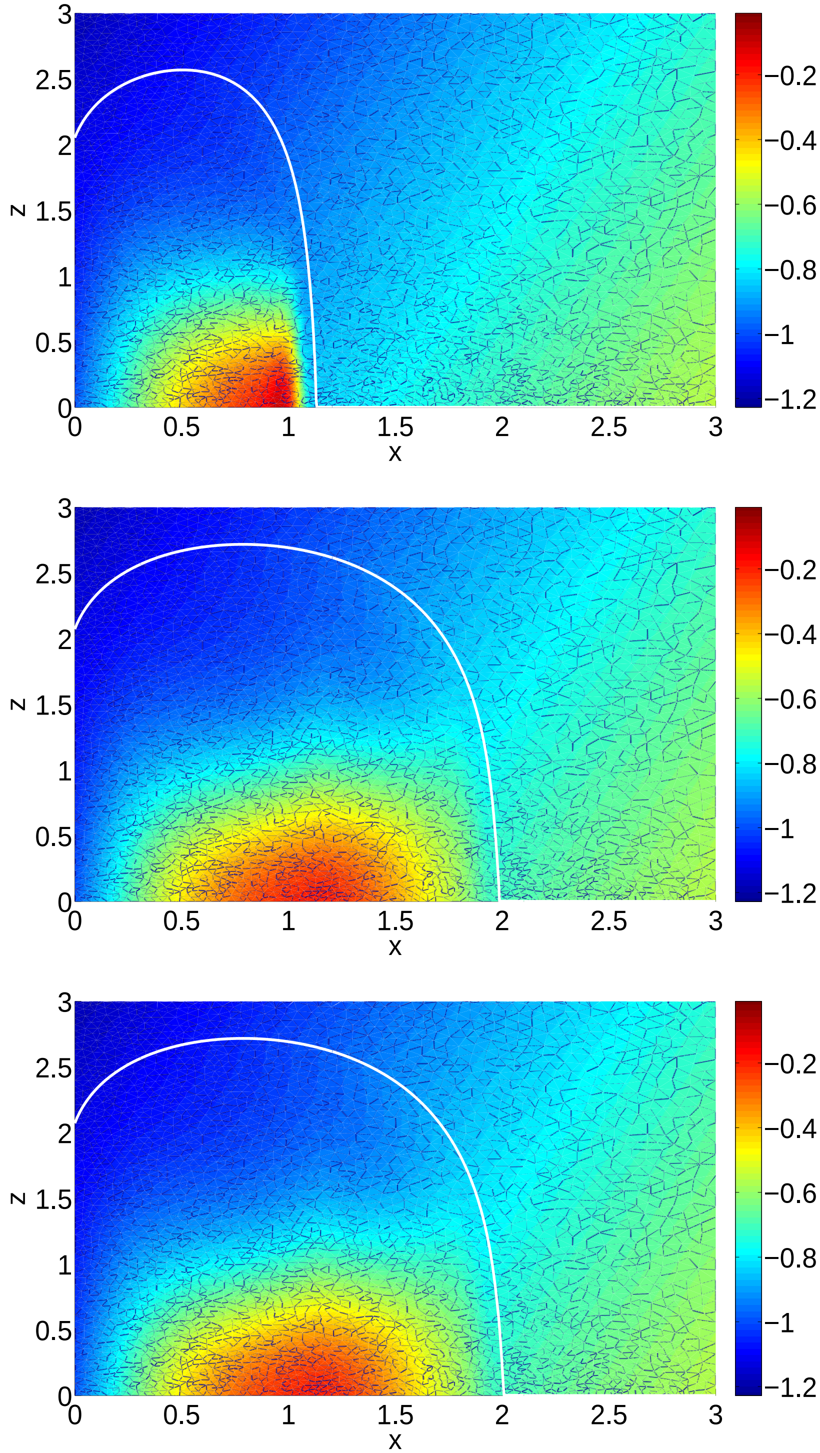

Figure 4.15: Evolution of temperature for the cold-based ice with prescribed flux. From top to bottom: $t = 5$, $t = 15$ and $t = 29$.

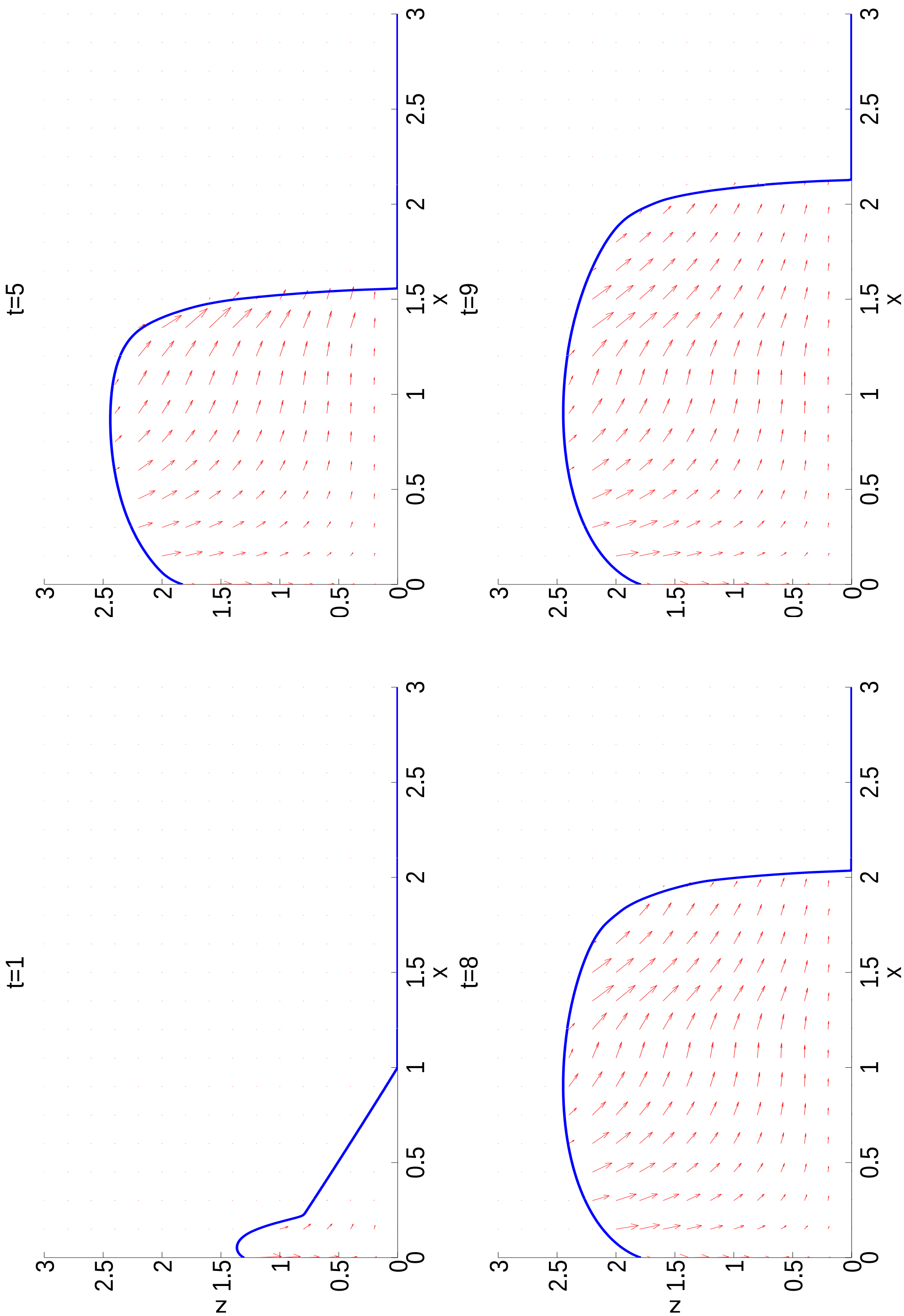

Figure 4.16: Evolution of profile and velocity field for the temperate-based ice with prescribed flux for $t = 1$, $t = 5$, $t = 8$ and $t = 9$ (steady state).

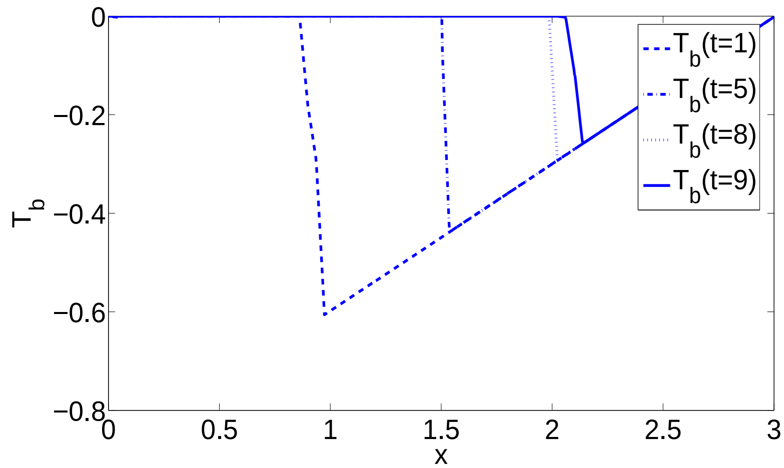

Figure 4.17: Basal temperature for the temperate-based ice with prescribed flux.

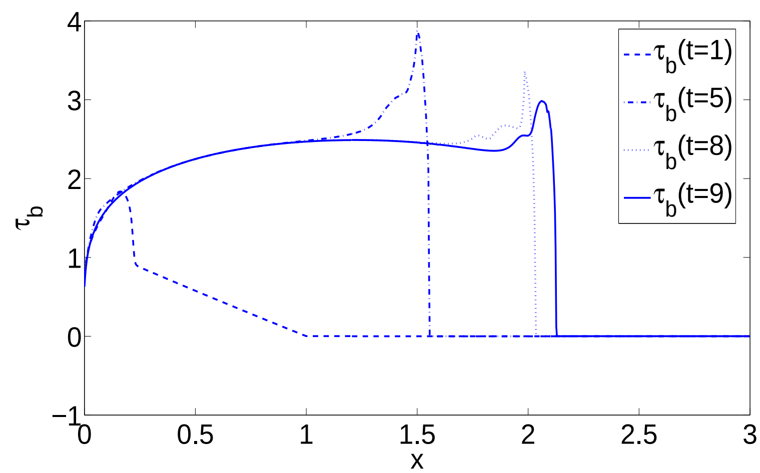

Figure 4.18: Basal stress for the temperate-based ice with prescribed flux.

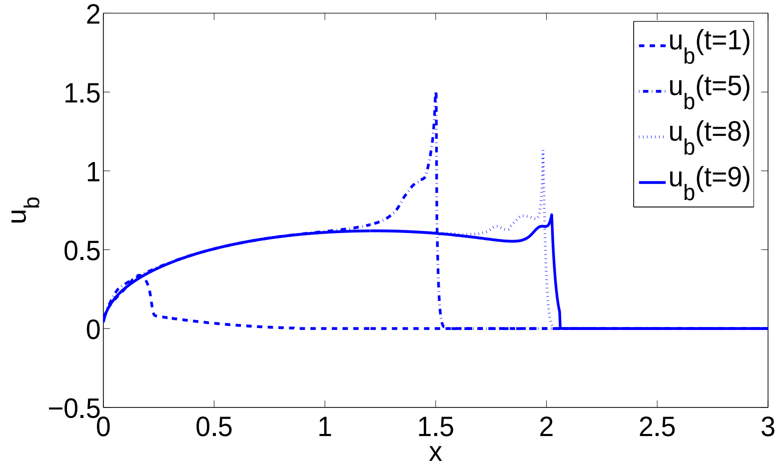

Figure 4.19: Basal velocity for the temperate-based ice with prescribed flux.

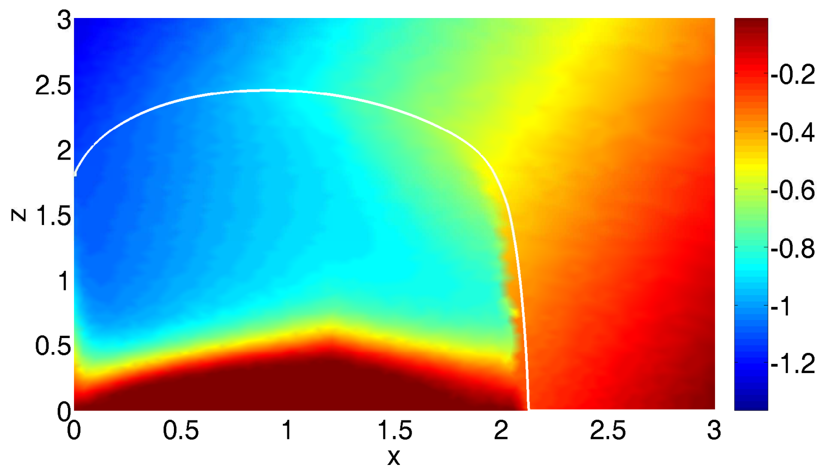

Figure 4.20: Temperature for the temperate-based ice with prescribed flux at $t = 9$.

In addition to the specific difficulties associated to the new profile model formulation, different appropriate techniques have been applied for the numerical solution of the temperature equation: an enthalpy formulation for the two phase Stefan problem, a characteristics method for the time discretization, duality methods associated to maximal monotone operators, a Newton method for the nonlinear term associated to thermal viscous dissipation and piecewise linear finite elements for spatial discretization. Moreover, specific numerical quadrature techniques are considered to compute the velocity field.

Once each subproblem has been solved with the appropriate numerical techniques, a fixed point iterative method is performed for the solution of the coupled problem, which essentially solves sequentially each of the subproblems.

This set of numerical techniques has been applied to several test examples. Thus, illustrative examples concerning the case of polar and temperate regimes have been considered. Moreover, after the remarks in Chapter 3 concerning the appropriate boundary conditions upstream, also the case of flux imposed or profile imposed boundary condition at the left boundary of the glacier are presented. Again, as in the isothermal model treated in Chapter 3, the computed numerical results show that flux imposed boundary results to be more realistic due to the fact that the Dirichlet boundary condition leads to almost infinite slopes at the left glacier boundary. Also notice that, in the case of flux imposed boundary condition, the same technique developed in Chapter 3 allows to obtain the exact position of the free boundary. This value has been very accurately verified by the computations, because the expected value for an imposed flux of $\Upsilon_0 = 0.1$ and the chosen accumulation-ablation function (4.74) is $x_{front}^{\infty} = 2.0954$ and the computed values are $x_{front}^{\infty} = 2.013$ in the polar case (Example 3) and $x_{front}^{\infty} = 2.130$ in the temperate case (Example 4).

Chapter 5

Temperature Dependent Shear Flow and the Absence of Thermal Runaway in Valley Glaciers

5.1 Introduction

In this chapter we propose other two-dimensional model for valley glaciers in order to reconsider the question of whether thermal runaway could be a viable mechanism for the onset of creep instability in surging glaciers. The explanation of the mechanism of why some glaciers surge has been a primary concern for glaciologists for many years. Meier and Post [66] established many key properties of surging glaciers, and these have been variously explained by a variety of theories since. A glacier surge occurs when the glacier starts to slide rapidly at its base, and following the pioneering studies of Kamb et al. on Variegated Glacier in the 1980's [60], it is now generally accepted that this rapid sliding is associated with subglacial water reaching elevated pressure. The same idea was indicated earlier by Lliboutry in his theoretical studies of glacier sliding [63, 64].

One possible way in which high water pressures could be achieved is through the enhanced production of basal water, which in turn could be due to enhanced strain heating. This notion led Clark et at. [25] to the suggestion that creep instability might be the cause of glacier surging, and in particular that the temperature in a glacier might undergo thermal runaway. Thermal runaway in shear flows of viscous fluids was studied by Gruntfest [48] and Joseph [58, 59], and it was suggested as a possible causative surge mechanism by Clarke, Nitsan and Paterson [25] and Yuen and Schubert [77]. These studies showed that multiple steady states were possible in glacier flow models of prescribed depth, but their interpretation was criticized by Fowler [31], on the basis that in reality one should prescribe the ice flux (via the net accumulation) and not the depth. Subsequently, Fowler and Larson [37, 38] showed that, at least when thermal advection was negligible, a non-isothermal model for glacier flow indeed had a unique solution, and moreover this was linearly stable, suggesting that surge-like oscillations were unlikely in that case.

The neglect of thermal advection was unlikely to be critical to those studies, since one would expect advection to have a stabilizing tendency. However, the possibility for thermal runaway could not be ruled out under conditions where the ice surface responds more slowly than the temperature field. In this case, thermal runaway could occur before the ice surface has time to respond.

The situation concerning thermal runaway is thus not entirely conclusive, and although it is not of active concern in valley glacier studies, the same issue arises in the study of ice streams, where the same precepts may be important [52, 70]. Whereas in simple one-dimensional combustion studies one can prove the existence of thermal runaway, for example Fujita [41], such precision is undoubtedly much harder in a glacier flow model involving a free boundary together with a nonlinear advection term. Our approach therefore is to seek an approximate theoretical framework which is both apparently conductive to the occurrence of thermal runaway, and susceptible to sufficient analysis that, within this framework, the issue can be satisfactorily resolved. While this falls short of an absolute proof one way or the other, it lends strong support to the more general validity of the conclusion, which is that runaway unlikely to occur.

In this chapter we examine the possibility of thermal runaway, by means of an approximation method based on the idea that shear is concentrated near the base of an ice flow [67]. Formally we assume that the parameter γ that appears in the Frank–Katmeneskii approximation (2.87) is large, indicating strong temperature dependence of the flow law. This allows us to solve the temperature equation analytically, and we are thus able to deduce an explicit evolution equation for the ice surface. Using this approach, we will show that thermal runaway is still not possible, and remains an unlikely cause of glacier surges.

We set out this chapter as follows. In Section 5.2, we take up the dimensionless model of Chapter 2 and impose a new set of boundary conditions for temperature to create a new asymptotical model. This new model is not a fully coupled model like in Chapter 4 but it is a semi-coupled profile-temperature model. Also in Section 5.2, we show how to reduce the model by solving the temperature equation asymptotically, and we derive an effective equation for the ice surface evolution. In Section 5.3, we present the numerical algorithms to solve the asymptotical model proposed in Section 5.2. These numerical algorithms are analogous to the numerical algorithm proposed in Chapter 3 to solve the profile problem because the two problems are very similar. Moreover, we do not need a numerical algorithm to solve the temperature problem because in this asymptotical model we deduce an explicit formula to compute this temperature. In Section 5.4 we show solutions of several cases corresponding to formation of cold-based and temperate-based glaciers, and emphasizing in doing so the important rôle played by meltwater refreezing in warming the basal ice. We also address the important issue of how best to prescribe the upstream boundary condition. Conclusions of the study follow in Section 5.5.

5.2 Asymptotic model

We depart from the dimensionless model derived in Chapter 2:

$$\begin{aligned}
\frac{DT}{Dt} &= \alpha\tau^{n+1}A(T) + \beta\frac{\partial^2 T}{\partial z^2}, \\
\frac{\partial u}{\partial z} &= A(T)\,\tau^n, \\
\tau &= \left(1 - \mu\frac{\partial \eta}{\partial x}\right)(\eta - z), \\
\frac{\partial \eta}{\partial t} &= a - \frac{\partial}{\partial x}\int_b^\eta u\,dz,
\end{aligned} \tag{5.1}$$

The boundary conditions are taken to be the prescription of a constant surface temperature $-\Delta\Theta$, thus the dimensionless surface temperature is

$$T = -1 \quad \text{at} \quad z = \eta. \tag{5.2}$$

The condition on the velocity is that of a basal sliding velocity u_b, at least if the basal temperature is at the melting point; however, if the basal temperature is below freezing, then we prescribe an effective geothermal heat flux G^*, and the basal velocity is then zero. The effective geothermal heat flux is the sum of the actual geothermal heat flux G and a term which represents the latent heat release by refreezing of surface (not basal) meltwater which finds its way to the base of the glacier through moulins and crevasses. If the quantity of ice melted which heats the base in this way is denoted V, measured as surface loss in elevation per year, then we have

$$G^* = G + \rho LV, \tag{5.3}$$

where L is the latent heat. It turns out that this heat source dwarfs the geothermal heat flux in glaciers, and is instrumental in causing them to become warm at the base. This condition does not imply that the basal temperature is at melting point: think of the temperature regulation of a freezer where one regularly adds ice cube trays containing water.

In dimensionless terms, these conditions take the alternate forms, all applied at the base $z = b$,

$$
\begin{aligned}
&T < 0, \quad -\frac{\partial T}{\partial z} = g_b, \quad u = 0, \\
&T = 0, \quad -\frac{\partial T}{\partial z} = g_b + \tau_b u, \quad 0 < u < u_b, \\
&T = 0, \quad 0 < -\frac{\partial T}{\partial z} < g_b + \tau_b u, \quad u = u_b, \\
&T = 0, \quad 0 > -\frac{\partial T}{\partial z}, \quad u = u_b,
\end{aligned} \tag{5.4}
$$

where

$$\tau_b = \left(1 - \mu \frac{\partial \eta}{\partial x}\right)(\eta - b) \tag{5.5}$$

is the basal stress, $u_b(\tau_b)$ is the fully temperate sliding law, and a function of the basal stress, and the dimensionless geothermal heat flux is

$$g_b = \frac{G^* d_2}{k \Delta \Theta}. \tag{5.6}$$

The four alternative conditions were provided by Fowler and Larson [38]. The first three are referred to by them as cold, subtemperate and temperate, respectively, and we may term the last condition as warm; it refers to the situation where the ice above the bed is temperate and contains moisture. In this case, an enthalpy variable generalizes the temperature, and the dimensionless temperature T is generalized to

$$T \to T + r\, St\, w, \tag{5.7}$$

where

$$r = \frac{\rho_w}{\rho}, \quad St = \frac{L}{c_p \Delta T}, \tag{5.8}$$

and ρ_w is the density of water, L is the latent heat, w is the volumetric water fraction of temperate ice; St is the Stefan number. In the case that warm basal ice occurs, the energy equation needs to be modified to allow for the different physical process (Darcy flow) which allows transport of enthalpy. This has been discussed by Fowler [35], for example, but is not pursued here.

Table 5.1 contains the typical sub-polar and polar values of the model parameters, and in Table 5.2 we estimate the other numerical parameters for polar and sub-polar values using their definition. We distinguish between two sets of values, recognizing that there is no one choice of values that can fit all locations. The primary difference lies in whether we suppose surface ablation occurs. In the normal case where this occurs (in sub-polar and temperate climates), some of the surface meltwater will find its way to the bed, and if the base is frozen, some of this water is likely to re-freeze, causing a release of latent heat. It may seem off to allow such basal re-freezing to occur at temperatures below the melting point: surely re-freezing implies that the basal temperature is at the melting point? The point is resolved by realizing that one makes a distinction between the instantaneous temperature of an ice-water interface and the average temperature of the combined system. In a freezer, one can import trays of hot water and remove them when frozen, replacing them with more hot water. While the water is freezing, its interfacial temperature will be at the melting point, but the air temperature will be significantly lower. If the average temperature of the freezer and its contents is computed, it will remain below the melting point, and the net effect of the water input is to provide an effective source of heat. The latent heat thus produced enhances the geothermal heat flux in a significant way. Where this does not occur (in polar, continental climate such as in Antarctica), there may be no melting at all, associated with a colder surface temperature (hence larger $\Delta\Theta$), and decreased precipitation (hence smaller $[a^*]$). These two climatic examples act as particular stereotypes in our investigations.

None of the parameters in table (5.2) are particularly small or large, but a number of them conspire to suggest a useful means of approximation. The rate factor decreases (if $\gamma = 2.5$) by a factor of 12 at the ice surface, and this decrease is enhanced by the stress dependence of the flow law. Half way to the surface, the creep rate is 3.5 times lower, but the consequent strain rate is then 28 times lower, because of the stress dependence. This effect is further enhanced by the relatively small value of β, which tends to concentrate the change of temperature (and thus also the shear) in a basal thermal boundary layer. Thus the shear is concentrated at the glacier bed, and we can formally base an approximation scheme on this observation by considering the limit in which $\gamma \gg 1$, noting that the limits $\beta \to 0$ and $n \to \infty$ enhance the quality of the approximation.

We write $\gamma T = \phi$, so that the temperature equation takes the form

$$\frac{1}{\alpha\gamma}\frac{\partial \phi}{\partial t} + \frac{1}{\alpha\gamma} u.\nabla\phi = \tau^{n+1} e^{\phi} + \frac{\beta}{\alpha\gamma}\frac{\partial^2 \phi}{\partial z^2}. \tag{5.9}$$

From this we see that ϕ will relax to equilibrium (if η is stationary) on a time scale of $\mathcal{O}\left(\frac{1}{\alpha\gamma}\right)$, and this steady state will be linear outside a boundary layer of thickness $\mathcal{O}\left(\sqrt{\frac{\beta}{\alpha\gamma}}\right)$, because the exponential term becomes transcendentally small away from the boundary. Note that the advective term becomes small in this approximation, so that the quasi-steady state for T is the solution of

$$\beta\frac{\partial^2 T}{\partial z^2} + \alpha\tau^{n+1} e^{\gamma T} = 0, \tag{5.10}$$

together with the boundary conditions from (5.2) and (5.4)[1]. Noting that the viscous heating term is $\alpha\tau\frac{\partial u}{\partial z}$, we can integrate this equation once to find

$$\beta \left.\frac{\partial T}{\partial z}\right|_b^{\eta} = \alpha\left[\tau_b u_b - \left(1 - \mu\frac{\partial \eta}{\partial x}\right)\int_b^s u\, dz\right], \tag{5.11}$$

and using $(5.1)_4$, we find that the evolution equation for η takes the form

$$\frac{\partial \eta}{\partial t} = a + \frac{\partial}{\partial x}\left[\frac{\beta \left.\frac{\partial T}{\partial z}\right|_b^{\eta} - \alpha\tau_b u_b}{\alpha\left(1 - \mu\frac{\partial \eta}{\partial x}\right)}\right]. \tag{5.12}$$

We can progress further by noting that, since the exponential term in (5.10) is negligible away from the base, we can replace τ in that equation by τ_b, and the

[1]There is a slight inaccuracy here. The advective term is certainly small in the boundary layer, but both the exponential and conductive terms become small in the bulk flow, so that in fact the outer problem for ϕ is the approximate equation $u \cdot \nabla\phi \approx 0$, if we suppose $\beta \ll 1$, the solution to which is $\phi = \phi(\psi)$, where ψ is a stream function for the flow. With the constant surface temperature condition (5.2), this makes no difference at all, and in fact even with a varying surface temperature, the boundary layer solution is formally the same, provided we take the dimensionless surface temperature $T = -1$ to be that at the head $x = 0$.

quasi-steady solution for T can then be written explicitly as

$$T = -\frac{2}{\gamma} \ln \left[B \cosh \left\{ \sqrt{\frac{\lambda}{2}} \frac{z}{B} + C \right\} \right], \tag{5.13}$$

where

$$\lambda = \frac{\alpha \gamma \tau_b^{n+1}}{\beta}, \tag{5.14}$$

and B must be positive in order that T be real. The temperature gradient is calculated from (5.13), and is

$$\frac{\partial T}{\partial z} = -\frac{\sqrt{2\lambda}}{\gamma B} \tanh \left\{ \sqrt{\frac{\lambda}{2}} \frac{z}{B} + C \right\}. \tag{5.15}$$

To keep things simple, we now suppose that $b = 0$, i.e, it is a flat inclined plane, and we suppose also that the sliding velocity u_b is negligible. Thus the sub-temperate part of the base shrinks to a point, and the temperate and warm parts of the base satisfy the same condition. Thus we suppose that $u = 0$ at $z = 0$ always, and

$$\begin{aligned} T < 0, &\quad -\frac{\partial T}{\partial z} = g_b, \\ T = 0, &\quad -\frac{\partial T}{\partial z} < g_b, \end{aligned} \tag{5.16}$$

also at $z = 0$.

The condition $T = -1$ at $z = \eta$ implies

$$\left| C + \sqrt{\frac{\lambda}{2}} \frac{\eta}{B} \right| = \frac{\gamma}{2} - \ln \frac{B}{2} - \ln \left[1 + \exp \left\{ -2 \left| \sqrt{\frac{\lambda}{2}} \frac{\eta}{B} + C \right| \right\} \right]. \tag{5.17}$$

Cold-based ice

It is well known [58, 59] that there are generally two solutions of the equation (5.10) for λ less than some critical value λ_c; in the present case these are distinguished as being a lower, cool branch, and an upper, warm branch.

For cold-based ice, we have in addition to (5.17) the equation

$$g_b = \frac{\sqrt{2\lambda}}{\gamma B} \tanh C, \tag{5.18}$$

which shows that $C > 0$. Since we take $\gamma \gg 1$, (5.18) implies that $B \ll 1$, and therefore (5.17) is approximately

$$C + \sqrt{\frac{\lambda}{2}}\frac{\eta}{B} = \frac{\gamma}{2} + \ln\frac{2}{B}. \tag{5.19}$$

If we first suppose that $C \leq \mathcal{O}(1)$, then

$$B \approx \frac{\sqrt{2\lambda}\eta}{\gamma}, \quad g_b\eta \approx \tanh C, \tag{5.20}$$

and

$$T|_0 \approx \frac{2}{\gamma}\ln\gamma > 0; \tag{5.21}$$

this solution therefore corresponds to the warm branch.

Alternatively, if $C \gg 1$, then

$$B \approx B_\infty = \frac{\sqrt{2\lambda}}{\gamma g_b}, \quad C \approx \frac{\gamma}{2}(1 - g_b\eta) + \ln\left(\gamma g_b\sqrt{\frac{2}{\lambda}}\right), \tag{5.22}$$

and in this case

$$T|_0 \approx -(1 - g_b\eta), \tag{5.23}$$

and this is negative if $g_b\eta < 1$, which is also the criterion that $C \gg 1$. Thus this cool lower branch is determined by (5.22), and thermal runaway occurs if $g_b\eta > 1$, except that in any case we then switch to the temperate-based case.

To compute $\frac{\partial T}{\partial z}\big|_0^\eta$, we use (5.15), together with the approximation

$$\tanh\xi \approx 1 - 2e^{-2\xi} \tag{5.24}$$

for large ξ. We then find that

$$\left.\frac{\partial T}{\partial z}\right|_0^\eta \approx -\frac{\lambda e^{-\gamma}}{\gamma^2 g_b}\left(e^{\gamma g_b\eta} - 1\right), \tag{5.25}$$

and hence we find in this case that η satisfies

$$\frac{\partial\eta}{\partial t} = a - e^{-\gamma}\frac{\partial}{\partial x}\left[\left(\frac{e^{\gamma g_b\eta} - 1}{\gamma g_b}\right)\eta^{n+1}\left(1 - \mu\frac{\partial\eta}{\partial x}\right)^n\right]. \tag{5.26}$$

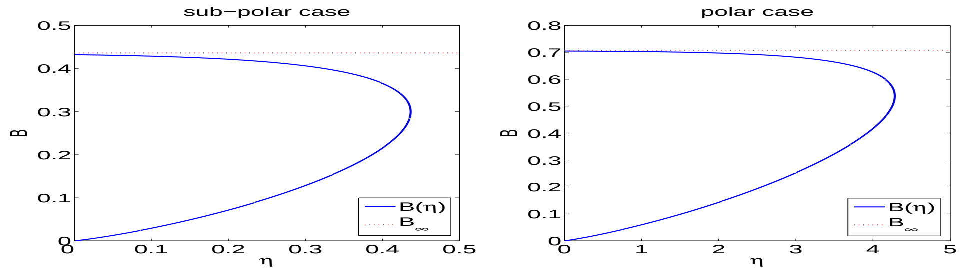

Figure 5.1: Exact and approximate values of $B(\eta)$ for the case of sub-polar and polar climates. For the sub-polar climate, we use values $\gamma = 2.5$, $g_b = 2.9$, and $\lambda = 5$, based on a temperate-based shear stress of $\tau_b \approx 0.8$, with $\alpha = 0.25$, $\beta = 0.29$; for the polar climate, we use values $\gamma = 5$, $g_b = 0.2$, and $\lambda = 0.25$, based on a cold-based shear stress of $\tau_b \approx 1.2$, with $\alpha = 0.13$, $\beta = 2.9$. In both cases, it is the upper (cool) branch of the solution which is to be taken.

Because, particularly in the sub-polar case, γ is not in fact that large, one must be careful that the approximations in (5.22) are reasonably accurate. Figure 5.1 shows two examples of the exact solutions for B as a function of η computed from the solution of (5.17) and (5.18), together with the approximation $B \approx B_\infty$. In each curve the upper branch is the stable cool branch, and one can see that the approximate value actually gives a good estimate, even though B_∞ is not so very small. This gives us some confidence in the use of (5.22).

Temperate-based ice

For the case that $T = 0$ at $z = 0$, we have instead of (5.18)

$$B \cosh C = 1. \tag{5.27}$$

From (5.15) and (5.13), we see that if $C > 0$, then $\left.\frac{\partial T}{\partial z}\right|_0 < 0$, and $T < 0$ in $z > 0$, whereas if $C < 0$, the opposite is true, and the basal ice is warm (actually, superheated). In addition, the cool branch is stable and the warm branch is unstable.

We can see from (5.27) that either $B = O(1)$ or $B \ll 1$. If $B = O(1)$, then (5.17) implies (since $\gamma \gg 1$) that $|C| \gg 1$, and hence in fact $B \ll 1$ is the only possibility.

The two possible solutions then correspond to $\pm C \gg 1$: for the stable, cool branch, $C \gg 1$, while for the unstable, warm branch, $-C \gg 1$. From (5.27), we have

$$|C| \approx -\ln\frac{B}{2} - \frac{B^2}{4}\dots, \tag{5.28}$$

and therefore, from (5.17), we obtain the approximations

$$\begin{aligned} C &\approx \ln\frac{2}{B}, \qquad B \approx \frac{\sqrt{2\lambda}\eta}{\gamma}, \quad C > 0, \\ C &\approx -\ln\frac{2}{B}, \qquad B \approx \frac{\sqrt{2\lambda}\eta}{\gamma}, \quad C < 0. \end{aligned} \tag{5.29}$$

Restricting our attention to the cool, stable case $C > 0$, we can now approximate $\frac{\partial T}{\partial z}\Big|_0^\eta$ as before, using the definitions in (5.15) and (5.29), and the approximation (5.24). The result is

$$\left.\frac{\partial T}{\partial z}\right|_0^\eta \approx -\frac{\lambda\left(1-e^{-\gamma}\right)\eta}{\gamma^2}. \tag{5.30}$$

Finally, using the definition of λ in (5.14), we find that for temperate basal conditions, the mass conservation equation (5.12) takes the form

$$\frac{\partial \eta}{\partial t} = a - \frac{\left(1-e^{-\gamma}\right)}{\gamma}\frac{\partial}{\partial x}\left[\eta^{n+2}\left(1-\mu\frac{\partial \eta}{\partial x}\right)^n\right]. \tag{5.31}$$

The temperate-based evolution equation applies while $-\frac{\partial T}{\partial z}\Big|_0 \approx \dfrac{\sqrt{2\lambda}}{\gamma B} < g_b$, it is,

$$g_b\eta > 1. \tag{5.32}$$

The warm and cool branches must come together when $C = \mathcal{O}(1)$, and thus $B = \mathcal{O}(1)$. Thermal runaway will thus occur if $B = \mathcal{O}(1)$. Formally this does not happen, since $B \ll 1$. If we suppose the approximate result in (5.29) can be extended, then it suggests that runaway will occur if $\sqrt{2\lambda}\eta > \gamma B$ for some value of $B = \mathcal{O}(1)$, or

$$\eta^{n+3}\left(1-\mu\frac{\partial \eta}{\partial x}\right)^{n+1} > \frac{\beta\gamma B^2}{2\alpha}, \tag{5.33}$$

but just as before, we can associate the transition from cool to warm branches with the passage of the basal heat flux, $-\frac{\partial T}{\partial z}\Big|_0$, through zero, and thus the onset of a region of basal moist ice; again, thermal runaway does not occur.

Global asymptotic model

Both cold and temperate based glacier models can be represented by the combined form

$$\frac{\partial \eta}{\partial t} = a - \frac{\partial}{\partial x}\left[K\eta^{n+2}\left(1-\mu\frac{\partial \eta}{\partial x}\right)^n\right], \tag{5.34}$$

where $K(\eta)$ can be defined by

$$K = \begin{cases} \dfrac{\left(e^{-\gamma(1-g_b\eta)} - e^{-\gamma}\right)}{\gamma g_b \eta}, & g_b\eta < 1 \quad \text{(cold)}, \\ \\ \dfrac{1-e^{-\gamma}}{\gamma}, & g_b\eta > 1 \quad \text{(temperate)}. \end{cases} \tag{5.35}$$

Note that K is a continuous function of η. The terms $e^{-\gamma}$ are formally negligible, but are retained for the purpose of indicating the appropriate continuity at $g_b\eta = 1$.

In computing the temperature field, we would use the approximation given by (5.13), where the values of B and C should be as described above. With the approximate formulae given by (5.22) and $(5.29)_1$, the temperature field will be continuous across the cold-temperate transition at $g_b\eta = 1$, but the basal temperature will not be exactly zero at the switch point, because (5.27) is only approximately satisfied there. Because it represents the actual melting point, we want to ensure that the transition occurs at $T|_0 = 0$, and the simplest way to do this, if we want to retain explicit approximations for B and C, rather than solving for them exactly at each value of x, is to make the same approximation in (5.13) as we do in deriving the approximate values of B and C.

Since this involves the supposition that B is small and C is large, we make the same approximation in (5.13), and after some algebra, this leads to the linear approximation

$$T = \begin{cases} -1 + g_b(\eta - z), & g_b\eta < 1, \quad \text{(cold)}, \\ \\ -\dfrac{z}{\eta}, & g_b\eta > 1, \quad \text{(temperate)}. \end{cases} \tag{5.36}$$

5.3 Numerical Methods

In deriving the effective non-isothermal surface evolution profile equation (5.34), we have tacitly assumed $\frac{\partial\eta}{\partial x} < \dfrac{1}{\mu}$, which physically implies the glacier surface is inclined downhill, as we expect. More generally, the derivation of the equation leads to the form

$$\frac{\partial\eta}{\partial t} = a - \frac{\partial}{\partial x}\left[K\eta^{n+2}\left|1-\mu\frac{\partial\eta}{\partial x}\right|^{n-1}\left(1-\mu\frac{\partial\eta}{\partial x}\right)\right], \tag{5.37}$$

and properly speaking, the equation must be solved in this form.

In this section we briefly describe the set of numerical methods that have been used for the three models.

5.3.1 Boundary conditions

The issue of boundary conditions for a valley glacier is an interesting one. The second order equation (5.37) requires two boundary conditions, upstream and downstream. That at the snout of the glacier, assuming it terminates on land, is simply

$$\eta = 0 \quad \text{at} \quad x = x_{front}, \tag{5.38}$$

where $x_{front}f$ is the position of the glacier front. The value of x_{front} is unknown (it is a free boundary), but the condition (5.38) is sufficient to determine it, since the equation is degenerate there (the diffusion coefficient is zero).

At the upstream end of the glacier $x = 0$, the position is less clear (as pointed in Chapters 3 and 4). We might suggest

$$\eta = 0 \quad \text{at} \quad x = 0, \tag{5.39}$$

but the flux

$$\Upsilon = K\eta^{n+2}\left|1-\mu\frac{\partial\eta}{\partial x}\right|^{n-1}\left(1-\mu\frac{\partial\eta}{\partial x}\right) \tag{5.40}$$

is then apparently zero unless $\frac{\partial\eta}{\partial x}$ is infinite. Indeed, the condition $\eta = 0$ then requires $\Upsilon \sim ax > 0$ near $x = 0$, and this requires $\frac{\partial\eta}{\partial x}$ to be infinite and *negative*. Thus the only way one can maintain $\eta = 0$ at the head is to have a finite flux, and (since η must be positive in $x > 0$), this must be a negative flux; that is to say, the glacier actually grows into an ice sheet with an ice divide downstream of the head.

Physically, we need to represent the bergschrund of the glacier. One way to do this is to allow a variable basal slope, thus replacing (5.37) by

$$\frac{\partial \eta}{\partial t} = a - \frac{\partial}{\partial x}\left[K\eta^{n+2}\left|\Theta - \mu\frac{\partial \eta}{\partial x}\right|^{n-1}\left(\Theta - \mu\frac{\partial \eta}{\partial x}\right)\right], \tag{5.41}$$

where Θ is the scaled basal slope. We can represent a bergschrund by specifying

$$\Theta \sim \frac{1}{x^{\nu}} \quad \text{as} \quad x \to 0, \tag{5.42}$$

where $0 < \nu < 1$ in order that the mountain height be finite. Then we can have positive downstream flux with $\Upsilon \sim ax$ near $x = 0$ if $\eta \sim x^{\sigma}$, where

$$\sigma = \frac{1}{n+2} + n\nu. \tag{5.43}$$

While this provides a convenient cosmetic resolution to the problem, and allows us to prescribe (5.39), it introduces unnecessary numerical complication. Thus in practice we have applied a flux boundary condition

$$\Upsilon = \Upsilon_0 \quad \text{at} \quad x = 0. \tag{5.44}$$

With a small positive value for Υ_0, then $\frac{\partial \eta}{\partial x} < \dfrac{1}{\mu}$, and η is finite at $x = 0$.

We write the equation (5.37) in the form

$$\frac{\partial \eta}{\partial t} + \frac{\partial}{\partial x}\left[F\left(\eta, \frac{\partial \eta}{\partial x}\right)\left(1 - \mu\frac{\partial \eta}{\partial x}\right)\right] = a \tag{5.45}$$

where

$$F\left(\eta, \frac{\partial \eta}{\partial x}\right) = K(\eta)\eta^{n+2}\left|1 - \mu\frac{\partial \eta}{\partial x}\right|^{n-1}, \tag{5.46}$$

and K is given by (5.35).

Equation (5.45) is valid for the function η when $\eta\,(x,t) > 0$, the set of whose points is an additional unknown. Thus, we use a fixed domain technique like in Chapter 3.

For this purpose, let $\mathcal{Q} = (0, t_A) \times [0,\ x_{\max}]$; in our computations we use $x_{\max} = 3$. If we extend the function η to be zero in the ice free region, then the extended function (still noted by η) satisfies the equations

$$\begin{aligned}
\frac{\partial \eta}{\partial t} + \frac{\partial}{\partial x}\left[F\left(\eta, \frac{\partial \eta}{\partial x}\right)\left(1 - \mu \frac{\partial \eta}{\partial x}\right)\right] - a &\geq 0 \quad \text{in} \quad \mathcal{Q}, \\
\eta &\geq 0 \quad \text{in} \quad \mathcal{Q}, \\
\left\{\frac{\partial \eta}{\partial t} + \frac{\partial}{\partial x}\left[F\left(\eta, \frac{\partial \eta}{\partial x}\right)\left(1 - \mu \frac{\partial \eta}{\partial x}\right)\right] - a\right\}\eta &= 0 \quad \text{in} \quad \mathcal{Q}, \\
\eta &= 0 \quad \text{on} \quad (0, t_A) \times \{x_{\max}\}, \\
F\left(\eta, \frac{\partial \eta}{\partial x}\right)\left(1 - \mu \frac{\partial \eta}{\partial x}\right) &= \Upsilon_0 \quad \text{on} \quad (0, t_A) \times \{0\}, \\
\eta\,(x, 0) &= 0 \quad \text{in} \quad \Omega.
\end{aligned} \tag{5.47}$$

Notice that in the ice covered region, the fact that $\eta\,(x,t) > 0$ together with equation $(5.47)_3$ implies equation (5.45).

Next, in order to solve numerically the complementarity problem $(5.47)_{1-4}$, an implicit finite difference scheme for time discretization is applied together with an iterative fixed point technique for the resulting nonlinear diffusive term.

So, for each $m = 0, 1 \ldots,$ we initialize $\eta^{m+1,0}$ and the following problem has to be solved at step $k+1$:

Find $\eta^{m+1,k+1}$ such that:

$$
\begin{aligned}
&\frac{\eta^{m+1,k+1}-\eta^m}{\Delta t} - \\
&\qquad \mu\frac{\partial}{\partial x}\left[F\left(\eta^{m+1,k},\frac{\partial\eta}{\partial x}^{m+1,k}\right)\frac{\partial\eta}{\partial x}^{m+1,k+1}\right] - b^{m+1,k} \geq 0 \quad \text{in} \quad \Omega, \\
&\qquad\qquad\qquad\qquad\qquad\qquad\qquad\qquad \eta^{m+1,k+1} \geq 0 \quad \text{in} \quad \Omega, \\
&\eta^{m+1,k+1}\left\{\frac{\eta^{m+1,k+1}-\eta^m}{\Delta t}\right. \\
&\left. -\mu\frac{\partial}{\partial x}\left[F\left(\eta^{m+1,k},\frac{\partial\eta}{\partial x}^{m+1,k}\right)\frac{\partial\eta}{\partial x}^{m+1,k+1}\right] - b^{m+1,k}\right\} = 0 \quad \text{in} \quad \Omega, \\
&\qquad\qquad\qquad\qquad\qquad\qquad\qquad\qquad \eta^{m+1,k+1} = 0 \quad \text{on} \quad x = x_{\max}, \\
&\qquad F\left(\eta^{m+1,k+1},\frac{\partial\eta}{\partial x}^{m+1,k+1}\right)\left(1-\mu\frac{\partial\eta}{\partial x}^{m+1,k+1}\right) = \Upsilon_0 \quad \text{on} \quad x = 0,
\end{aligned}
\tag{5.48}
$$

where

$$
b^{m+1,k} = a^{m+1} - \frac{\partial}{\partial x}\left[F\left(\eta^{m+1,k},\frac{\partial\eta}{\partial x}^{m+1,k}\right)\right]. \tag{5.49}
$$

In order to pose the variational formulation and the spatial discretization, we point out that the relation between variational inequalities, complementarity problems and obstacle problems can be reviewed in Elliott and Ockendon [30], for example.

Next, in order to discretize in space the variational inequality associated with (5.48), a piecewise linear Lagrange finite element space is used. Thus, for a given positive mesh stepsize Δx, a uniform finite element mesh τ_l is built for the domain Ω with nodes $x_i = (i-1)\Delta x,\ i = 1,\ldots,N+1$. The following classic spaces and sets are introduced:

$$
\begin{aligned}
V_l &= \{\varphi_l \in \mathcal{C}^0(\Omega) : \varphi_l|_E \in P_1\ \forall E \in \tau_l\}, \\
V_{0l} &= \{\varphi_l \in V_l : \varphi_l(x_{\max}) = 0\}, \\
K_l &= \{\varphi_l \in V_l : \varphi_l \geq 0 \text{ a.e. in } \Omega,\ \varphi_l(x_{\max}) = 0\},
\end{aligned}
\tag{5.50}
$$

where E denotes a standard finite element. In this way, the discretized problem can be written as follows:

Find $\eta_l^{m+1,k+1} \in K_l$ *such that:*

$$
\begin{aligned}
&\frac{1}{\Delta t}\int_\Omega \eta_l^{m+1,k+1}\left(\varphi_l - \eta_l^{m+1,k+1}\right) d\Omega + \\
&+\mu \int_\Omega F\left(\eta^{m+1,k}, \frac{\partial \eta}{\partial x}^{m+1,k}\right) \frac{\partial \eta_l}{\partial x}^{m+1,k+1} \frac{\partial}{\partial x}\left(\varphi_l - \eta_l^{m+1,k+1}\right) d\Omega \geq \\
&\geq \frac{1}{\Delta t}\int_\Omega \eta_l^{m}\left(\varphi_l - \eta_l^{m+1,k+1}\right) d\Omega + \int_\Omega b^{m+1,k}\left(\varphi_l - \eta_l^{m+1,k+1}\right) d\Omega + \\
&+\left(\Upsilon_0 - F\left(\eta^{m+1,k}\left(x_{\max}\right), \frac{\partial \eta}{\partial x}^{m+1,k}\left(x_{\max}\right)\right)\right)\left(\varphi_l(0) - \eta_l^{m+1,k+1}(0)\right), \quad \forall \varphi_l \in K_l.
\end{aligned}
\tag{5.51}
$$

In order to solve the discretized nonlinear problem (5.51) we use the same techniques described in Chapter 3.

5.4 Numerical Test

In this section we present numerical results corresponding to three particular cases: cold, temperate and polythermal (meaning that parts of the base are cold and parts temperate). The results have been obtained by using the numerical methods briefly described in the previous section, and detailed in Chapter 3.

The departure point for the numerical techniques is a fixed domain formulation for the moving boundary problem. Particularly, we select the spatial domain $\Omega = [0,\ x_{\max}]$, where $x_{\max}$ is sufficiently large that Ω always contains the glacier profile. In practice, we take $x_{\max} = 3$. Next, we fix the boundary conditions at both ends of the domain. As intimated above, these are

$$
\begin{aligned}
\eta &= 0 \quad \text{at} \quad x = x_{\max}, \quad t > 0, \\
\Upsilon &= \Upsilon_0 \quad \text{at} \quad x = 0, \quad t > 0,
\end{aligned}
\tag{5.52}
$$

where Υ is given by (5.40) (and K by (5.35)). The initial condition is taken as

$$
\eta = 0 \quad \text{for} \quad t = 0, \quad x \in \Omega. \tag{5.53}
$$

In all runs we have chosen the accumulation rate function to be

$$a(x) = 1 - x \tag{5.54}$$

and the Glen exponent $n = 3$.

For the numerical solution a spatial mesh stepsize $\Delta x = 10^{-4}$ and a timestep of $\Delta t = 10^{-6}$ have been used. Moreover, for the fixed point iteration to deal with the nonlinear diffusive term a stopping test based on the error between two iterations being less than 10^{-6} has been used, while for the duality method 10^{-9} has been chosen.

In these tests we have imposed the accumulation-ablation function and the flux at the left of the domain, so we can compute the x-axis point where flux are zero for steady state (it is, when $\partial\eta/\partial t = 0$). We rewrite equation (5.34) in steady state as follows:

$$a(x,t) = \frac{\partial}{\partial x}\Upsilon_0(t), \tag{5.55}$$

We integrate this equation between 0 and x_{front} (with x_{front} the point where $\Upsilon_0(t) = 0$) and we get:

$$\int_0^{x_{front}} a(x,t)\,dx = \int_0^{x_{front}} \frac{\partial}{\partial x}\Upsilon_0(t)\,dx \Rightarrow \int_0^{x_{front}} a(x,t)\,dx = -\Upsilon_0(t), \tag{5.56}$$

and as in these tests, the value of the accumulation-ablation function, $a(t,x)$, is given by equation (5.54), so we can obtain the following equation that link the position of the front of the glacier and the flux imposed at the left of the glacier,

$$2x_{front} - x_{front}^2 = -2\Upsilon_0(t). \tag{5.57}$$

5.4.1 Example 1. Cold-based ice

The first example corresponds to the polar parameters which may be appropriate for the case where the effective basal heating is very small, and we expect to find a cold-based glacier. The parameters used are

$$\gamma = 5,\ g_b = 0.2,\ \mu = 0.13,\ \alpha = 0.125,\ \beta = 2.9,\ \Upsilon_0 = 0.1. \tag{5.58}$$

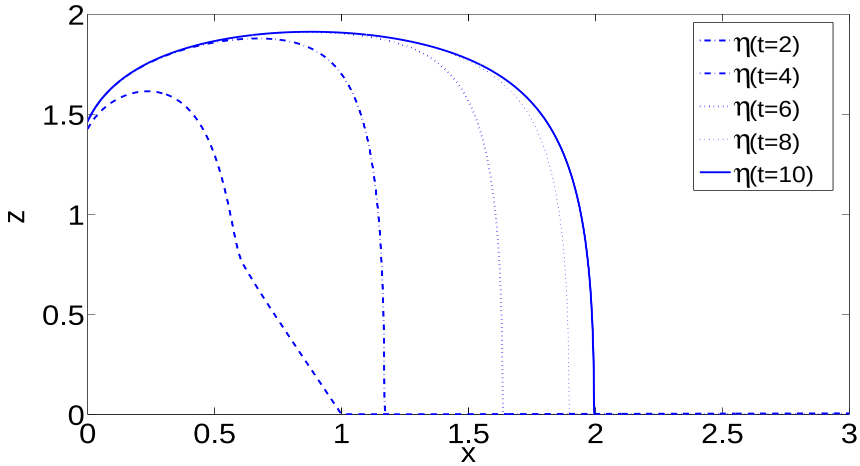

Figure 5.2: Evolution of the surface on solving (5.34) with the polar choice of parameters $\gamma = 5$, $g_b = 0.2$, $\mu = 0.13$, $\alpha = 0.125$, $\beta = 2.9$, $\Upsilon_0 = 0.1$.

With this set of parameters, the front of the glacier is at $x = 2.09$, that is the value of x_{front} when equation (5.57) is solved using $\Upsilon_0 = 0.1$. Figure 5.2 shows the computed profile evolution from $t = 2$ to $t = 10$ (when the profile has reached the steady state), after numerically solving equation (5.34) and we can check that x_{front} is the expected value. Figure 5.3 shows the computed temperature for $t = 10$ in the ice region, obtained from (5.36).

5.4.2 Example 2. Temperate-based ice

The second example corresponds to the sub-polar parameters for which the effective basal melting is large, and we expect a temperate-based glacier.[2] The parameters used are

$$\gamma = 2.5,\ g_b = 2.9,\ \mu = 0.13,\ \alpha = 0.25,\ \beta = 0.29,\ \Upsilon_0 = 0.5. \tag{5.59}$$

In this case, the expected front of the glacier is at $x = 2.41$, this value is computed solving equation (5.57) with $\Upsilon_0 = 0.5$. In Figure 5.4 we show the computed profile

[2]Over most of the domain. Near the snout of the glacier, the base must become cold according to the model.

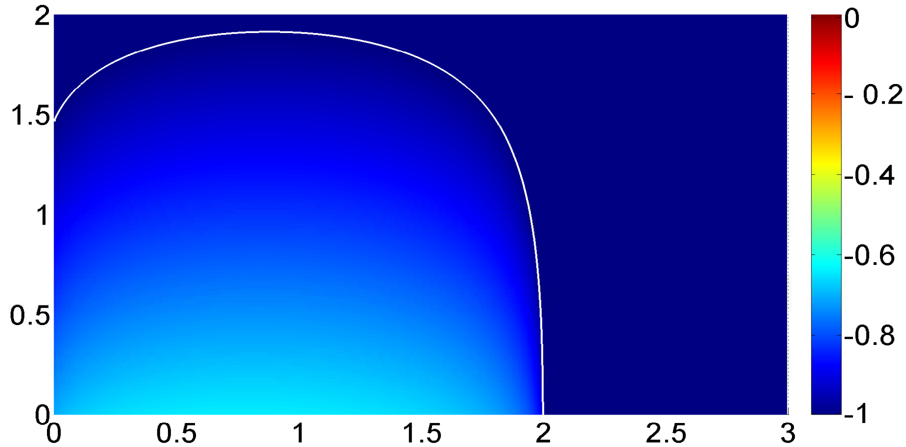

Figure 5.3: Ice temperature for the final steady state of the cold-based glacier; parameters as in Figure 5.2.

evolution from $t = 1$ to $t = 4$ (when it has again reached steady state), after numerically solving equation (5.34), and there we can check that the snout is at the expected coordinate. Figure 5.5 shows the computed temperature for $t = 4$ in the ice region, obtained from (5.36).

5.4.3 Example 3. Polythermal basal ice

The final example corresponds to a case where basal heat flux is smaller than for the sub-polar parameters. We expect that as g_b is reduced, the base will become increasingly cold at the head and snout, and that eventually the glacier will become cold based. Between the temperate-based and cold-based states, we find a mixed cold-temperate, or polythermal basal régime at the base of the glacier. The parameters used are

$$\gamma = 2.5,\ g_b = 1,\ \mu = 0.13,\ \alpha = 0.125,\ \beta = 2.9,\ \Upsilon_0 = 0.5. \qquad (5.60)$$

. The position of the front of the glacier in this case is the same that in the previous example, that is, $x = 2.41$, that is because the imposed interval, accumulation-ablation

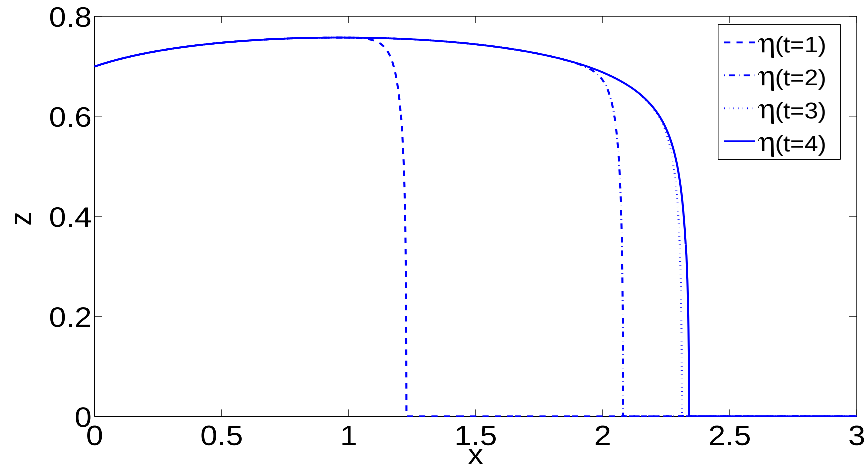

Figure 5.4: Evolution of the surface on solving (5.26) with the sub-polar choice of parameters $\gamma = 2.5$, $g_b = 2.9$, $\mu = 0.13$, $\alpha = 0.25$, $\beta = 0.29$, $\Upsilon_0 = 0.5$.

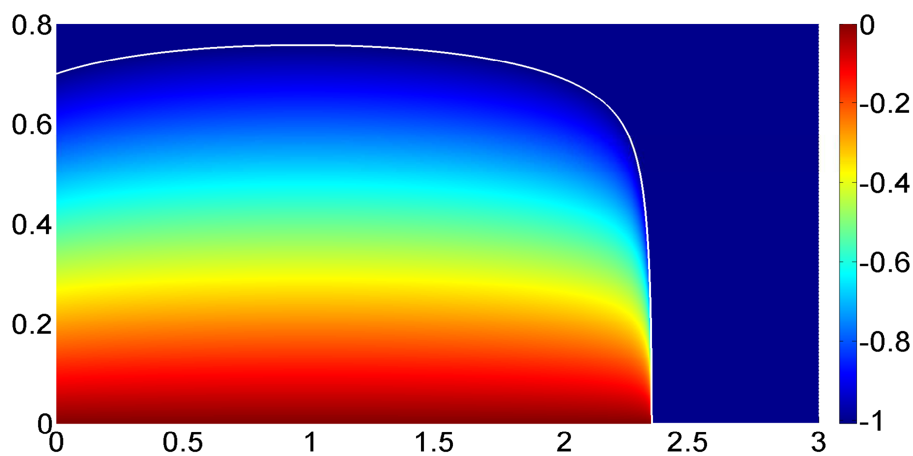

Figure 5.5: Ice temperature for the final steady state of the temperate-based glacier; parameters as in figure 5.4.

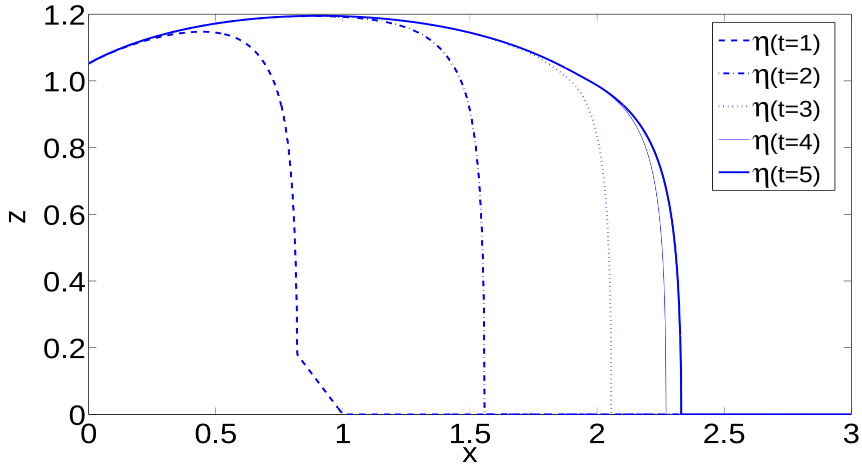

Figure 5.6: Evolution of the surface on solving (5.34) with the choice of parameters $\gamma = 2.5$, $g_b = 1$, $\mu = 0.13$, $\alpha = 0.125$, $\beta = 2.9$, $\Upsilon_0 = 0.5$.

function and flux at the left are the same that in the temperate-based ice example, $\Upsilon_0 = 0.5$. In Figure 5.6 we show the computed profile evolution from $t = 1$ to $t = 5$ (again at steady state), after numerically solving equation (5.34). Figure 5.7 shows the computed temperature for $t = 5$ in the ice region, obtained from (5.36).

5.5 Conclusions

Our principal aim in this chapter was to consider the issue of whether thermal runaway could properly happen in glacier flow, in a more comprehensive way than has been yet been done. In doing so, there are two problems to consider. The first is to consider whether thermal runaway can occur in the different possible basal thermal régimes which can exist at the base of the glacier, and the second is to consider whether, if runaway does occur, it leads in practice to an unlimited acceleration within the same basal thermal régime. Earlier work has shown that thermal runaway in shear flow models with fixed depth can occur, and this therefore remains a possibility if the temperature equation can respond more rapidly than the ice surface. Formally,

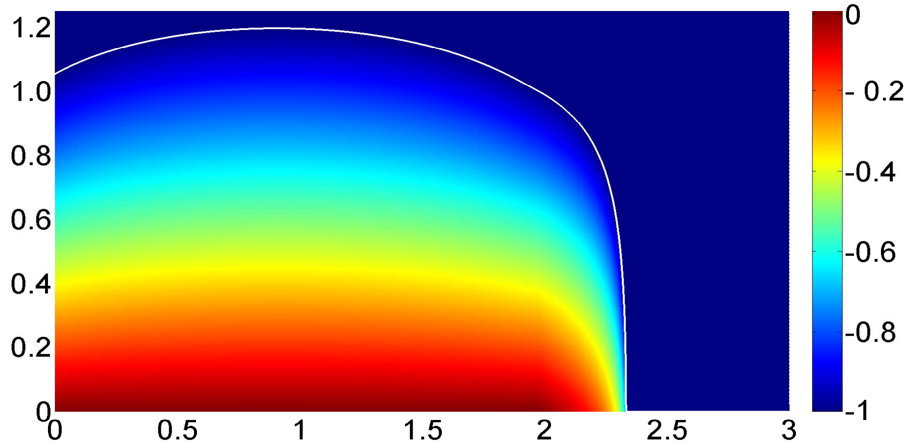

Figure 5.7: Ice temperature for the final steady state of the polythermal based glacier; parameters as in Figure 5.6.

this is the case for strongly temperature-dependent rheology, here taken as the limit $\gamma \gg 1$. In indulging this limit, we therefore provide a glacier flow model which would seem most likely to produce runaway, if it can occur at all. However, we have found that the progressive adjustment of thermal boundary conditions from cold to sub-temperate to temperate never in practice allows runaway occur, because one simply switches basal boundary conditions at the point where runaway could occur. The possibility of runaway when the basal ice (not boundary condition) becomes temperate, and internal moisture is generated, remains a possibility, but realistic modelling of temperate ice, allowing for moisture drainage, has not been done.

In building our approximate model to address this problem, we have constructed an effective non-isothermal ice surface evolution equation (5.38) which represents in a realistic way the evolution of the ice surface when the flow law is temperature dependent. The derivation of this equation suggests that temperature variation has very little effect on the overall motion of the glacier, other than mildly adjusting the depth scale of the flow.

A particular revelation of this exercise has been the unexpected inadequacy of geothermal heat. As measured by the parameter g_b, we have shown that a glacier remains cold-based until its depth $\eta > \frac{1}{g_b}$. If g_b is computed using normal values of geothermal heat flux, we find that it is so small that basal ice will never reach the melting point. In reality, entirely cold-based glaciers are something of a rarity, and we consider this to be due to the overwhelming importance of latent heat release by buried surface meltwater and rainwater. In the absence of such enhanced basal heating, glaciers would remain frozen at their base.

Symbol	Meaning	Typical value	Polar value
$[a^*]$	accumulation rate	$1\,\mathrm{m\,y^{-1}}$	$0.1\,\mathrm{m\,y^{-1}}$
A_m	flow rate factor	$0.17\,\mathrm{bar^{-n}\,y^{-1}}$	
c_p	specific heat	$2\,\mathrm{kJ\,kg^{-1}\,K^{-1}}$	
d_2	depth	$132\,\mathrm{m}$	
E	creep activation energy	$78.8\,\mathrm{kJ\,mole^{-1}}$	
g	gravity	$9.81\,\mathrm{m\,s^{-2}}$	
G	geothermal heat flux	$60\,\mathrm{mW\,m^{-2}}$	
G^*	effective geothermal heat flux	$1\,\mathrm{W\,m^{-2}}$	$60\,\mathrm{mW\,m^{-2}}$
H	elevation loss	$1\,\mathrm{km}$	
k	thermal conductivity	$2.2\,\mathrm{W\,m^{-1}\,K^{-1}}$	
d_1	length	$10\,\mathrm{km}$	
L	latent heat	$3.3\times10^5\,\mathrm{J\,kg^{-1}}$	
n	Glen exponent	3	
R	gas constant	$8.3\,\mathrm{J\,mole^{-1}\,K^{-1}}$	
Θ_m	melting temperature	$273\,\mathrm{K}$	
$[U]$	velocity	$76\,\mathrm{m\,y^{-1}}$	
V	effective surface melt rate	$0.1\,\mathrm{m\,y^{-1}}$	$0\,\mathrm{m\,y^{-1}}$
$\Delta\Theta$	surface temperature deficit	$20\,\mathrm{K}$	$40\,\mathrm{K}$
$\kappa = k/\rho c_p$	thermal diffusivity	$1.2\times10^{-6}\,\mathrm{m^2\,s^{-1}}$	
ρ	ice density	$917\,\mathrm{kg\,m^{-3}}$	
$[\tau^*]$	stress	$1.2\,\mathrm{bar}$	
$\sin\chi$	slope	0.1	

Table 5.1: Parameter values. The accumulation rate, surface temperature, surface melt rate, and consequent effective geothermal heat flux take two values, representing the essentially polar and sub-polar régimes.

Parameter	Definition	Sub-polar value	Polar value
r	(5.8)	1.1	
St	(5.8)	8.25	4.13
α	$(2.54)^3$	0.25	0.13
β	$(2.53)^2$	0.29	2.9
γ	(2.86)	2.5	5
g_b	(5.6)	2.9	0.17
μ	(2.36)	0.13	

Table 5.2: Dimensionless parameter values, using the estimates in table 5.1. Based on the different sub-polar (typical) and polar values, we compute two different estimates for parameters, as indicated. Where no polar value is indicated, the estimates do not differ.

Chapter 6

Conclusions

Our objective in this work has been to contribute to the mathematical modelling and numerical simulation of glaciers beheviour in the frame of shallow ice approximation (SIA) models. For this purpose,isothermal and non isothermal models are formulated in terms of systems of highly nonlinear partial differential equations, which eventually involve moving boundary problems. For the numerical solution of the complex models a variety of numerical techniques are proposed. In this final conclusion section, we summarizes some of the conclusions already presented in each chapter.

More precisely, for the profile problem arising in the isothermal model the main novelty relies on their formulation in terms of a new obstacle problem associated to a highly nonlinear convection-diffusion equation. We use fixed domain formulations where the unknown moving boundary between the ice covered and ice free regions is implicitly obtained. The modelling of prescribed profile and prescribed flux at the glacier head leads to two different fixed domain formulations, the second one being the more innovative in view of the existing literature. The main advantage with respect to some possible front-tracking alternatives (posing the nonlinear equation in the unknown ice covered domain) comes from our use of a fixed domain and a fixed mesh instead of updating the mesh associated to the ice covered domain at each time step. For the numerical solution, a combination of characteristics method for time discretization, a duality method for the nonlinear obstacle formulation and an appropriate explicit treatment of the nonlinear diffusive term have been considered.

Moreover, piecewise linear Lagrange finite elements for the spatial discretization have been used.

Numerical results illustrate the performance of the proposed numerical algorithm and techniques when applied to an academic example with closed form analytical solution. When addressing problems with not know analytical solution, in polar regimes the results show the presence of an infinite slope when a zero profile condition at the head is prescribed. This is motivated by the appearance of unrealistic negative fluxes at the head in this formulation. Therefore, an original and more realistic formulation with prescribed flux at the head is proposed and numerical methods are suitably adapted.

In the non isothemal case, main innovative aspect is the consideration of a non isothermal model for the profile equation, thus fully coupled with the shallow ice approximation for the velocity and the temperature equation. This new profile model is posed in terms of a new obstacle problem associated to an integro-differential equation, the numerical solution of which is addressed by the same techniques that in the isothermal model jointly with numerical integration for the nonlocal diffusion coefficient function.

In addition to the specific difficulties associated to the new profile model formulation, different appropriate techniques have been applied for the numerical solution of the temperature equation: an enthalpy formulation for the two phase Stefan problem, a characteristics method for the time discretization, duality methods associated to maximal monotone operators, a Newton method for the nonlinear term associated to thermal viscous dissipation and piecewise linear finite elements for spatial discretization. Moreover, specific numerical quadrature techniques are considered to compute the velocity field.

Once each subproblem has been solved with the appropriate numerical techniques, a fixed point iterative method is performed for the solution of the coupled problem, which essentially solves sequentially each of the subproblems.

This set of numerical techniques has been applied to several test examples. Thus, illustrative examples concerning the case of polar, polythermal and temperate regimes have been considered. Moreover, after the remarks in Chapter 3 concerning the appropriate boundary conditions upstream, also the case of flux imposed or profile imposed boundary condition at the left boundary of the glacier are presented. Again, as in the isothermal model treated in Chapter 3, the computed numerical results show that flux imposed boundary results to be more realistic due to the fact that the Dirichlet boundary condition leads to almost infinite slopes at the left glacier boundary. Also notice that, in the case of flux imposed boundary condition, the same technique developed in Chapter 3 allows to obtain the exact position of the free boundary. This value has been very accurately verified by the computations.

Also, the issue of whether thermal runaway, our principal aim in that chapter was to consider the issue of whether thermal runaway could properly happen in glacier flow, in a more comprehensive way than has been yet been done. In doing so, there are two problems to consider. The first is to consider whether thermal runaway can occur in the different possible basal thermal régimes which can exist at the base of the glacier, and the second is to consider whether, if runaway does occur, it leads in practice to an unlimited acceleration within the same basal thermal régime. Earlier work has shown that thermal runaway in shear flow models with fixed depth can occur, and this therefore remains a possibility if the temperature equation can respond more rapidly than the ice surface. Formally, this is the case for strongly temperature-dependent rheology, here taken as the limit $\gamma \gg 1$. In indulging this limit, we therefore provide a glacier flow model which would seem most likely to produce runaway, if it can occur at all. However, we have found that the progressive adjustment of thermal boundary conditions from cold to sub-temperate to temperate never in practice allows runaway occur, because one simply switches basal boundary conditions at the point where runaway could occur. The possibility of runaway when the basal ice (not boundary condition) becomes temperate, and internal moisture is generated, remains a possibility, but realistic modelling of temperate ice, allowing for moisture drainage, has not been done.

In building our approximate model to address this problem, we have constructed an effective non-isothermal ice surface evolution equation (5.38) which represents in a realistic way the evolution of the ice surface when the flow law is temperature dependent. The derivation of this equation suggests that temperature variation has very little effect on the overall motion of the glacier, other than mildly adjusting the depth scale of the flow.

A particular revelation of this exercise has been the unexpected inadequacy of geothermal heat. As measured by the parameter g_b, we have shown that a glacier remains cold-based until its depth $\eta > \dfrac{1}{g_b}$. If g_b is computed using normal values of geothermal heat flux, we find that it is so small that basal ice will never reach the melting point. In reality, entirely cold-based glaciers are something of a rarity, and we consider this to be due to the overwhelming importance of latent heat release by buried surface meltwater and rainwater. In the absence of such enhanced basal heating, glaciers would remain frozen at their base.

The main general conclusion is that the proposed set of numerical techniques results to be appropriate for the numerical solution of the complex shallow ice mathematical models that govern the thermomechanical behaviour of polar, polythermal and temperate glaciers, as it is also illustrated by the numerical results. We also point out that the here developed work concerning to modelling and numerical simulation poses interesting open problems related to the theoretical analysis of different particular and global models.

Appendix A

Monotone Operators and Yosida Approximations

A.1 Monotone operators

Throughout the present work, several nonlinear terms appearing in the complex mathematical models are numerically solved by means of the particular duality method introduced in Bermúdez–Moreno [5]. The justification of this duality method requires some concepts and results of the theory about maximal monotone operators. The concepts and results are summarized in this appendix. A more detailed explanation and the proof of some results can be found in Brezis [10].

Let us consider a Hilbert space W, equipped with the inner product denoted by $(\cdot, \cdot)$ and the associated norm $|\cdot|$.

Definition 1 An operator G is an application of W in the set of parts of W, denoted by $P(W)$.

Definition 2 Let us denote the domain of the operator G by the set

$$D(G) = \{x \in W / G(x) \neq 0\}.$$

Definition 3 Let us denote the image of the operator G by the set

$$R\left(G\right)=\bigcup_{x\in W}G\left(x\right).$$

Definition 4 The operator G is univalued if for all $x\in W$, $G\left(x\right)$ contains at most one element. Otherwise, the operator is multivalued.

Definition 5 The graph of operator G is the $W\times W$ subset given by

$$\left\{\left(x,y\right)\in W\times W/y\in G\left(x\right)\right\}.$$

Definition 6 The operator G is monotone if $\forall u_1\in G\left(y_1\right)$ and $\forall u_2\in G\left(y_2\right)$ it verifies that

$$\left(u_1-u_2,y_1-y_2\right)\geq 0.$$

In the set of operators of W we define the following order relation in terms of the graphs inclusion:

$$G_1\subset G_2\Leftrightarrow\forall x\in W,G_1\left(x\right)\subset G_2\left(x\right).$$

The set of monotone operators is inductive with respect to this relation, since it is different of the empty set, and for the given fully ordered chain of monotone operators

$$G_1\subset G_2\subset\ldots\subset G_j\subset G_{j+1}\subset\ldots,\quad j\in J,$$

the monotone operator

$$G:x\in W\rightarrow G\left(x\right)=\bigcup_{j\in J}G_j\left(x\right).$$

is an upper bound for the chain. Zorn Lemma ensures the existence of maximal elements in the monotone operators set.

Definition 7 An operator G is maximal monotone if it is a maximal element in the monotone operators set with respect to the previous relation.

The following characterization is important in the maximal monotone operators study.

Proposition 1 If G is a monotone operator, the following three properties are equivalent:

1. G is maximal.
2. $\operatorname{rang}(I+G)=W$.
3. $\forall\lambda>0, (I+\lambda G)^{-1}$ is a contraction from W to W.

Definition 8 Let be G a given maximal monotone operator and $\lambda>0$, the resolvent of G of parameter λ is the operator from W to W, defined by

$$J_\lambda=(I+\lambda G)^{-1}, \quad \lambda>0.$$

Definition 9 Let be G a maximal monotone operator and $\lambda>0$, the Yosida approximation of G of parameter λ is the univalued operator defined by

$$G_\lambda=\frac{I-J_\lambda}{\lambda}, \quad \lambda>0.$$

In terms of the previous definition, the following proposition holds (see [5] for details).

Proposition 2 Let G be a maximal monotone operator. Then, for the real numbers λ and ω such that $\lambda\omega<1$, $\lambda>0$ and $\omega\geq 0$, given $f\in W$, there exists a $y\in W$ such that $f\in(1-\lambda\omega)\,y+\lambda G(y)$. The following result (see [5] for details) is fundamental to justify the duality algorithm proposed to solve the problems throughout this Thesis.

Lemma 1 Let be G a maximal monotone operator in W. They are equivalent:

1. $u\in G(y)-wy$.
2. $u=G_\lambda^\omega(y+\lambda u)\,, \quad \lambda>0,$

where G_λ^ω denotes the Yosida approximation with real parameter λ of the operator $G-\omega I$.

In the previous result it appears the Yosida approximation of operator $G-\omega I$, the computation of which (in terms of Yosida approximation of G) we detail in the following remark:

Remark 1 If we denote by J_λ the resolvent operator of G and by J_λ^ω the resolvent operator of $G-\omega I$, i.e.,

$$J_\lambda = (I+\lambda G)^{-1}, \quad J_\lambda^\omega = (I+\lambda(G-\omega I))^{-1},$$

then the following identity holds:

$$J_\lambda^\omega(x) = J_{\frac{\lambda}{1-\lambda\omega}}\left(\frac{x}{1-\lambda\omega}\right).$$

More precisely, for $y \in J_\lambda^\omega(x)$ we have

$$x \in (I+\lambda(G-\omega I))(y) \Leftrightarrow \frac{x-(1-\lambda\omega)y}{\lambda} \in G(y) \Leftrightarrow \frac{\frac{x}{1-\lambda\omega}-y}{\frac{\lambda}{1-\lambda\omega}} \in G(y),$$

and, consequently,

$$y \in J_{\frac{\lambda}{1-\lambda\omega}}\left(\frac{x}{1-\lambda\omega}\right).$$

Next, if we compute the Yosida approximation of $G-\omega I$, denoted by G_λ^ω, we get

$$\begin{aligned}
G_\lambda^\omega(x) &= \left(\frac{I-J_\lambda^\omega}{\lambda}\right)(x) = \frac{1}{\lambda}\left[\frac{x}{1-\lambda\omega} - J_{\frac{\lambda}{1-\lambda\omega}}\left(\frac{x}{1-\lambda\omega}\right) - \frac{\lambda\omega}{1-\lambda\omega}x\right] \\
&= \frac{1}{1-\lambda\omega}\frac{1-\lambda\omega}{\lambda}\left[\frac{x}{1-\lambda\omega} - J_{\frac{\lambda}{1-\lambda\omega}}\left(\frac{x}{1-\lambda\omega}\right)\right] - \frac{\omega}{1-\lambda\omega}x \\
&= \frac{1}{1-\lambda\omega}G_{\frac{\lambda}{1-\lambda\omega}}\left(\frac{x}{1-\lambda\omega}\right) - \frac{\omega}{1-\lambda\omega}x,
\end{aligned}$$

where $G_{\frac{\lambda}{1-\lambda\omega}}$ denotes the Yosida approximation of the operator G with parameter $\frac{\lambda}{1-\lambda\omega}$.

A.2 Yosida approximation of the enthalpy operator in the thermal problem

In the thermal problem appearing in Chapter 4, the operator $E\circ\Lambda^{-1}$ is maximal monotone. Thus, using the previuos remark, the Yosida approximation of parameter λ of the operator $(E\circ\Lambda^{-1})-\omega I$ can be written as follows:

$$\left(E\circ\Lambda^{-1}\right)_\lambda^\omega(\Theta) = \frac{1}{1-\lambda\omega}\left(E\circ\Lambda^{-1}\right)_{\frac{\lambda}{1-\lambda\omega}}\left(\frac{\Theta}{1-\lambda\omega}\right) - \frac{\omega}{1-\lambda\omega}\Theta.$$

Therefore, if we denote

$$\begin{aligned}\bar{\lambda} &= \frac{\lambda}{1-\lambda\omega},\\ \bar{\Theta} &= \frac{\Theta}{1-\lambda\omega},\end{aligned}$$

then we get the following identity:

$$\left(E\circ\Lambda^{-1}\right)_{\lambda}^{\omega}(\Theta) = \frac{1}{1-\lambda\omega}\left(E\circ\Lambda^{-1}\right)_{\bar{\lambda}}\left(\bar{\Theta}\right) - \omega\bar{\Theta},$$

where

$$\left(E\circ\Lambda^{-1}\right)_{\bar{\lambda}}\left(\bar{\Theta}\right) = \frac{\bar{\Theta} - J_{\bar{\lambda}}\left(\bar{\Theta}\right)}{\bar{\lambda}}, \quad J_{\bar{\lambda}} = \left[I + \bar{\lambda}\left(E\circ\Lambda^{-1}\right)\right]^{-1}.$$

In the particular case where density (ρ), specific heat (c) and thermal conductivity (k) are constant at each solid and liquid phase, we have the following expressions for the enthalpy, the Kirchoff variable change and its inverse:

$$E(\Theta) = \begin{cases} \rho_s c_s \Theta & \text{if } \Theta < T_m, \\ \left[\rho_s c_s T_m, \rho_s c_s T_m + \rho_s L_c\right] & \text{if } \Theta = T_m, \\ \rho_l c_l \Theta + \left(\rho_s c_s - \rho_l c_l\right) T_m + \rho_s L_c & \text{if } \Theta > T_m, \end{cases} \tag{A.1}$$

$$\Lambda(\Theta) = \begin{cases} k_s \Theta & \text{if } \Theta < T_m, \\ k_s T_m & \text{if } \Theta = T_m, \\ k_l \Theta + \left(k_s - k_l\right) T_m & \text{if } \Theta > T_m, \end{cases} \tag{A.2}$$

$$\Lambda^{-1}(\Theta) = \begin{cases} \frac{1}{k_s}\Theta & \text{if } \Theta < k_s T_m, \\ T_m & \text{if } \Theta = k_s T_m, \\ \frac{1}{k_l}\Theta + \left(1 - \frac{k_s}{k_l}\right) T_m & \text{if } \Theta > k_s T_m, \end{cases} \tag{A.3}$$

where the subindexes s and l indicate the solid and liquid phases respectively, L_c is the latent heat and T_m is the phase change temperature.

Moreover, if we denote

$$\begin{aligned} A_1 &= k_s T_m + \bar{\lambda}\rho_s c_s T_m, \\ A_2 &= k_s T_m + \bar{\lambda}\rho_s c_s T_m + \bar{\lambda}\rho_s L_c, \end{aligned}$$

then the resolvent operator $J_{\bar{\lambda}}$ is given by the following expression:

$$J_{\bar{\lambda}}\left(\bar{\Theta}\right)=\begin{cases}\frac{1}{1+\frac{\bar{\lambda}\rho_s c_s}{k_s}}\bar{\Theta} & \text{if} \quad \bar{\Theta}<A_1,\\ k_s T_m & \text{if} \quad A_1\leq\bar{\Theta}\leq A_2,\\ \frac{1}{1+\frac{\bar{\lambda}\rho_l c_l}{k_l}}\bar{\Theta}+\frac{(k_s\rho_l c_l-k_l\rho_s c_s)\bar{\lambda}T_m-\rho_s k_l\bar{\lambda}L_c}{k_l+\bar{\lambda}\rho_l c_l}T_m & \text{if} \quad \bar{\Theta}>A_2,\end{cases} \tag{A.4}$$

and therefore, $(E\circ\Lambda^{-1})_{\bar{\lambda}}$ is given by:

$$\left(E\circ\Lambda^{-1}\right)_{\bar{\lambda}}\left(\bar{\Theta}\right)=\begin{cases}\frac{\rho_s c_s}{k_s\left(1+\frac{\bar{\lambda}\rho_s c_s}{k_s}\right)}\bar{\Theta} & \text{if} \quad \bar{\Theta}<A_1,\\ \frac{1}{\bar{\lambda}}\left(\bar{\Theta}-k_s T_m\right) & \text{if} \quad A_1\leq\bar{\Theta}\leq A_2,\\ \frac{1}{1+\frac{\bar{\lambda}\rho_l c_l}{k_l}}\left(\frac{\rho_l c_l}{k_l}\bar{\Theta}+k_s T_m\left(\frac{\rho_s c_s}{k_s}-\frac{\rho_l c_l}{k_l}\right)+\rho_s L_c\right) & \text{if} \quad \bar{\Theta}>A_2,\end{cases}$$

In the particular case of the Stefan problem posed in Chapter 4, the previous expressions result to be simplified to obtain:

$$\begin{aligned}E\left(\Theta\right) &= \begin{cases}\Theta & \text{if} \quad \Theta<0,\\ [0,\,L_c] & \text{if} \quad \Theta=0,\\ L_c & \text{if} \quad \Theta>0,\end{cases}\\ \Lambda\left(\Theta\right) &= \beta\Theta,\\ \Lambda^{-1}\left(\Theta\right) &= \frac{1}{\beta}\Theta,\end{aligned}$$

so, we have:

$$\begin{aligned}J_{\bar{\lambda}}\left(\bar{\Theta}\right) &= \begin{cases}\frac{1}{1+\frac{\bar{\lambda}}{\beta}}\bar{\Theta} & \text{if} \quad \bar{\Theta}<0,\\ 0 & \text{if} \quad 0\leq\bar{\Theta}\leq\bar{\lambda}L_c,\\ \bar{\Theta}-\bar{\lambda}L_c & \text{if} \quad \bar{\Theta}>\bar{\lambda}L_c,\end{cases}\\ \left(E\circ\Lambda^{-1}\right)_{\bar{\lambda}}\left(\bar{\Theta}\right) &= \begin{cases}\frac{\bar{\Theta}}{\beta+\bar{\lambda}} & \text{if} \quad \bar{\Theta}<0,\\ \frac{\bar{\Theta}}{\bar{\lambda}} & \text{if} \quad 0\leq\bar{\Theta}\leq\bar{\lambda}L_c,\\ L_c & \text{if} \quad \bar{\Theta}>\bar{\lambda}L_c,\end{cases}\end{aligned}$$

where $\beta=k_s=k_l$. Moreover, when $\lambda\omega=1/2$, the Yosida approximation of operator

$(E \circ \Lambda^{-1}) - \omega I$ of parameter $1/2\omega$ is given by:

$$\left(E \circ \Lambda^{-1}\right)^{\omega}_{\frac{1}{2\omega}}(\Theta) = \begin{cases} 2\frac{2\Theta}{\beta + \frac{1}{\omega}} - 2\omega\Theta & \text{if} \quad \Theta < 0, \\ 2\omega\Theta & \text{if} \quad 0 \leq \Theta \leq \frac{L_c}{2\omega}, \\ 2L_c - 2\omega\Theta & \text{if} \quad \Theta > \frac{L_c}{2\omega}, \end{cases}$$

A.3 Yosida approximation of the Heaviside operator in the thermal problem

Also when considering the Signorini basal boundary condition in the nonlinear thermal problem treated in Chapter 4, the multivalued Heaviside operator H appears. So we need to obtain the Yosida approximation of the maximal monotone operator $H \circ \Lambda^{-1}$ which is denoted by $\left[I + \bar{\lambda}\,(H \circ \Lambda^{-1})\right]^{-1}$. We just have to repeat expressions (A.1)–(A.4) with the following data:

$$T_m = 0, \quad \rho_s c_s = 0, \quad \rho_l c_l = 0, \quad \rho_s L_c = 1, \quad k_s = 1, \quad k_l = 1.$$

So, we get the following expression for the resolvent of the operator $H \circ \Lambda^{-1}$:

$$\left[I + \bar{\lambda}\left(H \circ \Lambda^{-1}\right)\right]^{-1}(\bar{\Theta}) = \begin{cases} \bar{\Theta} & \text{if} \quad \bar{\Theta} < 0, \\ 0 & \text{if} \quad 0 \leq \bar{\Theta} \leq \bar{\lambda}, \\ \bar{\Theta} - \bar{\lambda} & \text{if} \quad \bar{\Theta} > \bar{\lambda}, \end{cases}$$

and the following one for the Yosida approximation:

$$\left(H \circ \Lambda^{-1}\right)_{\bar{\lambda}}(\bar{\Theta}) = \begin{cases} 0 & \text{if} \quad \bar{\Theta} < 0, \\ \frac{\bar{\Theta}}{\bar{\lambda}} & \text{if} \quad 0 \leq \bar{\Theta} \leq \bar{\lambda}, \\ 1 & \text{if} \quad \bar{\Theta} > \bar{\lambda}. \end{cases}$$

Finally, using the operator $(H \circ \Lambda^{-1})^{\omega}_{\lambda}$ for the particular case $\lambda\omega = 1/2$ is

$$\left(H \circ \Lambda^{-1}\right)^{\omega}_{\frac{1}{2\omega}}(\Theta) = \begin{cases} -2\omega\Theta & \text{if} \quad \Theta < 0, \\ 2\omega\Theta & \text{if} \quad 0 \leq \Theta \leq \frac{1}{2\omega}, \\ 2\left(1 - \omega\Theta\right) & \text{if} \quad \Theta > \frac{1}{2\omega}. \end{cases}$$

A.4 Yosida approximation of the subdifferential of the indicatrix function of a convex

In the profile problems appearing in Chapters 3 and 4, the nonnegative profile function constraint gives rise to an associated convex set in the variational inequality formulation.

The use of a duality method for the numerical solution involves the consideration of a maximal monotone operator defined as the subdifferential of the indicatrix of the convex set. At this section we detail the required computation for the use of Bermudez–Moreno technique [5].

Let be W a Hilbert space, K a closed convex subset of W and ∂I_K the subdifferential of the indicatrix function of the convex K. Then, the operator ∂I_K is maximal monotone.

If K_λ^ω denotes the Yosida approximation of the operator $\partial I_K - \omega I$, this particular Yosida approximation can be easily expressed in terms of the function P_K, which denotes the projection over the set K.

Note the Remark 1 in this appendix allow us to write:

$$K_\lambda^\omega(x) = \frac{1}{1-\lambda\omega} K_{\frac{\lambda}{1-\lambda\omega}}\left(\frac{x}{1-\lambda\omega}\right) - \frac{\omega}{1-\lambda\omega}x,$$

and, if we denote by:

$$\begin{aligned} \bar{\lambda} &= \frac{\lambda}{1-\lambda\omega}, \\ \bar{x} &= \frac{x}{1-\lambda\omega}, \end{aligned}$$

we can obtain the following identity:

$$K_\lambda^\omega(x) = \frac{1}{1-\lambda\omega} K_{\bar{\lambda}}(\bar{x}) - \omega\bar{x},$$

where

$$K_{\bar{\lambda}} = \frac{1}{\bar{\lambda}}\left(\bar{x} - J_{\bar{\lambda}}(\bar{x})\right), \qquad J_{\bar{\lambda}} = \left(I + \bar{\lambda}\partial I_K\right)^{-1}.$$

Next, we compute the resolvent operator $J_{\bar{\lambda}} = \left(I + \bar{\lambda}\partial I_K\right)^{-1}$.

Given $x \in W$, let be $y \in J_{\bar{\lambda}}(x) = \left(I + \bar{\lambda}\partial I_K\right)^{-1}(x)$. Then, we have the equivalence:

$$x \in \left(I + \bar{\lambda}\partial I_K\right)(y) \Leftrightarrow \frac{x-y}{\bar{\lambda}} \in \partial I_K(y).$$

So, if we use the definition of subdifferential we have

$$I_K(z) - I_K(y) \geq \left(\frac{x-y}{\bar{\lambda}}, z-y\right), \qquad \forall z \in W.$$

Therefore, the previous inequality leads to:

$$y \in K, \quad I_K(z) \geq \left(\frac{x-y}{\bar{\lambda}}, z-y\right), \qquad \forall z \in W,$$

or equivalently:

$$0 \geq \left(\frac{x-y}{\bar{\lambda}}, z-y\right), \qquad \forall z \in K.$$

So, we have

$$y \in K, \qquad (x, z-y) \leq (y, z-y), \qquad \forall z \in K.$$

and the element can be characterized as:

$$y = P_K(x).$$

Thus, we can express $K_{\bar{\lambda}}$ in the following way:

$$K_{\bar{\lambda}}(\bar{x}) = \frac{\bar{x} - P_K(\bar{x})}{\bar{\lambda}}.$$

Finally, the expression of K_{λ}^{ω} for the particular case $\lambda\omega = 1/2$ is given by:

$$K^{\omega}_{\frac{1}{2\omega}}(x) = \begin{cases} -2\omega x & \text{if} \quad x \geq 0, \\ 2\omega x & \text{if} \quad x < 0. \end{cases}$$

Appendix B

Computer implementation

B.1 GLANUSIT: a software toolbox for the numerical simulation of large ice masses evolution

In this section we present the GLAciology NUmerical SImulation Toolbox (GLANUSIT), that consist of a software application which provides a user friendly environment for the numerical simulation of glaciers. This toolbox implements the numerical algorithms proposed in this Thesis to solve the global coupled model. Nevertheless, as it is a modular toolbox, it can be changed easily to incorporate other partial models or improvements of the existing ones.

Both the highly specific techniques and the complexity of the coupling between submodels explain the fact that there is no software toolbox for the numerical simulation of the coupled process. A possible alternative, which consist of the solution of the even more complex departure continuum mechanics models [55], might be offered by certain commercial codes like FLUENT or COMSOL. Nevertheless, in such approach, the equations become more complicated and the presence of several moving boundaries is neither available in the models nor in the codes. Nowadats, therefore there exits a computer system that implements the Shallow Ice Approximation, this system is called SICOPOLIS [45], but this system is valid for ice sheets, not for glaciers. Also for ice sheets a previous version of GLANUSIT has been developed as it is described in [15]. Therefore, GLANUSIT is a software application motivated by this previous necessities.

As in most finite element software libraries, the numerical methods developed in GLANUSIT kernel are written in FORTRAN 90 language. The existence of periodically improved FORTRAN compilers for personal computers and for cluster of computers motivates the choice of this language for the GLANUSIT kernel implementation. Moreover, to present GLANUSIT in a user-friendly environment, we have select the multifunction system MATLAB. Note that there exist several MATLAB toolboxes (PDE Toolbox, COMSOL) to solve systems of partial differential equations with some finite element methods [65], which do not include those handled by GLANUSIT. The appearance of their graphical user interfaces has been taken as a reference. The combination of numerical computing in FORTRAN codes with the interface in the MATLAB environment can be additionally justified by several reasons. First, the use of MATLAB in finite element computations becomes very slow for fine enough meshes to obtain the required accurate results. Secondly, the use of FORTRAN90 for the interface programming part should be a possible alternative, more tedious than the easier to handle MATLAB commands. Thirdly, MATLAB allows to execute FORTRAN codes as internal functions.

B.1.1 Software design

In order to analyze and design the appropriate environment for the here described software toolbox, GLANUSIT, Object Oriented Methodology (OOM) is nowadays the most adequate software development technology [42]. Particularly, Unified Modelling Language (UML) can be used to easily describe the object-oriented model of the environment [7]. Thus, in the case of this software application, the system contains a session manager, a data management, a postprocessing and a main kernel (core) which implements the numerical techniques for solving the model (see Figure B.1).

In the designing process, the main system requirements were: an input data and

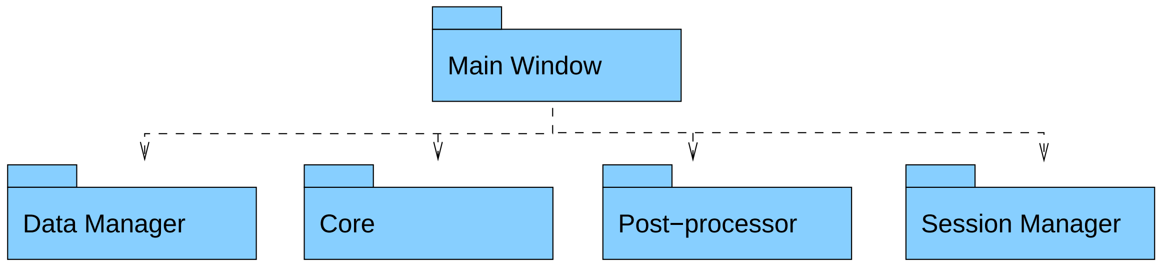

Figure B.1: Modules of GLANUSIT system

a results management both user friendly and implemented with a graphical interface. Moreover, our system must allow include new functionalities, both at the input and output interface and it must let us introduce easily improvements in the core of the system [15]. Concerning to the potential users, the software has been designed so that not only researchers with more physical, glaciological or environmental science background and interest, but also applied mathematicians and numerical analysts can take the maximum advantage. Thus, for example, the possibility of adjusting the parameters associated to the numerical methods is available.

In the session manager subsystem the basic element is the session (which identifies the user's workspace) characterized by its name, directory, state and associated folders and files. In Figure B.2 the possible session states are sketched. In GLANUSIT the session manager controls the current available menu at the interface.

The data management package contains the controls of two data types: the physical data and the options and parameters of the numerical methods, Two windows at the interface are available for reading, storing, showing, printing and updating both data sets (see Fig. B.3). Moreover, the data manager transforms the physical data according to the shallow ice scaling to obtain the corresponding dimensionless values (see Chapter 2 for details about the shallow ice scaling). These dimensionless data are the ones actually used by the numerical methods. Then, before the postprocessing process, the inverse scaling of the dimensionless computed results to recover the physical magnitudes is performed.

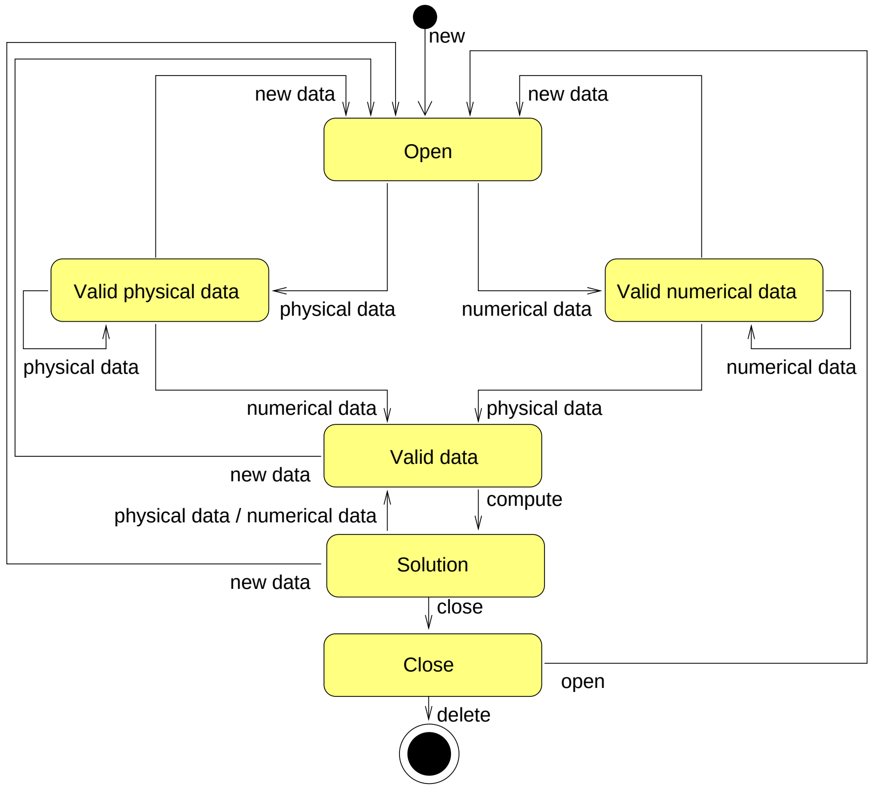

Figure B.2: States of GLANUSIT system

The postprocessor module provides the resources for analyzing the different physical magnitudes computed by the numerical methods. For this purpose, the user can choose among asking for numerical values, plotting or displaying movies of the different magnitudes. In the first case, to obtain the numerical valued of a $1D$ basal magnitude (sliding velocity, basal temperature, basal stress and ice width above a basal point) or a $2D$ one (velocity, temperature and stress), the appropriate data (time and spatial coordinates) have to be introduced (see Fig. B.4). In the second case, the user selects the set of magnitudes (either $1D$ or $2D$) to be plotted for a prescribed time (see Fig. B.5). In the third case, a movie with the evolution of the selected magnitudes is played (see Fig. B.6). The core module contains the FORTRAN90 code which develops the specific numerical methods to solve the complex global shallow ice approximation model. The execution of the code is activated at

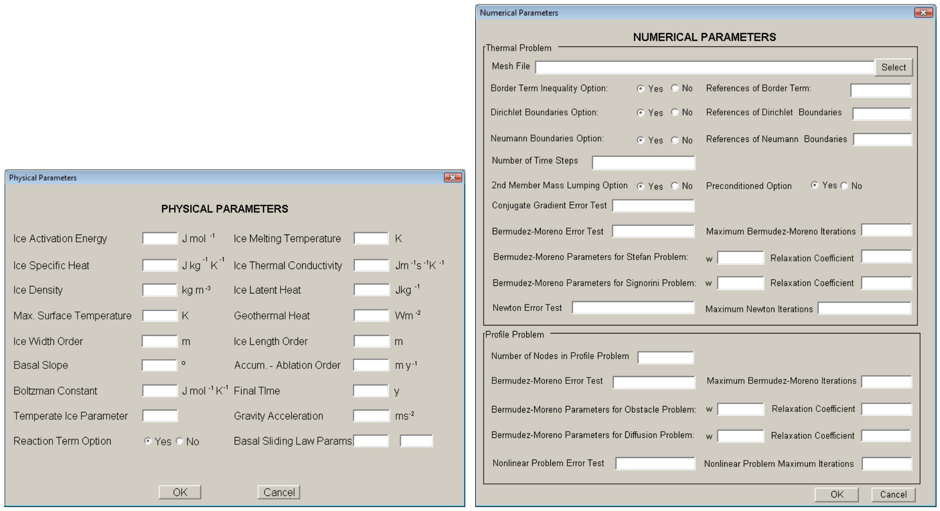

Figure B.3: Input Data

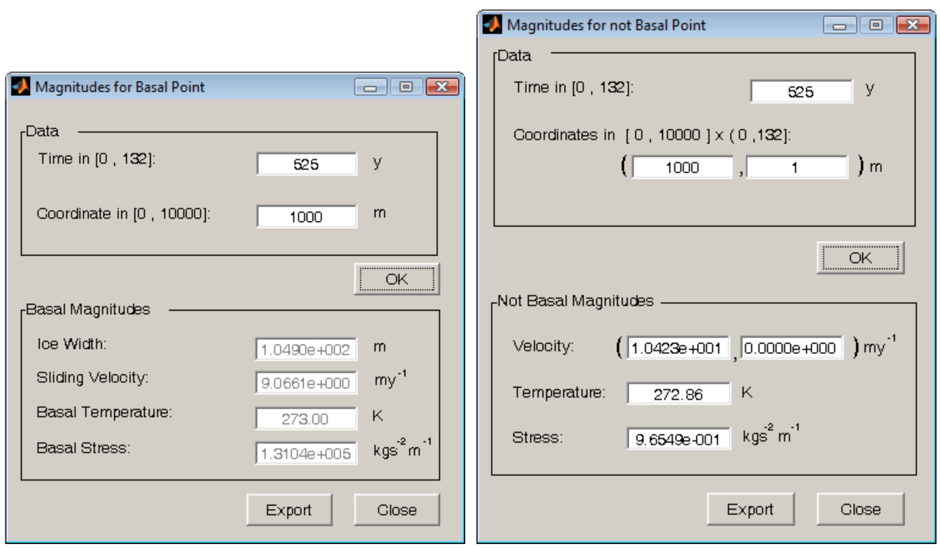

Figure B.4: Numerical Solutions

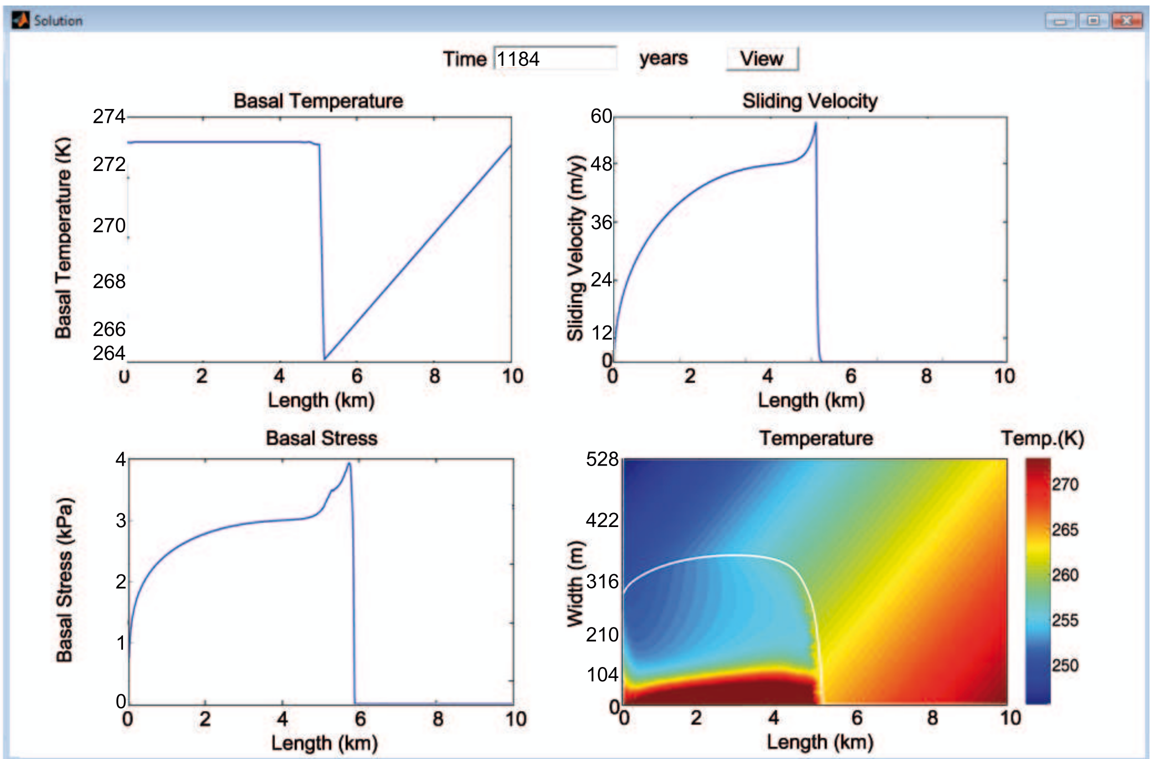

Figure B.5: Graphical Solution

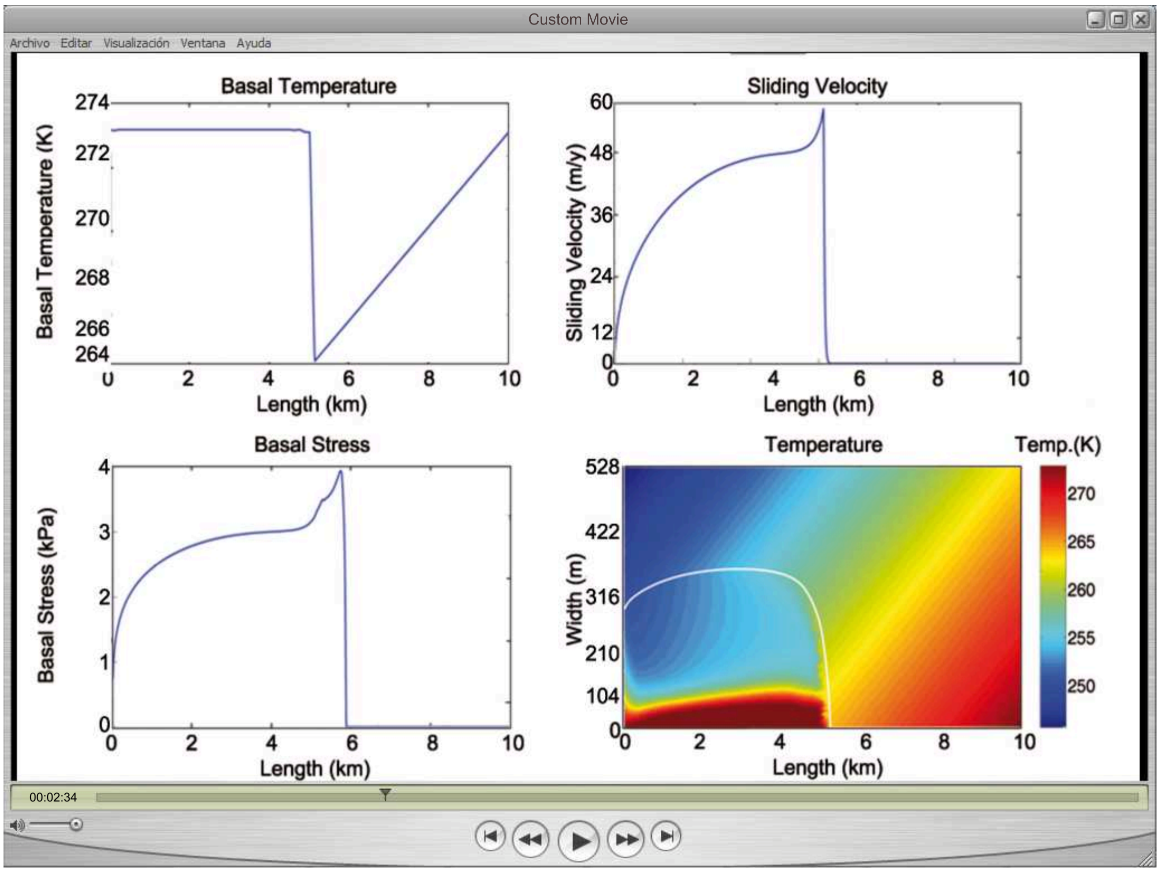

Figure B.6: Video Solution

the Compute menu in the interface. A main program reads the dimensionless physical data and the options and parameters associated to the numerical methods in the respective data files. Once the algorithm has computed the different dimensionless values, they are rescaled so that the user can access to the real magnitudes in the different formats provided by the postprocessor module.

B.2 Parallel implementation of the glacier problem

The algorithm described in Section 4.5.5 is implemented in a computer intensive program, that requires significant CPU time when it runs over a sequential machine. In this section we present a vectorial version to be run more efficiently than the sequential one.

The structure of this program is very similar to the one developed to simulate the behaviour of ice sheets. We have previously built a parallel version for the ice sheets program and we run it over a machine with eight biprocessor Intel Xeon IV of 1.6GHz servers and 1 Gb of RAM and we have achieved speedups from 1.15 over two processors to 1.20 over five processors (see further details in [16]). These speedups indicate that the program is not very suitable to be parallelized. Moreover, the parallel version is not scalable because adding more processors hardly increases the speedup. This is due to the special characteristics of the program structure. As most of these special characteristics are also kept in the program for glaciers we have decided to vectorize the algorithm instead of parallelizing it. In the following section we present the particular characteristics of the algorithm for glaciers simulation and the vectorization technique.

B.2.1 Program characteristics

As we can see in the flowchart of the program sketched in Fig. B.7, we have an iterative process which is composed by a time loop where the computed results at each time iteration are used in the following time iteration.

The functional block that computes the profile at each time step, $f_{profile}$, implements the algorithm described in Section 4.5.1. The functional block that computes the temperature at each time step, $f_{temperature}$, implements the algorithm described at the end of Section 4.5.4. Both algorithms are further sketched in Figs. B.8 and B.9. At each time step, the computation of the profile and the temperature combines fixed point techniques, finite elements and duality methods that involve additional nested iterative processes. Furthermore, the total number of iterations for these nested loops is a priori unknown because it depends on several convergence criteria.

A first approach to develop a parallel version of the algorithm could be to split the different functional blocks that appear in Fig. B.7 into different processors, but this is clearly not a valid approximation because the loads between the different computations should be unbalanced, as each block of the flowchart does not consume similar execution times. Thus, for example, the computation of profile is more complex and time consuming than the computation of the temperature in the atmosphere. These arguments led us to try a loop level parallelism.

B.2.2 Parallel implementation

First, notice that in Fig. B.7 each functional block (except those ones corresponding to profile and temperature computation) just involves a loop execution. The same occurs in Fig. B.8 and B.9, where the exceptions are the functional blocks corresponding to the linear system solvers. Therefore, we exploit a loop-level parallelism using the Streaming SIMD Extensions (SSE) to vectorize the code.

The SSE is a Simple Instruction Multiple Data (SIMD) instructions set extension, so the SSE allows to execute simultaneously the same operation on multiple pieces of data. SIMD results to be specially well suited for matrix and vector operations, that are the basic instructions of our program.

In the case of the profile problem, the linear system solver is the bottleneck for the parallelization because it involves a direct method for solving a tridiagonal system.

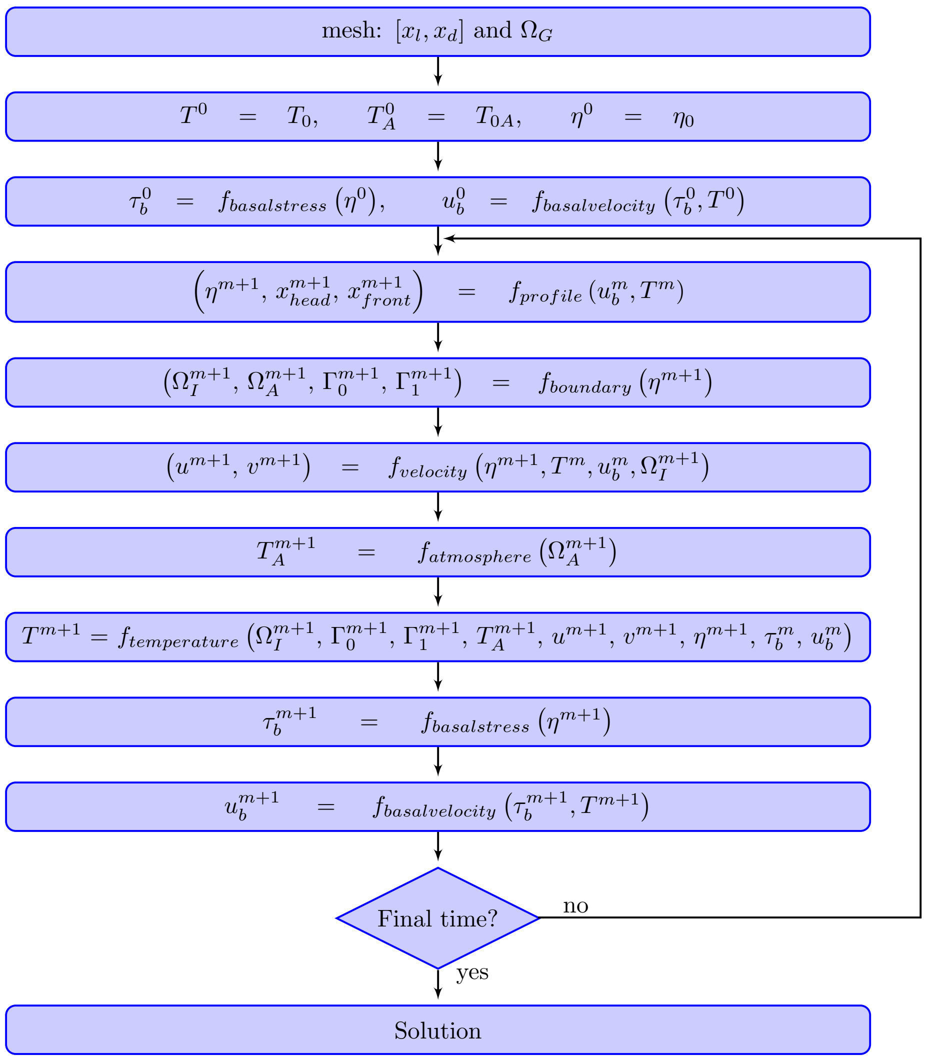

Figure B.7: Flowchart of the algorithm described in Section 4.5.5

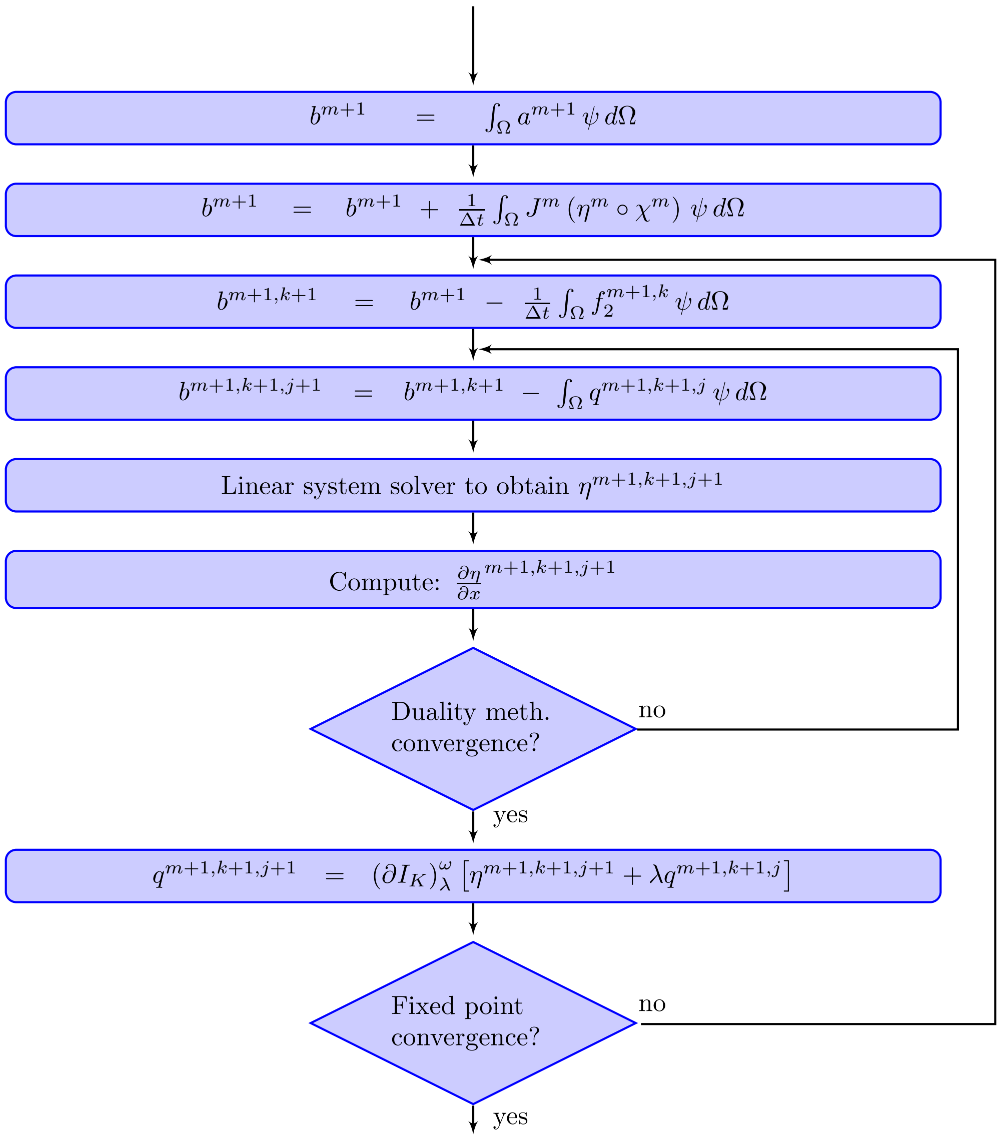

Figure B.8: Flowchart of the algorithm described in Section 4.5.1 to obtain the profile at each time step

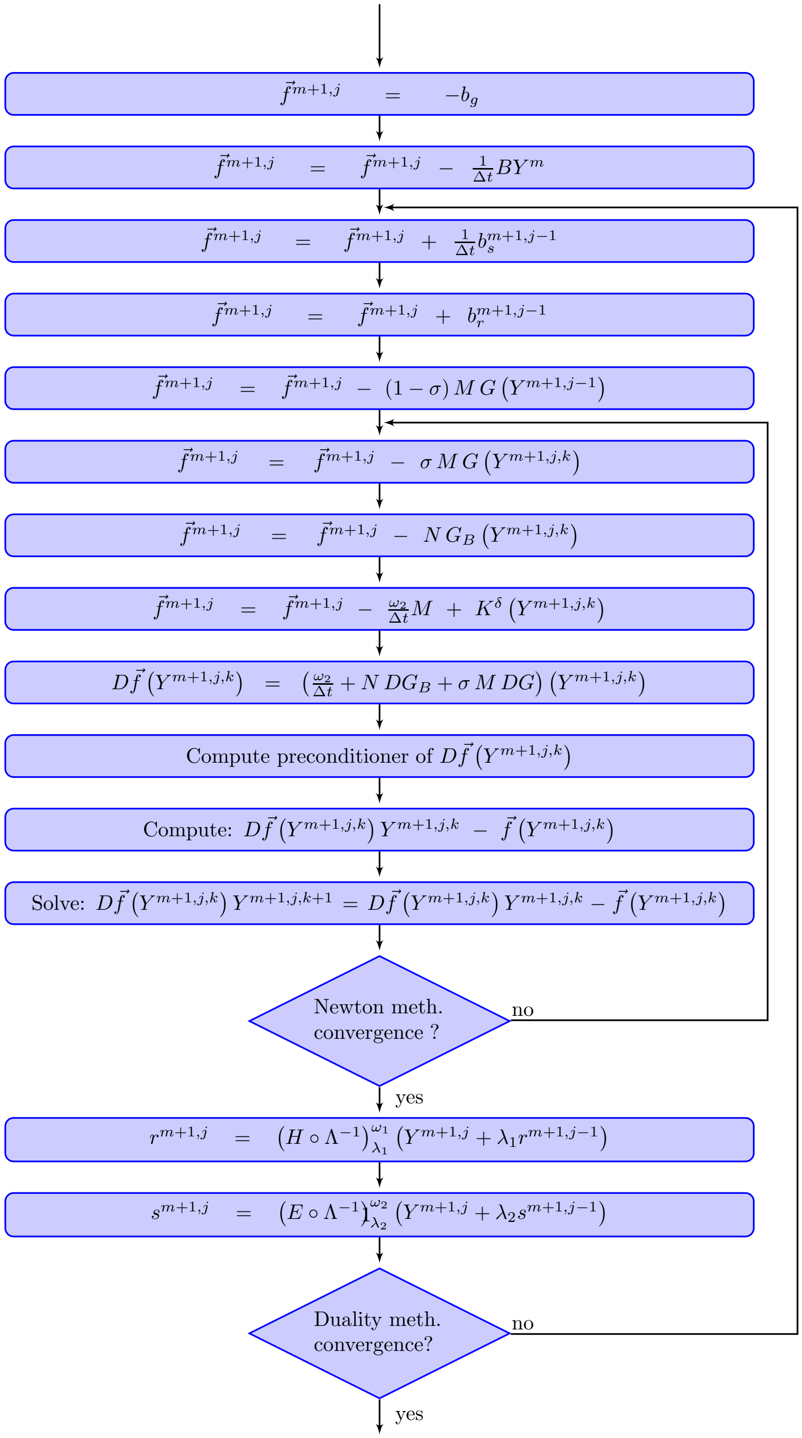

Figure B.9: Flowchart of the algorithm described in Section 4.5.4 to obtain the temperature at each time step

N	100	10000
without SSE	11m 35s	275m 31s
with SSE	3m 59s	19d 3h 40m 55s

Table B.1: Execution time to compute the profile problem with analytical solution without prescribed flux and $\Delta t = 10^{-6}$(see Section 3.6.1).

At this point, notice that in the tridiagonal case, if the system size is small enough to be stored in the computer memory then it is not efficient to parallelize. This is mainly due to the strong dependence between the data that would involve a great number of communications among the processors.

In the case of the temperature problem, the linear system solver is based on the biconjugate gradient method that is more suitable to be parallelized. Nevertheless in this case the bottleneck of the algorithm is the sparsity of the matrix, that involves a great number of communications after each matrix and vectorial computation.

Table B.1 shows the execution times obtained using the SSE to vectorize the code. With this approach we divide by almost 3 the computational time. This improvement is much better than the time reduction obtained with parallelization in the ice sheets where 1.2 was the maximum speedup obtained. Moreover, when we compute the solution for the nonisothermal problem without use the SSE the total time to reach the steady state solution is 29d and with SSE the total time to reach the steady state is 9d and 13h. This approach divides by 3 the computational and once again it is much better than the time reduction that we can obtain with parallelization, that in the coupled problem of ice sheets the maximum speedup obtained was 1.15.

Bibliography

[1] A. Aschwanden and H. Blatter. Mathematical modeling and numerical simulation of polythermal glaciers. *J. Geophys. Res.*, 114:F01027, 2009. doi: 10.1029/2008JF001028.

[2] M. Bercovier, O. Pironneau, and V. Sastri. Finite elements and characteristics for some parabolic-hyperbolic problems. *Appl. Math. Modelling*, 7(2):89–96, 1983. doi: 10.1016/0307-904X(83)90118-X.

[3] A. Bermúdez and J. Durany. La méthode des caractétistiques pour les problémes de convection-diffusion stationaries. *Modélisation mathématique et analyse numérique*, 21:7–26, 1987.

[4] A. Bermúdez, J. Durany, M. Posse, and C. Vázquez. An upwind method for solving transport-diffusion-reaction systems. *Int. J. Numer. Methods Eng.*, 28(9):2021–2039, 1989. doi: 10.1002/nme.1620280904.

[5] A. Bermúdez and C. Moreno. Duality methods for solving variational inequalities. *Comput. Math. Appl.*, 7(1):43–58, 1981. doi: 10.1016/0898-1221(81)90006-7.

[6] H. Blatter and K. Hutter. Polythermal conditions in arctic glaciers. *J. Glaciol.*, 37(126):261–269, 1990.

[7] G. Booch, J. Rumbaugh, and I. Jacobson. *Unified modelling language user's guide*. Addison Wesley, Boston, USA, 1998.

[8] M. Boukrouche and F. Saidi. Non-isothermal lubrication problem with Tresca fluid-solid interface law. Part I. *Nonlinear Analysis: Real World Applications*, 7:1145–1166, 2006. doi: 10.1016/j.nonrwa.2005.10.008.

[9] M. Boukrouche and F. Saidi. Non-isothermal lubrication problem with Tresca fluid-solid interface law. Part II Asymptotic behaviour of weak solutions. *Nonlinear Analysis: Real World Applications*, 9:1680–1701, 2008. doi: 10.1016/j.nonrwa.2007.05.003.

[10] H. Brezis. *Operateurs maximales monotones.* Mathematics Studies 5. North Holland P.C., Amsterdam, 1973.

[11] E. Bueler, J. Brown, and C. Linge. Exact solutions and the verification of numerical models for isothermal ice sheets. *J. Glaciol.*, 51(173):291–306, 2005.

[12] E. Bueler, J. Brown, and C. Linge. Exact solutions to the thermomechanically coupled shallow ice approximation: effective tools for verification. *J. Glaciol.*, 53(182):499–516, 2007.

[13] N. Calvo, J. I. Díaz, J. Durany, E. Schiavi, and C. Vázquez. On a doubly nonlinear parabolic obstacle problem modelling ice sheet dynamics. *SIAM J. App. Math.*, 63(2):683–707, 2003. `http://www.jstor.org/stable/3648788`.

[14] N. Calvo, J. Durany, R. Toja, and C. Vázquez. Numerical methods for a fixed domain formulation of the glacier profile problem with alternative boundary conditions. *submitted*.

[15] N. Calvo, J. Durany, R. Toja, and C. Vázquez. Glanusit: A software toolbox for the numerical simulation of large ice masses evolution. *Adv. Eng. Software*, 36(6):410–422, June 2007. doi: 10.1016/j.advengsoft.2006.09.009.

[16] N. Calvo, J. Durany, R. Toja, and C. Vázquez. Numerical techniques for ice masses dynamics simulation by using a complete shallow ice approximation. *Proc. Appl. Math. Mech.*, 7(1):2100053–2100054, 2007. doi: 10.1002/pamm.200700540.

[17] N. Calvo, J. Durany, R. Toja, and C. Vázquez. Numerical methods for a coupled profile-velocity-temperature problem in polythermal glaciers. In Mohammed Seaïd Mofdi El Amrani and Naji Yebari, editors, *Proceedings of 1st Hispano-Moroccan Days on Applied Mathematics and Statistics HMAMS*, pages 473–478, 2008.

[18] N. Calvo, J. Durany, R. Toja, and C. Vázquez. Métodos numéricos para un problema acoplado perfil-velocidad-temperatura en glaciares politérmicos. In SEMNI and APMTAC, editors, *Actas del Congreso de Métodos Numéricos en Ingeniería*, 2009.

[19] N. Calvo, J. Durany, R. Toja, and C. Vázquez. Simulación numérica de un modelo de frontera libre para la evolución del perfil de un glaciar. In SEMA, editor, *Actas del XXI Congreso de Ecuaciones Diferenciales y Aplicaciones - XI Congreso de Matemática Aplicada*, 2009.

[20] N. Calvo, J. Durany, and C. Vázquez. Numerical approach of temperature distribution in a free boundary polythermal ice sheet. *Numer. Math.*, 83(4):557–580, 1999. doi: 10.1007/s002119900081.

[21] N. Calvo, J. Durany, and C. Vázquez. Numerical computation of ice sheet profiles with free boundary models. *Appl. Numer. Math.*, 35(2):111–128, 2000. doi: 10.1016/S0168-9274(99)00052-5.

[22] N. Calvo, J. Durany, and C. Vázquez. Finite elements numerical solution of a coupled profile-velocity-temperature shallow ice sheet approximation model. *J. Comput. Appl. Math.*, 158:31–41, 2003. doi: 10.1016/S0377-0427(03)00466-7.

[23] N. Calvo, J. Durany, and C. Vázquez. A new fully nonisothermal coupled model for the simulation of ice sheet flow. *Physica D*, 238(15):1362–1371, 2010. doi: 10.1016/j.physd.2008.11.003.

[24] P. G. Ciarlet. *The Finite Elements Method for Elliptic Problems*, volume 4 of *Studies in mathematics and its applications*. North–Holland, 1978.

[25] G. K. C. Clarke, U. Nitsan, and W. S. B. Paterson. Strain heating and creep instability in glaciers and ice sheets (paper 6r0950). *Rev. Geophys. Space Phys.*, 15(2):235–247, May 1977. `http://www.agu.org/journals/rg/v015/i002/RG015i002p00235/RG015i002p00235.pdf`.

[26] J. I. Díaz. *The Mathematics of Models for Climatology and Environment*. Springer, 1997.

[27] J. I. Díaz and E. Schiavi. On a degenerate parabolic/hyperbolic system in glaciology giving rise to a free boundary. *Nonlinear Anal.*, 38:649–673, 1999. doi: 10.1016/S0362-546X(99)00101-7.

[28] J. Douglas and T. Russell. Numerical methods for convection dominated diffusion problems based on combining the method of characteristics with finite element or finite difference. *SIAM J. Numer. Anal.*, 19(5):871–885, 1982.

[29] G. Duvaut. *Méchanique des milieux continus*. Sciences. Master. Masson, Paris, 1990.

[30] C. M. Elliott and J.R. Ockendon. *Weak and variational methods for moving boundary problems*, volume 59 of *Research Notes in Mathematics*. Pitman Advanced Publishing Program, Boston, 1982.

[31] A. C. Fowler. The existence of multiple steady states in the flow of large ice masses. *J. Glaciol.*, 25(91):183–184, 1980.

[32] A. C. Fowler. Subtemperate basal sliding. *J. Glaciol.*, 32(110):3–5, 1986.

[33] A. C. Fowler. *Glaciers and Ice Sheets*. Number 26 in NATO ASI Ser. I. Springer, 1997.

[34] A. C. Fowler. *Mathematical Models in the Applied Sciences*. Cambridge University Press, Cambridge, 1997.

[35] A. C. Fowler. *Modelling the flow of glaciers and ice sheets*, pages 201–221. Continuum mechanics and applications in geophysics and the environment. Eds. B. Straughan, R. Greve, H. Ehrentraut and Y. Wang, Springer–Verlag, Berlin, 2001.

[36] A. C. Fowler and D. A. Larson. On the flow of polythermal glaciers, part i: Model and preliminary analysis. *Proc. R. Soc. A*, 363(1713):217–242, 1978. `http://www.jstor.org/stable/79748`.

[37] A. C. Fowler and D. A. Larson. Thermal stability properties of a model of glacier flow. *Geophys. J. R. Astron. Soc.*, 63(2):347–359, 1980. doi: 10.1111/j.1365-246X.1980.tb02625.x.

[38] A. C. Fowler and D. A. Larson. The uniqueness of steady state flows of glaciers and ice sheets. *Geophys. J. R. Astron. Soc.*, 63(2):333–345, 1980. doi: 10.1111/j.1365-246X.1980.tb02624.x.

[39] A. C. Fowler and E. Schiavi. A theory of ice sheets surges. *J. Glaciol.*, 44(146):104–118, 1998.

[40] A. C. Fowler, R. Toja, and C. Vázquez. Temperature-dependent shear flow and the absence of thermal runaway in valley glaciers. *Proc. R. Soc. A*, 446:363–382, 2010. doi: 10.1098/rspa.2009.0335.

[41] H. Fujita. On the nonlinear equations $\delta u + e^u = 0$ and $\partial u/\partial t = \delta v`e^v$. *Bull. Am. Math. Soc.*, 75(1):132–135, 1969. `http://projecteuclid.org/euclid.bams/1183530216`.

[42] E. Gamma, R. Helm, R. Johnson, and J. Vlissides. *Design patterns: elements of reusable object-oriented software.* Addion Wesley, Boston, USA, 1996.

[43] J. W. Glen. The creep of polycrystalline ice. *Proc. R. Soc. London, Ser. A*, (228):519–538, 1955. `http://www.jstor.org/stable/99642`.

[44] R. Glowinski. *Numerical methods for nonlinear variational problems.* Springer Series in Computational Physics. Springer, New York, 1984.

[45] R. Greve. *Thermomechanisches Verhalten polythermer Eisschilde - Theorie, Analytik, Numerik.* Doctoral thesis, Department of Mechanics, Darmstadt University of Technology, Germany, 1995.

[46] R. Greve and H. Blatter. *Dynamics of Ice Sheets and Glaciers.* Springer, Paris, 2009.

[47] J.M. Grove. The little ice age in the massif of mont blanc. *Transactions of the Institute of Brisisth Geographers*, (40):129–143, December 1966. `http://www.jstor.org/stable/621573`.

[48] I. J. Gruntfest. Thermal feedback in liquid flow: plane shear at constant stress. *J. Rheol.*, 7(1):195–207, March 1963. doi: 10.1122/1.548954.

[49] M. E. Gurtin. *An Introduction to Continuum Mechanics.* Academic Press, 1981.

[50] W. D. Harrison. Temperature of a temperate glacier. *J. Glaciol.*, 11(61):15–29, 1972.

[51] F. Hecht and E. Saltel. *EMC2 Wysiwyg 2D finite elements mesh generator.* INRIA (Institut National de Recherche en Informatique et en Automatique, 1995.

[52] R. C. A. Hindmarsh. Consistent generation of ice-streams via thermo-viscous instabilities modulated by membrane stresses. *Geophys. Res. Lett.*, 36:L06502, 2009. doi: 10.1029/2008GL036877.

[53] R. C. A. Hindmarsh and A. J. Payne. Time-step limits for stable solutions of the ice sheet equations. *Ann. Glaciol.*, 23:74–85, 1996.

[54] K. Hutter. *Theoretical Glaciology.* Reidel, Dordrecht, 1981.

[55] A. Huybrechts. *The Antarctic ice sheet and environmental changes: a three dimensional modelling study.* PhD thesis, in: Ber. Polarforsh, Vol. 99, Alfred Polar Institute for Polar and Marine Research, Bremerhaven, Germany, 1992. doi: 10013/epic.10099.d001.

[56] A. Huybrechts and A. J. Payne. Eismint benchmarks for testing ice sheet models. *Ann. Glaciol.*, 23:1–12, 1996.

[57] IPCC. Climate change 2007: Synthesis report. contributing of working groups i, ii and iii to the fourth assesment report of the intergovernmental panel on climate change. Technical report, IPCC, Geneva, Switzerland, 2007. `http://www.ipcc.ch/publications_and_data/publications_ipcc_fourth_assessment_report_synthesis_report.htm`.

[58] D. D. Joseph. Variable viscosity effects on the flow and stability of flow in channels and pipes. *Phys. Fluids*, 7:1761–1771, 1964. `http://www.aem.umn.edu/people/faculty/joseph/archive/docs0/64_2.pdf`.

[59] D. D. Joseph. Stability of frictionally-heated flow. *Phys. Fluids*, 8:2195–2200, 1965. `http://www.aem.umn.edu/people/faculty/joseph/archive/docs0/65_2.pdf`.

[60] B. Kamb and 7 others. Glacier surge mechanism: 1982–1983 surge of variegated glacier, alaska. *Science*, 227(4686):469–479, 1985. doi: 10.1126/science.227.4686.469.

[61] E. Le Meur, O. Gagliardini, T. Zwinger, and J. Ruokolainen. Glacier flow modelling: a comparison of the shallow ice approximation and the full-stokes solution. *C.R. Phys.*, 5(7):709–722, September 2004. doi: 10.1016/j.crhy.2004.10.001.

[62] L. Lliboutry. *Very slow flows of solids.* Martinus Nijhoff, Dordrecht, 1987.

[63] L. A. Lliboutry. *Traite de Glaciologie.* Masson, Paris, 1964.

[64] L. A. Lliboutry. General theory of subglacial cavitation and sliding of temperate glaciers. *J. Glaciol.*, 7:21–58, 1968.

[65] Mathworks. *The language of technical computing.* Mathworks Inc., 2000.

[66] M. F. Meier and A. Post. What are glacier surges? *Can. J. Earth Sci.*, 6(4):807–817, 1969. doi: 10.1139/e69-08110.1139/e69-08110.1139/e69-081.

[67] J. F. Nye. The motion of ice sheets and glaciers. *J. Glaciol.*, 3(26):493–507, 1959.

[68] C. Parés, J. Macías, and M. Castro. Duality methods with an automatic choice of parameters. application to shallow water equations in conservative form. *Numer. Math*, 89:161–189, 2001. `http://resolver.scholarsportal.info/resolve/0029599x/v89i0001/161_dmwaacsweicf`.

[69] W. S. B. Paterson. *The physics of glaciers.* Pergamon, Oxford, 1981.

[70] A. J. Payne and P. W. Dongelmans. Self-organization in the thermomechanical flow of ice sheets. *J. Geophys. Res.*, 102(B6):12,219–12,233, 1997. `http://www.agu.org/journals/jb/v102/iB06/97JB00513/`.

[71] O. Pironneau. On the transport-diffusion algorithm and its applications to navier-stokes equations. *Numer. Math.*, 38:309–332, 1982. doi: 10.1007/BF01396435.

[72] S.D. Richardson and J.M. Reynolds. An overview of glacial hazars in the himalayas. *Quaternary International*, 65–66:31–47, 2000. doi: 10.1016/S1040-6182(99)00035-X.

[73] F. Saito, A. Abe-Ouchi, and H. Blatter. An improved numerical scheme to compute horizontal gradients at the ice sheet margins: Its effects on the simulated ice thickness and temperature. *Ann. Glaciol.*, 46(1):87–96, 2007. doi: 10.3189/172756407782871594.

[74] G. D. Smith and L. W. Morland. Viscous relations for the steady creep of polycristaline ice. *Cold Reg. Sci. Technol.*, 5(2):141–150, 1981. doi: 10.1016/0165-232X(81)90048-3.

[75] R. Stöckli, E. Vermote, and Nazmi Saleous. The blue marble next generation - a true color earth dataset including seasonal dynamics from modis. *NASA Goddard Space Flight Center*, 2005. `http://earthobservatory.nasa.gov/Features/BlueMarble/bmng.pdf`.

[76] H.A. Van der Vorst. Bi-cgstab: a fast and smoothly converging variant of bi-cg for the solution of nonsymmetric linear systems. *SIAM J. Sci. Stat. Comput.*, 13(2):631–644, March 1992. doi: 10.1137/0913035.

[77] D. A. Yuen and G. Schubert. The role of shear heating in the dynamics of large ice masses. *J. Glaciol.*, 24(90):195–212, 1979.

[78] O. C. Zienkiewicz and R. L. Taylor. *El Método de los Elementos Finitos*, volume 1–2. CIMNE, cuarta edición edition, 1994.